Intelligent Power Control System of Three-Phase Grid-Connected PV System

三相併網型太陽光電系統之智慧型功率控制

Chair Prof. Faa-Jeng Lin
PhD, Fellow IEEE/IET
linfj@ee.ncu.edu.tw

Dec. 18, 2019

Abstract

- A PC-based intelligent power control system of the three-phase grid-connected photovoltaic (PV) system for active and reactive power control during grid faults is developed.
- Considering low voltage ride through (LVRT) requirements and current limit of three-phase inverter.
- Two fuzzy-neural-network (FNN) based intelligent controllers are proposed.
  - Probabilistic wavelet fuzzy neural network (PWFNN) controller
  - Takagi-Sugeno-Kang type probabilistic fuzzy neural network with asymmetric membership function (TSKPFNN-AMF) controller
- A dual mode operation control method of the converter and inverter of the three-phase grid-connected PV system is proposed.
- Various types of voltage sags and test scenarios are designed to investigate the LVRT capability of the grid-connected PV system.
- The control performances of the proposed controllers are superior to other controllers.
  - Higher complexity of structure and current harmonic distortion of injected current during grid faults are the main defects.

Contents

Background

- The price of the photovoltaic (PV) system declines of around **75%** in less than 10 years.
- The cumulative installed capacity of the world has been reached to **178 GW** in the end of **2014.**
- EPIA predicts the worldwide total installed capacity of the PV system in **2019** could reach between 396 and 540 GW with the highest probability scenario being around **450 GW.**
- Taiwan has decided to raise the official PV installation target from **13 GW** to **20 GW** in 2025 (currently, **728 MW**).

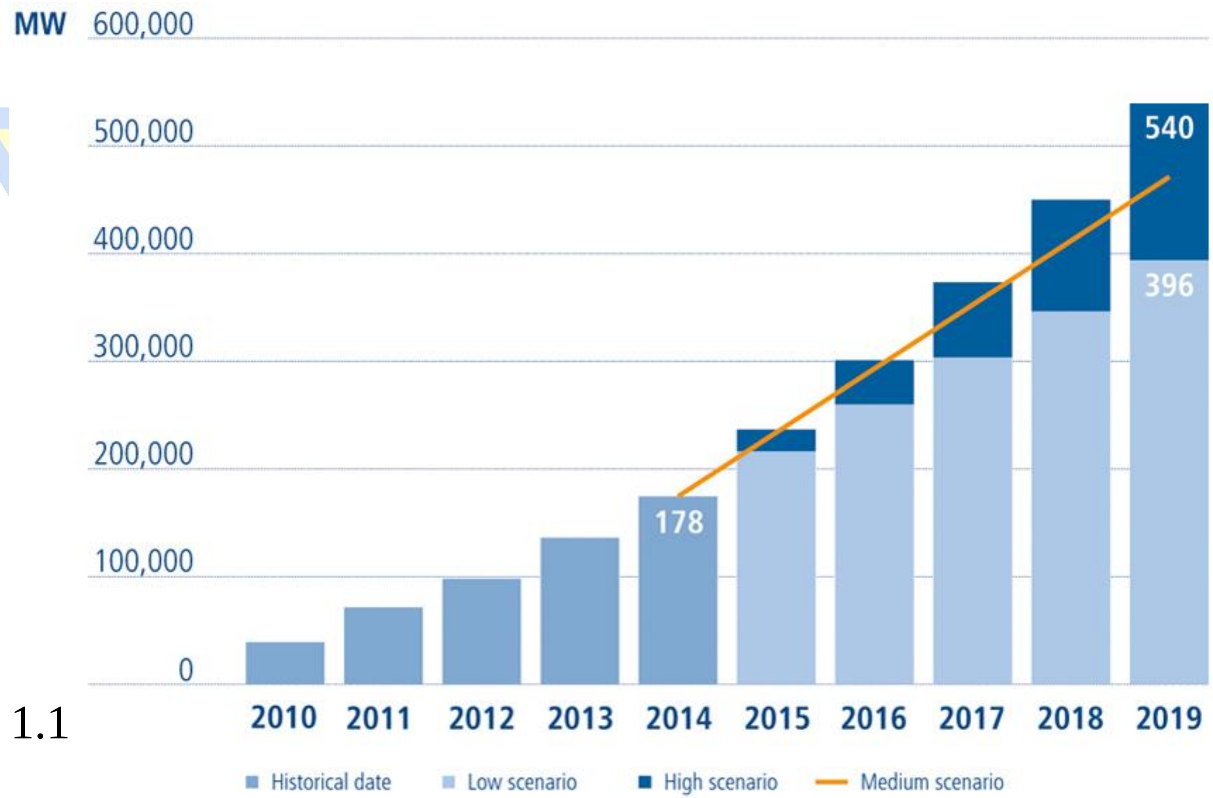

Fig. 1.1

Background

- A grid-connected PV system is mainly composed of two parts: (1) PV panel, (2) inverter.
- Optional elements:
  - Transformer (In Spain, the transformer is mandatory for galvanic isolation requirement).
  - DC-DC boost converter.
- Single-stage or two-stage
  - **Single-stage:** mainly used for medium or high power applications
    - **Pros:** simple-structure, reliable and efficient energy conversion.
    - **Cons:** higher dc-link voltage , efficiency worsened by the less accurate MPPT, partial shading issue.
  - **Two-stage:** mainly adopted in residential PV applications
    - **Pros:** place with partial shading, complicated roof structures, small space, various roof orientations.
    - **Cons:** efficiency may be lowered by the DC-DC stage, compensated by the accuracy MPPT, cost.

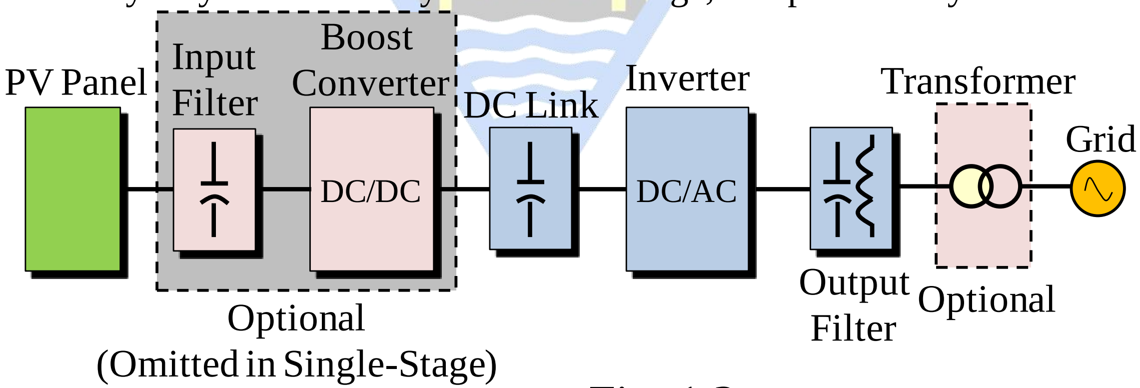

Fig. 1.2

Electrical Characteristic of PV Cell

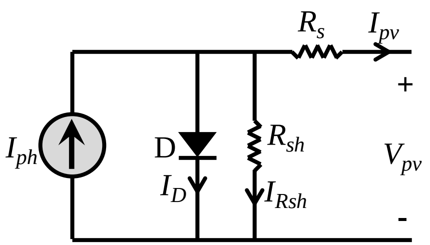

Fig. 1.3

$$P_{pv} = I_{pv}V_{pv} = I_{ph}V_{pv} - I_{rs}V_{pv}\left[\exp\left(\frac{V_{pv}}{AV_T}\right) - 1\right] \tag{1.5}$$

- The short circuit current of the PV panel highly depends on the irradiance.
- High irradiance leads to large short circuit current.
- High temperature leads to small open circuit voltage.

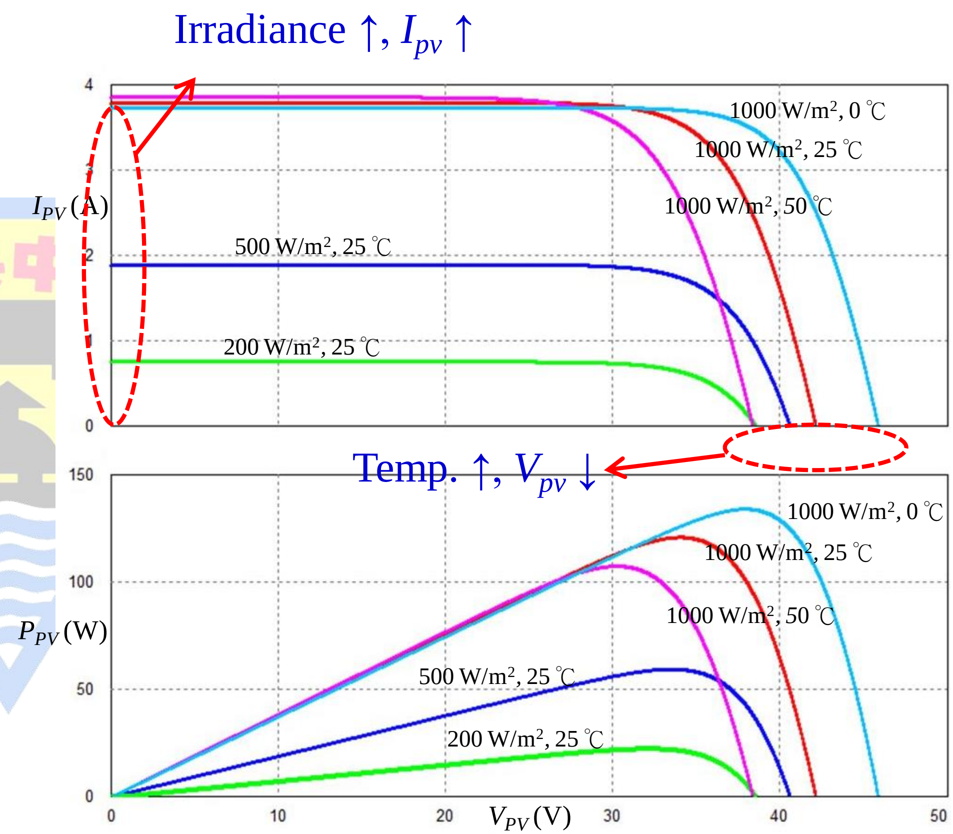

Fig. 1.4

Photovoltaic Cell Electrical Characteristics

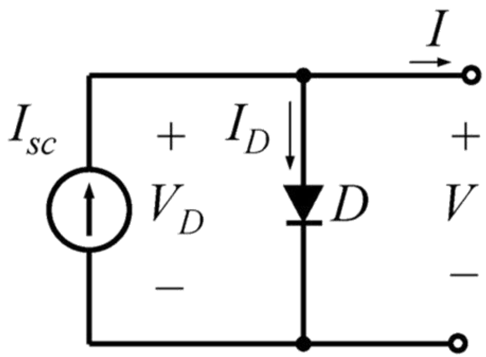

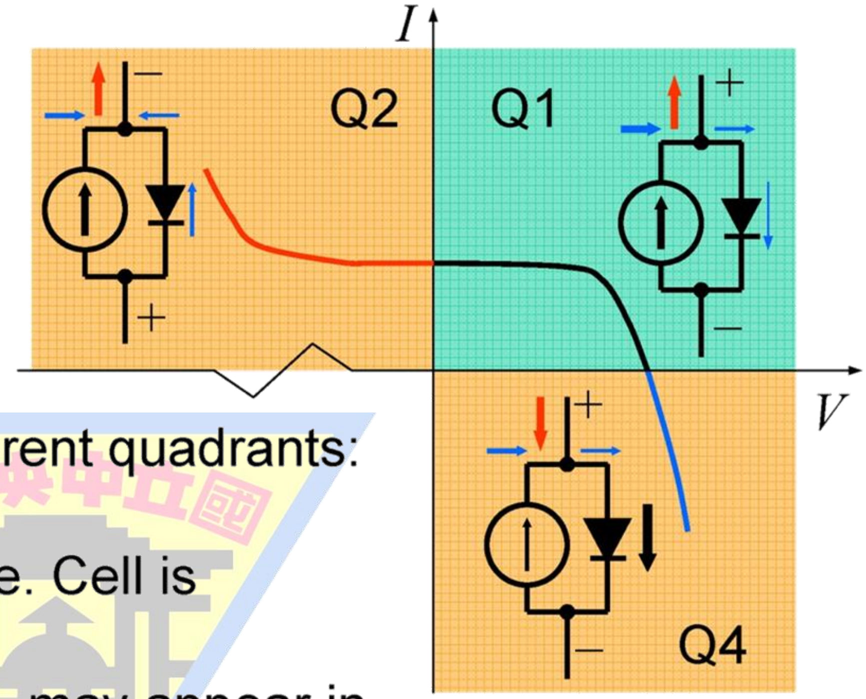

- PV cell may operate in different quadrants: Q1, Q2, Q4.
- Q1 is normal operating zone. Cell is generating power.
- Q2 has reverse cell voltage, may appear in series-connected cells. Cell is dissipating power.
- Q4 has reverse cell current, may appear in parallel-connected cells. Cell is dissipating power.

Series String PV Cell Under Shaded Condition

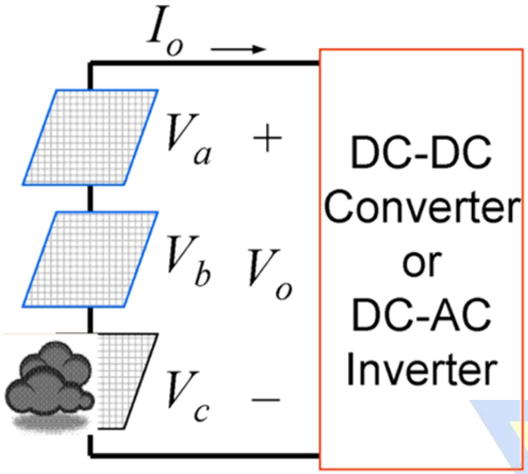

$$V_o = V_a + V_b + V_c$$

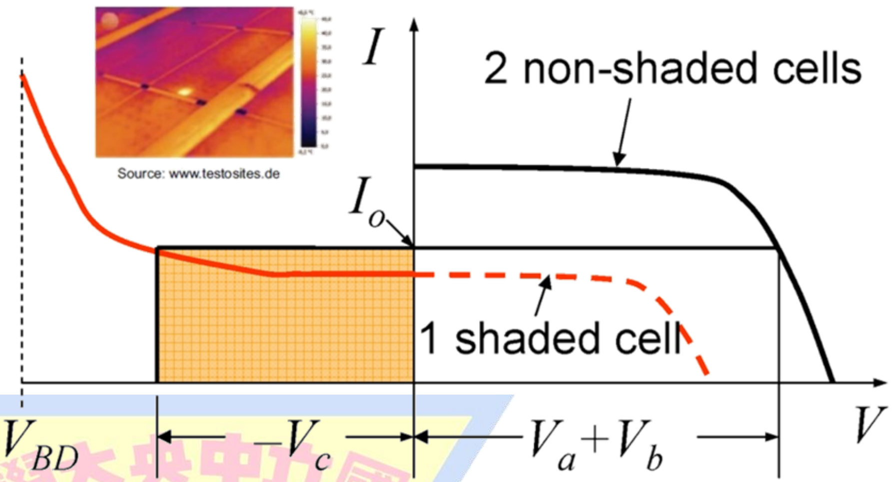

Potential hot spot or failure when $V_c > V_{BD}$

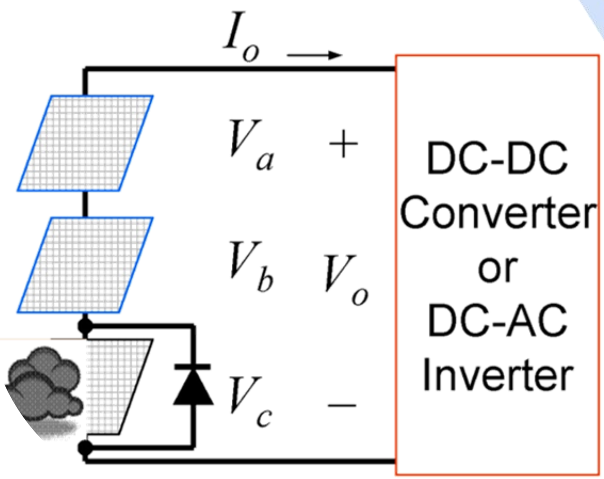

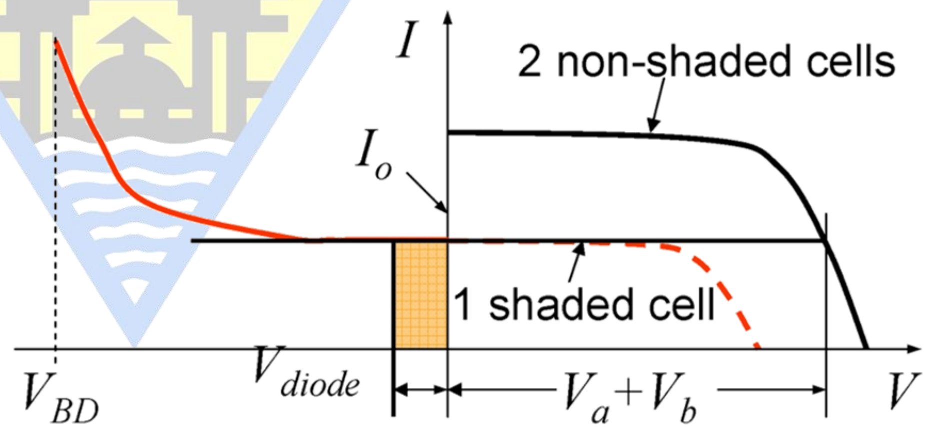

Adding anti-paralleled diode avoids failure

Bypass Diode Power Dissipation

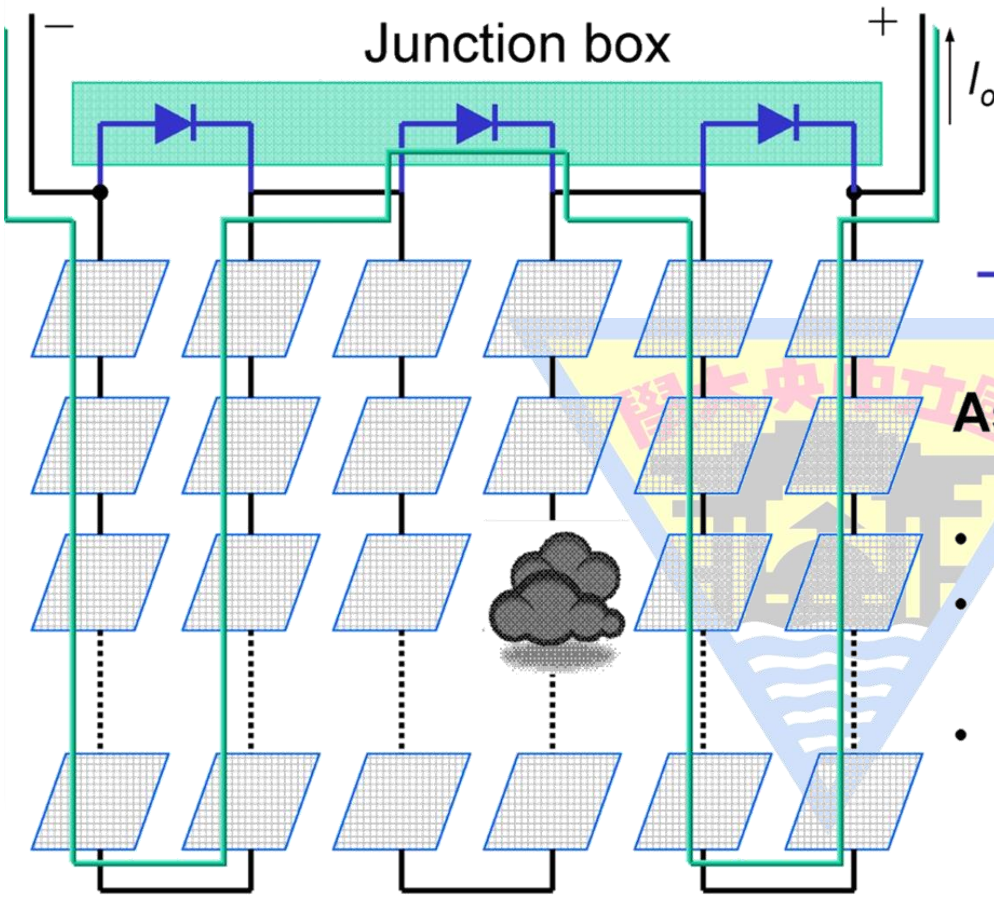

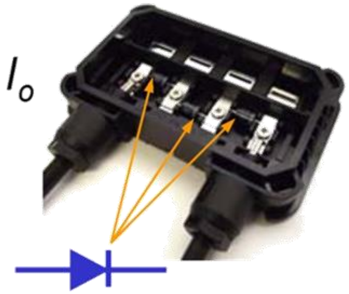

Overheated Bypass Diodes

Assume I_o = 8A. Diode dissipations:

- **Si diode: 0.7V·8A = 5.6W**
- **Schottky diode:**
  0.4V·8A = 3.2W
- **Active diode (synchronous rectification):**
  $(8A)^2 \cdot (5m\Omega)$ = 0.32W

Active Bypass Diode (MOSFET Body Diode with Synchronous Rectification)

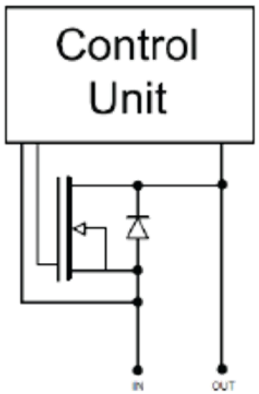

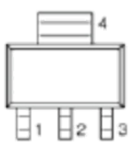

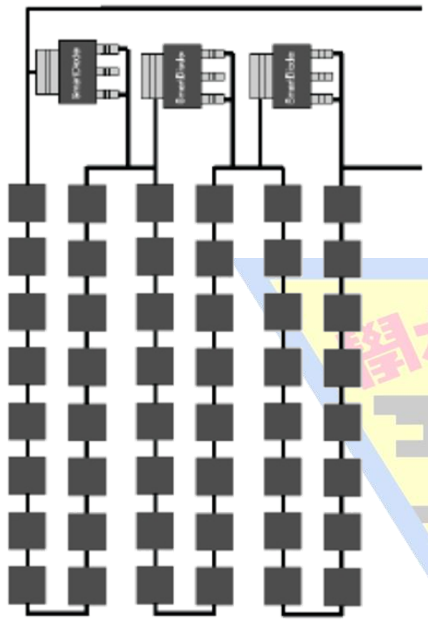

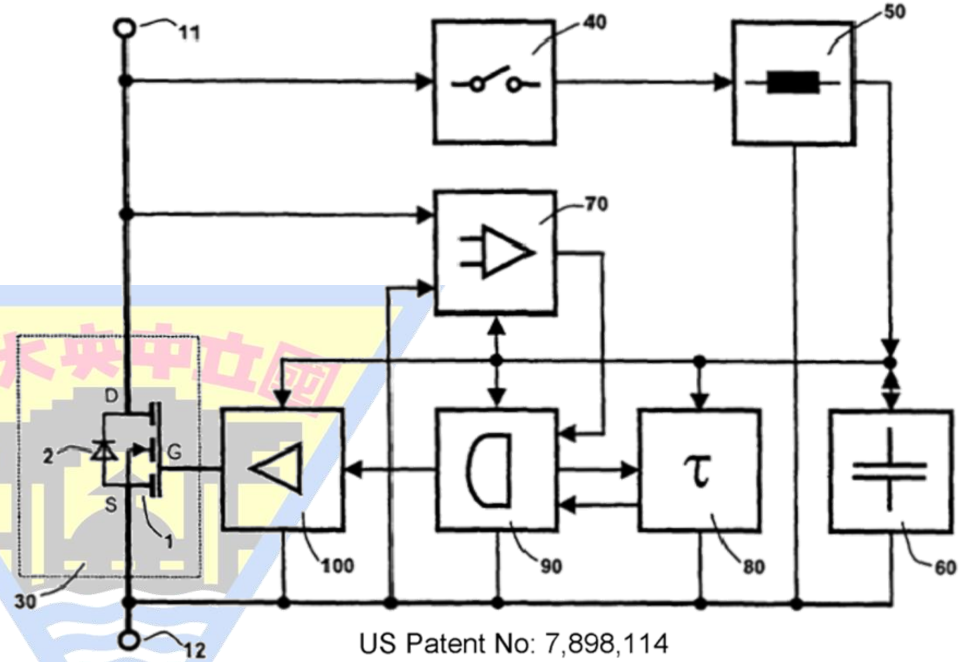

US Patent No: 7,898,114
Protective circuit device for a solar module

Maximum Power Point of a PV Cell

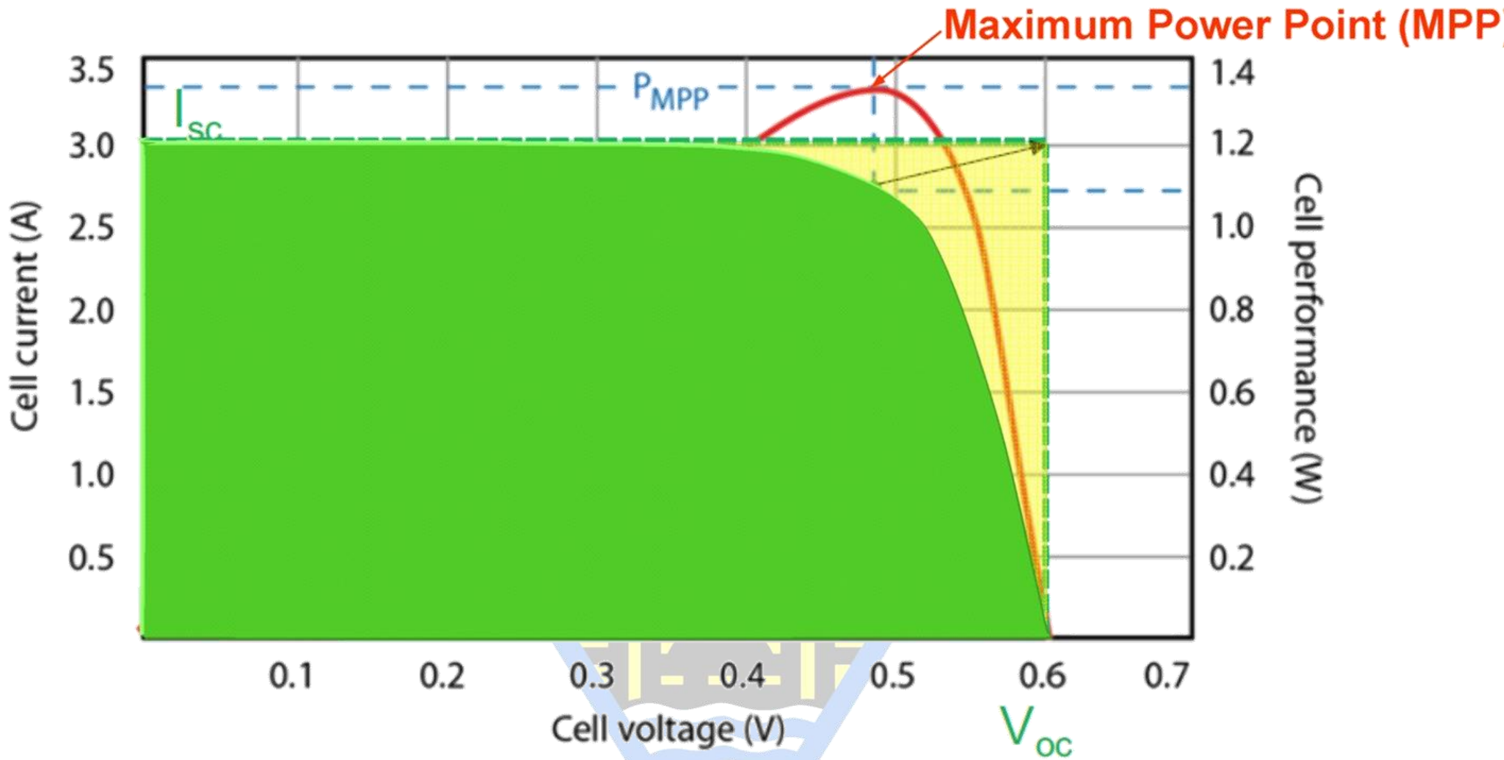

- Typically, $I_{sc} \cong 1.05$ to $1.15\, I_{MPP}$, $V_{MPP} \cong 0.8 V_{oc}$
- Defining fill factor (FF)

$$FF = \frac{P_{MPP}}{V_{oc} I_{sc}} = \frac{V_{MPP} I_{MPP}}{V_{oc} I_{sc}}$$

- Typical fill factors are:
  - C-Si: 0.75 ~ 0.85
  - A-Si: 0.5 ~ 0.7

Example PV Panel VI Characteristics
Kyocera KD180GX-LP

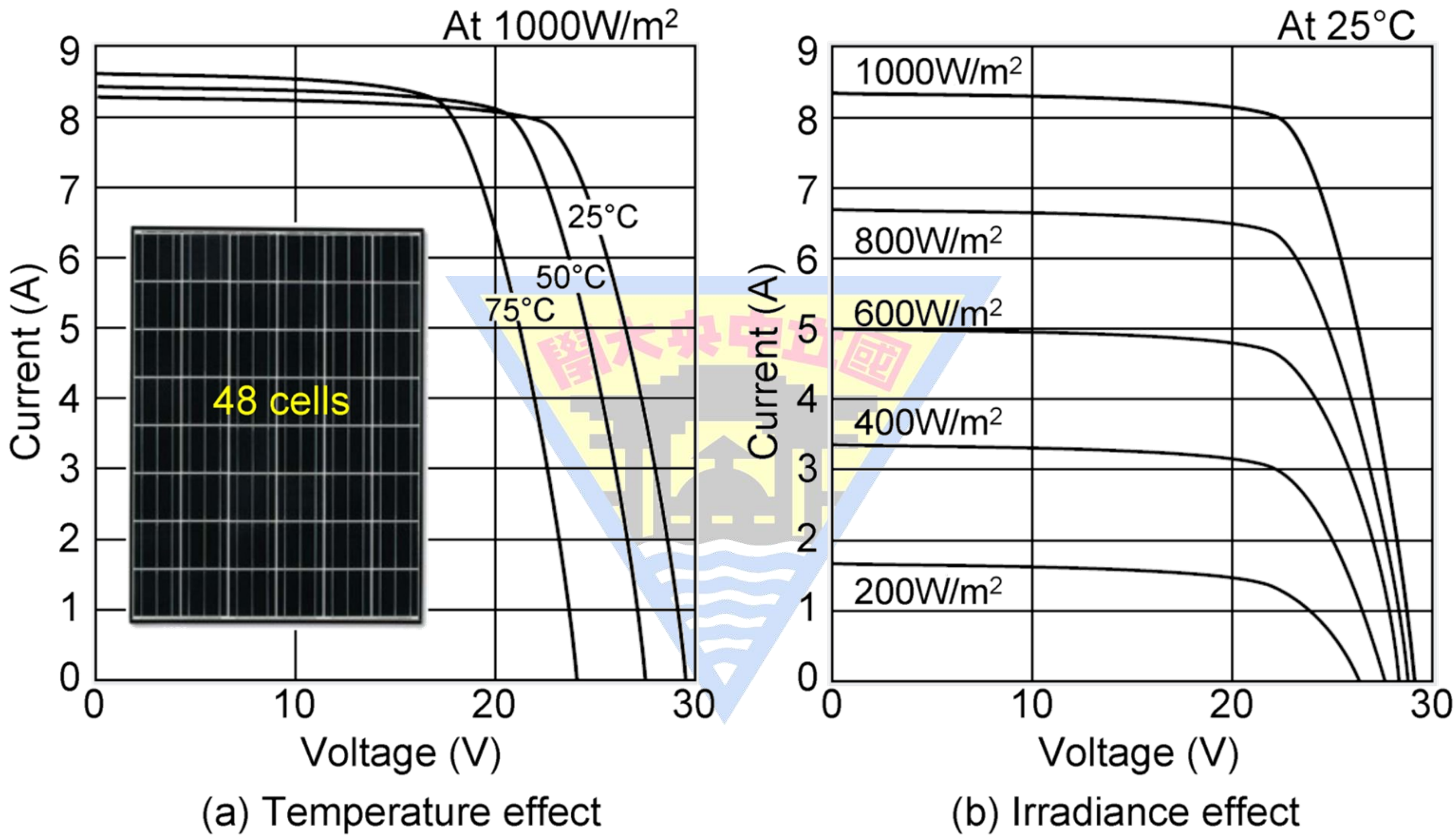

Multiple Peaks Due to Shading Effect with 3-Bypass Diode Configuration

Shading condition:

- **Modules a & b: full-sun condition**
- **Module c: shaded condition**

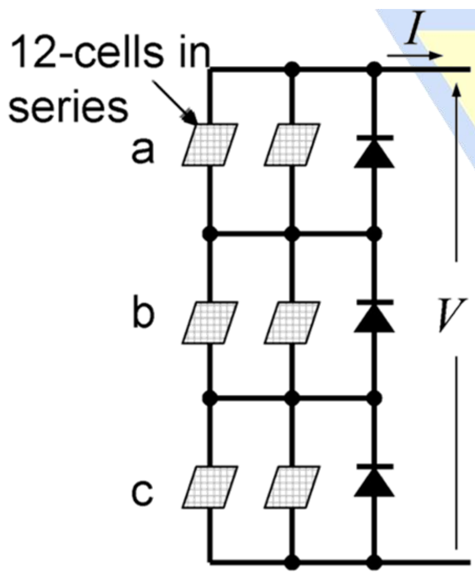

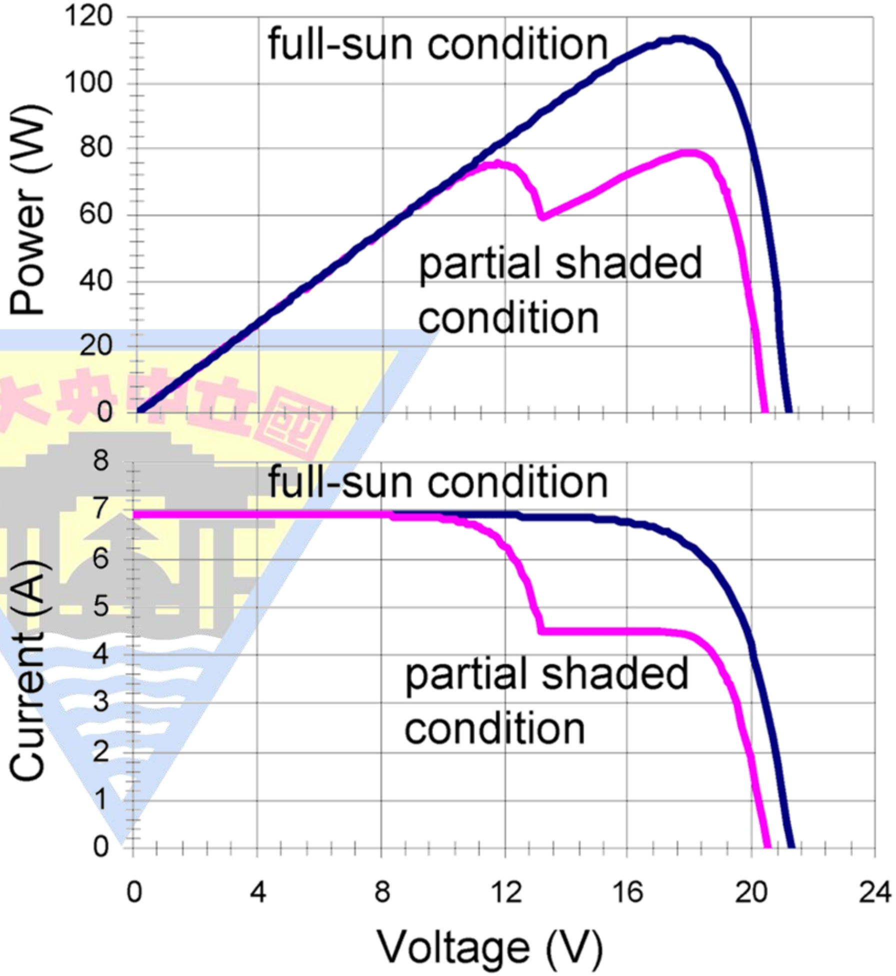

Case with Mismatched Panels and Different Irradiation Levels Among Them

Two different types of PV panels in series with different irradiation levels among them can result in multiple MPPs

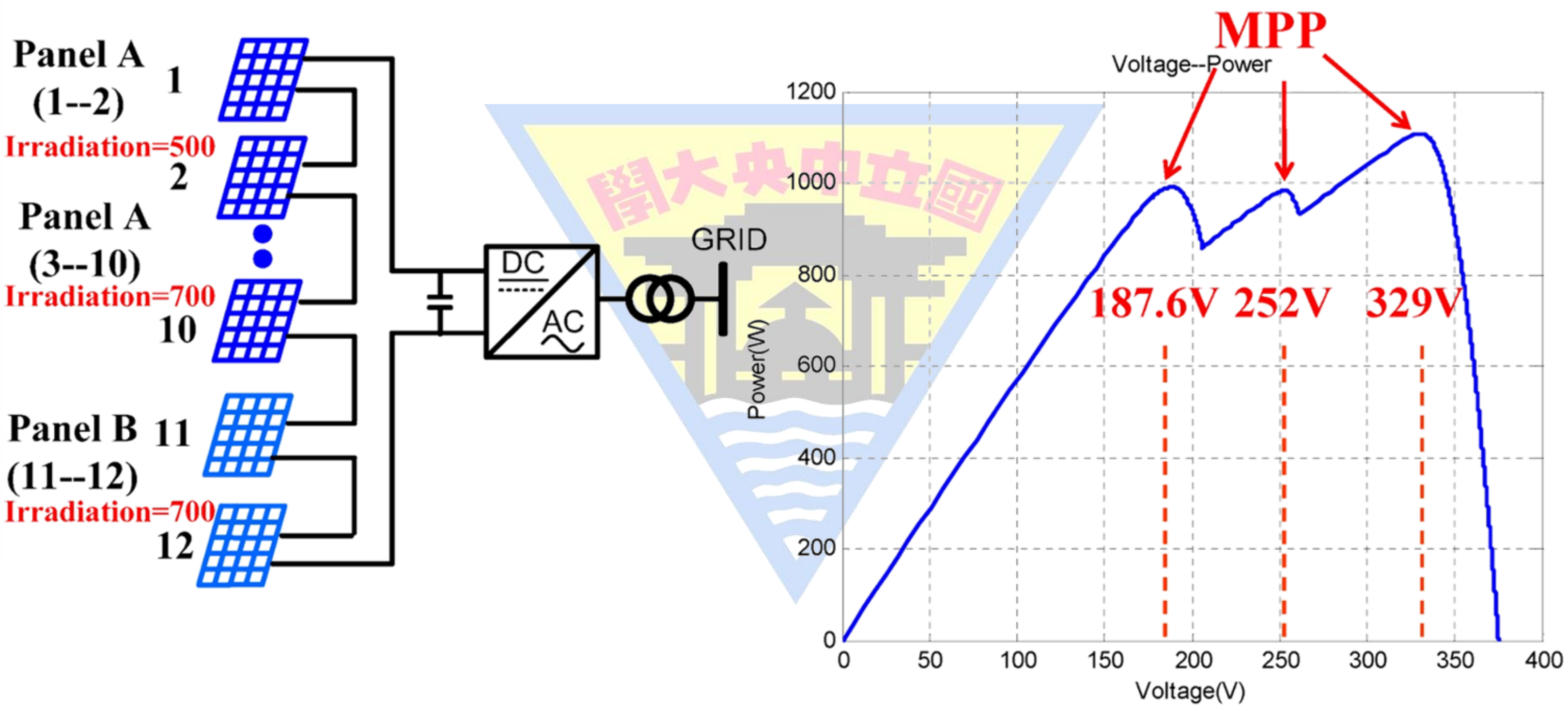

Maximum Power Point Tracking (MPPT)

- MPP control is required to harness as much energy as possible.
- Poor MPPT method is equivalent to having additional loss.
- Important MPPT design considerations:
  - Tracking speed
  - Control loop stability
  - Oscillation around MPP including double line frequency oscillation
  - Global MPP versus local MPP
  - Which stage performs MPPT, DC-DC stage or DC-AC stage?
  - Control of VPV or IPV?
  - Step size?
  - Digital versus analog
- Almost 20 distinct published methods, ranging from ripple correlation control (a fast method that uses converter ripple to find the MPP) to fuzzy logic controls.

Fractional Open-Circuit Voltage

- **For most PV cell types, there is a nearly linear relationship between V_{MPP} and V_{OC}, $V_{MPP} \approx x V_{oc}$**
- ***x* depends on PV material, typically 0.74 to 0.8 V_{oc}**
- **Measure V_{OC} at infrequent intervals, then use the known fraction as the basis for control**
- **Only an approximation → operation practically never exactly at the MPP**

✓ **Simple, low cost, fast, and robust**

× **Poor accuracy, lost power during V_{oc} measurement**

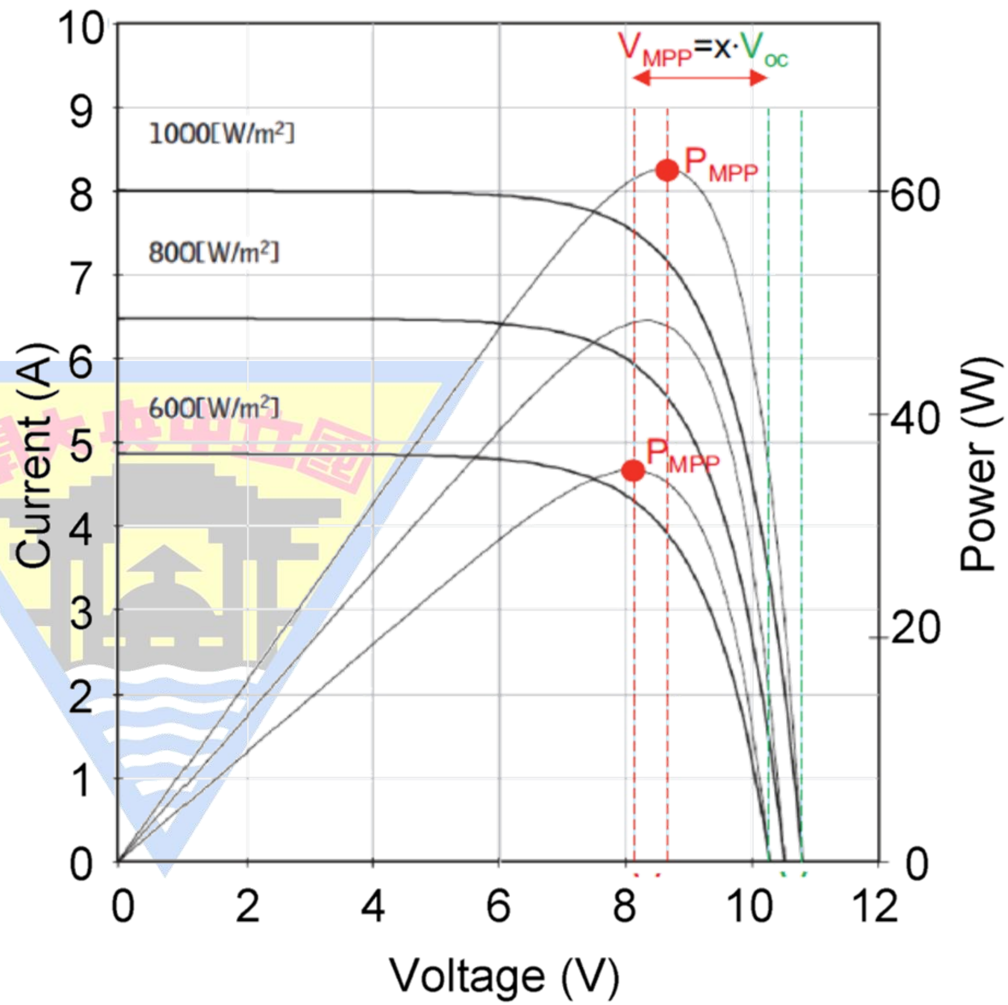

Hill-Climbing/Perturb & Observe Methods

- Alter the operating point, by changing a duty ratio slightly.
- Check whether the power rises or falls.
- Keep changing to get higher power.

Perturbation	Change in Power	Next Perturbation
Positive	**Positive**	**Positive**
Positive	**Negative**	**Negative**
Negative	**Positive**	**Negative**
Negative	**Negative**	**Positive**

Key Features

- Clear and effective.
- Convergence depends on perturbation step size and converter settling times.
- Goes to a *local* maximum power point.

Incremental Conductance Method

$$P_{pv}=V_{pv}I_{pv}\Rightarrow\frac{dP_{pv}}{dV_{pv}}=I_{pv}+V_{pv}\frac{dI_{pv}}{dV_{pv}}$$

$$\frac{1}{V_{pv}}\frac{dP_{pv}}{dV_{pv}}=\frac{I_{pv}}{V_{pv}}+\frac{dI_{pv}}{dV_{pv}}$$

- At MPP, $dP_{pv}/dV_{pv}=0$:

$$\frac{dI_{pv}}{dV_{pv}}=-\frac{I_{pv}}{V_{pv}}=-\frac{I_{MPP}}{V_{MPP}}$$

- When *V* or *I* changes, re-assess d*i*/d*v* and compare to –*I*/*V*. If equal, stay the point, else move back to MPP depending on d*i*/d*v* (> or <) –*I*/*V*

✓ Less oscillations around MPP, more accurate tracking than P&O

× More computation burden

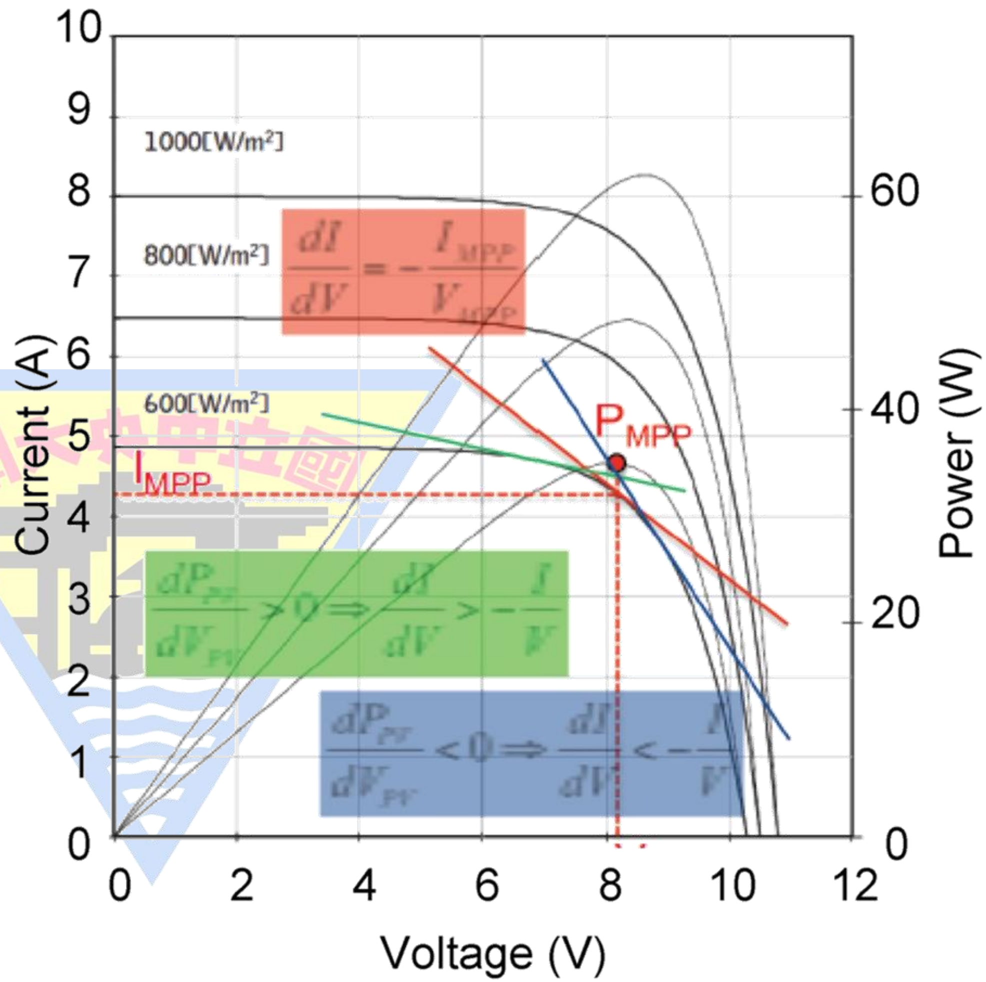

Ripple Correlation Method

A: $\frac{di}{dt}\frac{dp}{dt} > 0 \Rightarrow I < I^*$

B: $\frac{di}{dt}\frac{dp}{dt} < 0 \Rightarrow I > I^*$

MPP occurs at $\frac{di}{dt}\frac{dp}{dt} = 0 \Rightarrow I = I^*$

therefore duty cycle $d = k\int \frac{di}{dt}\frac{dp}{dt}dt$

Similarly with a negative *k*, we have $d = k\int \frac{dv}{dt}\frac{dp}{dt}dt$

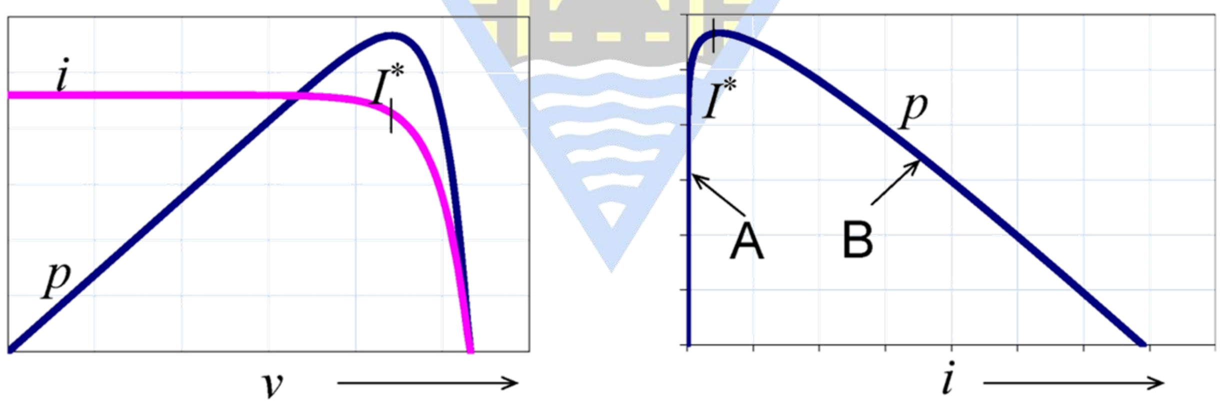

MPPT Implementation with Analog RCC Method for a Boost Converter

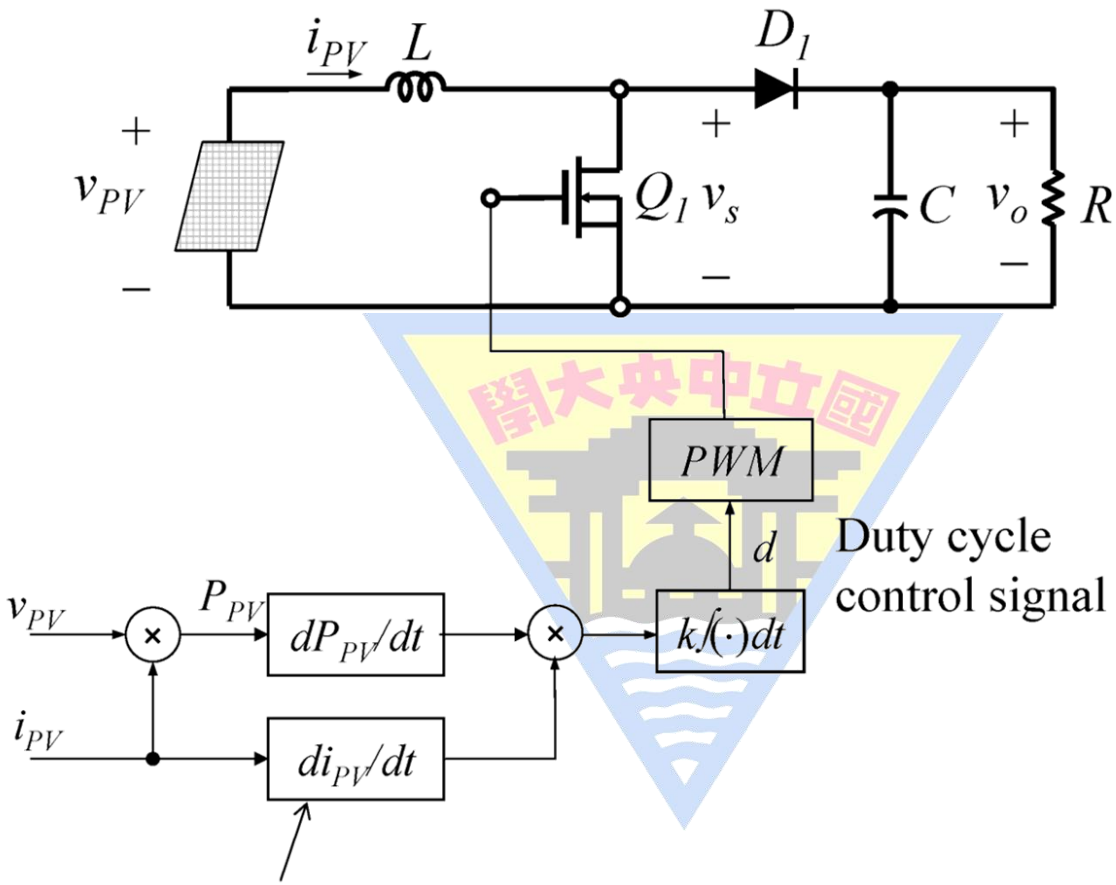

Note: this block can be replaced with dv/dt

PV Power Conversion System Architectures

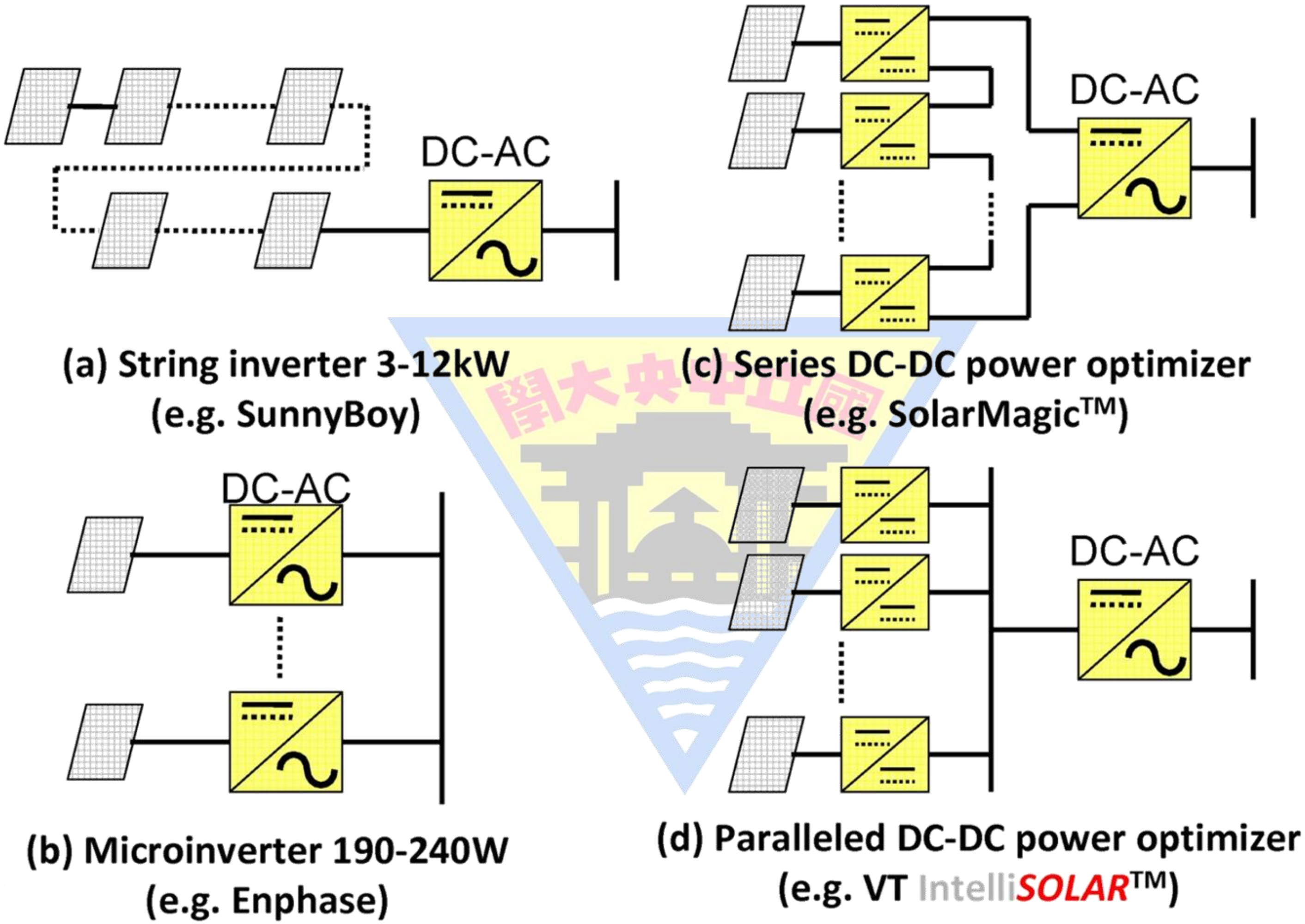

萌芽技術前瞻原創性說明

- 技術原創性
  - 單級轉換架構(轉換效率提升及降低成本)
  - MPPT採增量電導法(提升太陽光電之發電量)
  - 二階廣義積分器鎖相迴路(三相或單相故障時仍可與市電同步與併網)
  - 低電壓穿透功能(提供虛功及具回復市電故障功能可防止發電系統崩潰)
  - 模糊類神經網路智慧型控制(控制實/虛功率反應速度快)

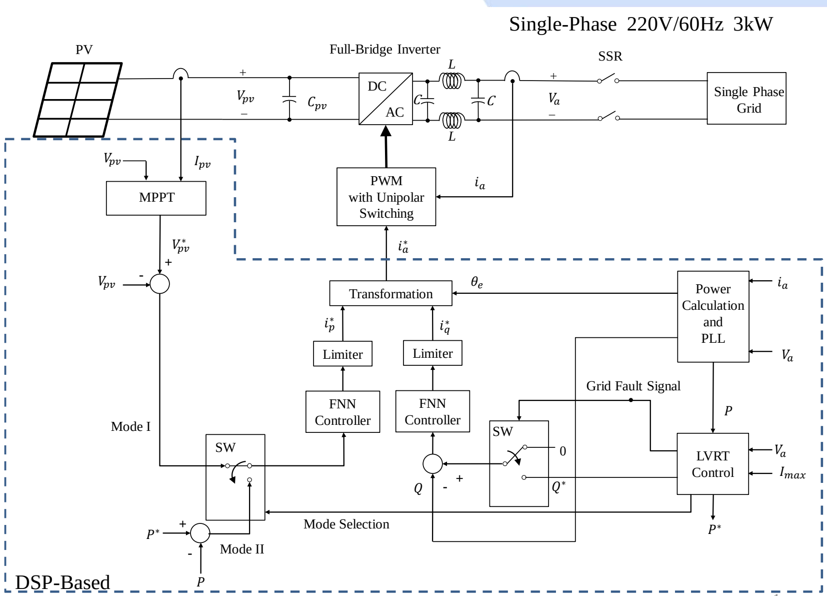

圖三、Single-Phase Single Stage (Inverter)

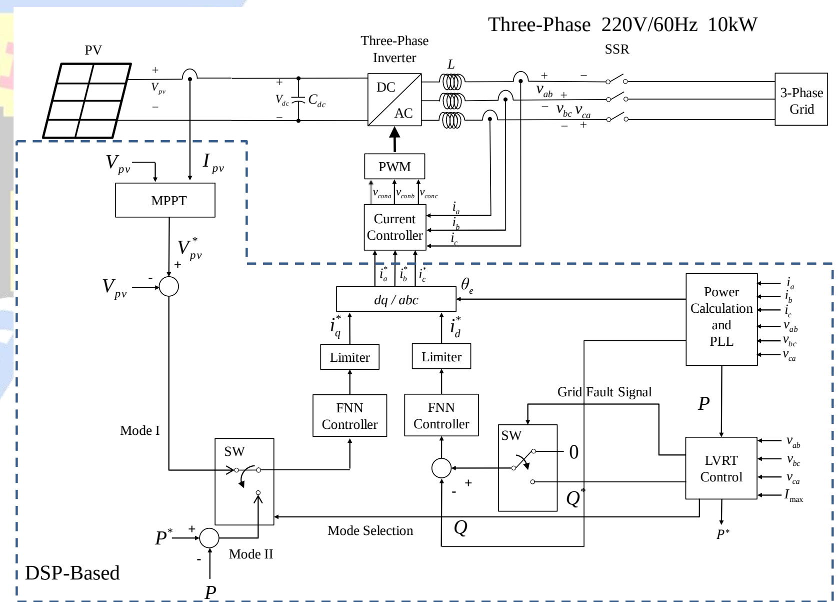

圖二、Three-Phase Single Stage (Inverter)

本計畫之智慧型太陽光能發電系統（單相）本計畫之智慧型太陽光電系統（三相）

103017TW
非MOST
領證及1-3年
年費

中華民國專利證書

發明第 I522767 號

發 明 名 稱：太陽光能發電系統

專 利 權 人：國立中央大學

發 明 人：林法正、呂光欽、李軒宇

專利權期間：自2016年 2 月21日至2034年 6 月16日止

上開發明業經專利權人依專利法之規定取得專利權

經濟部智慧財產局 局長 王美花

中華民國 105 年 2 月 21 日

注意：專利權人未依法繳納年費者，其專利權自原繳費期限屆滿後消滅。

國立中央大學 NCU

103017US
非MOST
領證

The United States of America

The Director of the United States Patent and Trademark Office

Has received an application for a patent for a new and useful invention. The title and description of the invention are enclosed. The requirements of law have been complied with, and it has been determined that a patent on the invention shall be granted under the law.

Therefore, this

United States Patent

Grants to the person(s) having title to this patent the right to exclude others from making, using, offering for sale, or selling the invention throughout the United States of America or importing the invention into the United States of America, and if the invention is a process, of the right to exclude others from using, offering for sale or selling throughout the United States of America, or importing into the United States of America, products made by that process, for the term set forth in 35 U.S.C. 154(a)(2) or (c)(1), subject to the payment of maintenance fees as provided by 35 U.S.C. 41(b). See the Maintenance Fee Notice on the inside of the cover.

Michelle K. Lee

Director of the United States Patent and Trademark Office

US009276498B2

(12) **United States Patent**
Lin et al.

(10) **Patent No.:** **US 9,276,498 B2**
(45) **Date of Patent:** **Mar. 1, 2016**

(54) **PHOTOVOLTAIC POWER GENERATION SYSTEM**

(71) Applicant: **National Central University**, Zhongli, Taoyuan County (TW)

(72) Inventors: **Faa-Jeng Lin**, Zhongli (TW); **Kuang-Chin Lu**, Zhongli (TW); **Hsuan-Yu Lee**, Zhongli (TW)

(73) Assignee: **NATIONAL CENTRAL UNIVERSITY**, Zhongli, Taoyuan County (TW)

(*) Notice: Subject to any disclaimer, the term of this patent is extended or adjusted under 35 U.S.C. 154(b) by 0 days.

(21) Appl. No.: **14/533,695**

(22) Filed: **Nov. 5, 2014**

(65) **Prior Publication Data**

US 2015/0365014 A1 Dec. 17, 2015

(30) **Foreign Application Priority Data**

Jun. 17, 2014 (TW) .... 103120773 A

(51) **Int. Cl.**
H02M 1/12 (2006.01)
H02M 7/44 (2006.01)
H02M 1/44 (2007.01)
H02M 1/32 (2007.01)
H02M 1/00 (2007.01)
G05F 1/70 (2006.01)
F03D 9/00 (2006.01)

(52) **U.S. Cl.**
CPC ***H02M 7/44*** (2013.01); ***H02M 1/00*** (2013.01); ***H02M 1/32*** (2013.01); ***H02M 1/44*** (2013.01); *F03D 9/003* (2013.01); *G05F 1/70* (2013.01); *H02M 2001/0003* (2013.01)

(58) **Field of Classification Search**
CPC H02M 1/32; H02M 1/44; H02M 1/00; H02M 2001/0003; G05F 1/70; F03D 9/003
USPC 363/40, 74; 323/207; 361/18; 327/141
See application file for complete search history.

(56) **References Cited**

U.S. PATENT DOCUMENTS

8,467,205 B2 *	6/2013	Petter	F03D 9/003	361/53
2011/0075456 A1 *	3/2011	Tan	H02M 7/48	363/74
2011/0130889 A1 *	6/2011	Khajehoddin	H02J 3/383	700/298
2011/0317460 A1 *	12/2011	Garces Rivera	H02M 7/48	363/127
2014/0240880 A1 *	8/2014	Chen	H02H 7/22	361/62
2014/0307494 A1 *	10/2014	Wu	H02M 7/48	363/97

* cited by examiner

Primary Examiner — Jessica Han
Assistant Examiner — Demetries A Gibson
(74) *Attorney, Agent, or Firm* — Muncy, Geissler, Olds & Lowe, P.C.

(57) **ABSTRACT**

A photovoltaic power generation system includes a photovoltaic power generation module, a capacitor, a DC/AC voltage converter, a filter, a relay, a PWM controller, a calculation module, a control module, and a grid. The control module traces the maximum power of the photovoltaic power generation module, and detects whether the grid is abnormal or not. Finally, the DC power outputted from the photovoltaic power generation module is transferred to the AC power and outputted to the grid via the DC/AC voltage converter by using the PWM controller.

10 Claims, 5 Drawing Sheets

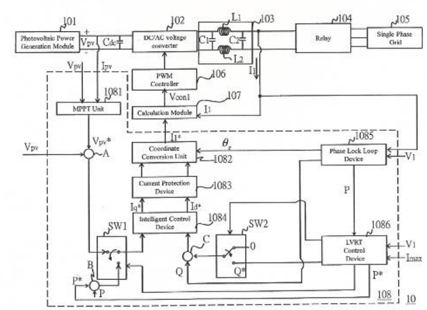

萌芽技術前瞻原創性說明

- **智財背景調查**

　　本計畫針對美國、台灣、大陸進行專利檢索，該些專利大多在探討低電壓穿越、暫態回復或最大功率追蹤，與本計畫智慧型太陽光能發電系統之系統配置及實施方式具有相當的差異。本計畫高效率智慧型太陽光能變頻器在單級轉換架構、最大功率追蹤、低電壓穿透及智慧型實虛功率控制等技術領先現有廠商，且具有技術前瞻性。

廠商國別	重要專利權人	專利數量	活動年期	平均專利年齡
美國	General Electric Company	7	5	3
大陸	天津電氣傳動設計研究所	4	2	2
大陸	中節能綠洲(北京)太陽能科技	3	2	2
台灣	台達電子工業股份有限公司（Delta）	2	2	2
德國	Sma Solar Technology Ag	1	1	3

註：活動年期：專利權人有專利產出之活動期數。平均專利年齡：將各專利之年齡總和，除以專利件數所得之值。

市場/技術競爭優勢說明

- 技術競爭優勢與效益
  - 現行太陽光能發電系統均無本計畫之領先技術。
  - 提高產生發電量、回復市電故障、提高市電併網效能、可做最大功率追蹤等功能，以及具備多功能、價格低廉、系統體積縮減、符合IEEE 1547a最新技術標準等優勢。
  - 生產成本與銷售價格相對低廉且具有較佳的運作效能。

比較項目	現行之太陽光能發電系統	本計畫之太陽光能發電系統	本計畫優勢分析
轉換架構	兩級	單級	轉換效率提升及降低成本
最大功率追蹤	擾動法	增量電導法	提升太陽光電之發電量
鎖相迴路	一般鎖相迴路	二階廣義積分器鎖相迴路	三相或單相故障時仍可與市電同步與併網
暫態控制	傳統比例積分控制器	模糊類神經網路	控制實/虛功率反應速度快
低電壓穿越	無	有	可防止發電系統因電壓驟降而導致發電系統崩潰

市場/技術競爭優勢說明

- 現有產品與本計畫「智慧型太陽光能變頻器」之成本評比

現有產品元件	本計畫元件	品項說明	預估成本	本計畫總成本（NT）
DC/AC功率級	DC/AC功率級	太陽能直流電轉換市電交流電	0.8萬	1.5萬
驅動級與電源	驅動級與電源	脈衝寬度調變驅動信號	0.1萬	
控制板與控制晶片	控制板與控制晶片	整體變頻器的控制功能核心	0.1萬	
散熱片與外殼	散熱片與外殼	組裝及測試	0.5萬	
DC/DC功率級		太陽能直流電升壓轉換	0.5萬	

- 本計畫之「智慧型太陽光能變頻器」與國內外廠商之競爭分析

廠商名稱	國家	型號	輸出功率（kW）	MPPT數	效率（%）	體積	售價
ABB	瑞士	Power-One	3～10	2+	90.6～97.2	大	€900～4600
SMA	德國	Sunny Boy	0.7~7	1～2	91.6～95.5	大	€150～3400
Kaco		Powador	3～8	1+	91.5～96.6	大	€770～6400
Xantrex	加拿大	GT	2.5～5	1	93.1～95.2	大	$200～1200
Fronius	奧地利	IG	1.3～40	1	91.4～98.8	大	$1000～4200
Mastervolt	美國	Mastervolt	0.5～60	1+	92.1～96.2	大	$180～4800
GE		GE	2～50	1+	90.5～97.2	大	£800～2500
台達電	台灣	PV、SI	1.8～5	0～1	91～96.5	大	約NT25000
飛瑞		PV	1.5～10	0～3	93～97	大	約NT25000
本計畫規格			**3～10**	**1**	**93～97**	**中**	**NT20000(3kW)**
本計畫優劣勢評比			**相當**	**相當**	**相當**	**優**	**優**

Contents

Three-Phase Grid-Connected PV System

- PV panel is emulated by Chroma 62100H- 600S (153 VDC, 1 kW); Utility grid is emulated by KIKUSUI PCR2000LE AC power (3×2kVA)
- Y-connected 100Ω/phase resistive load, 1 kVA three-phase inverter, 3 kVA Y-△ step-up transformer.
- 16-bit A/D converter (PCI-1716), 12-bit D/A converter (MRC-6810)

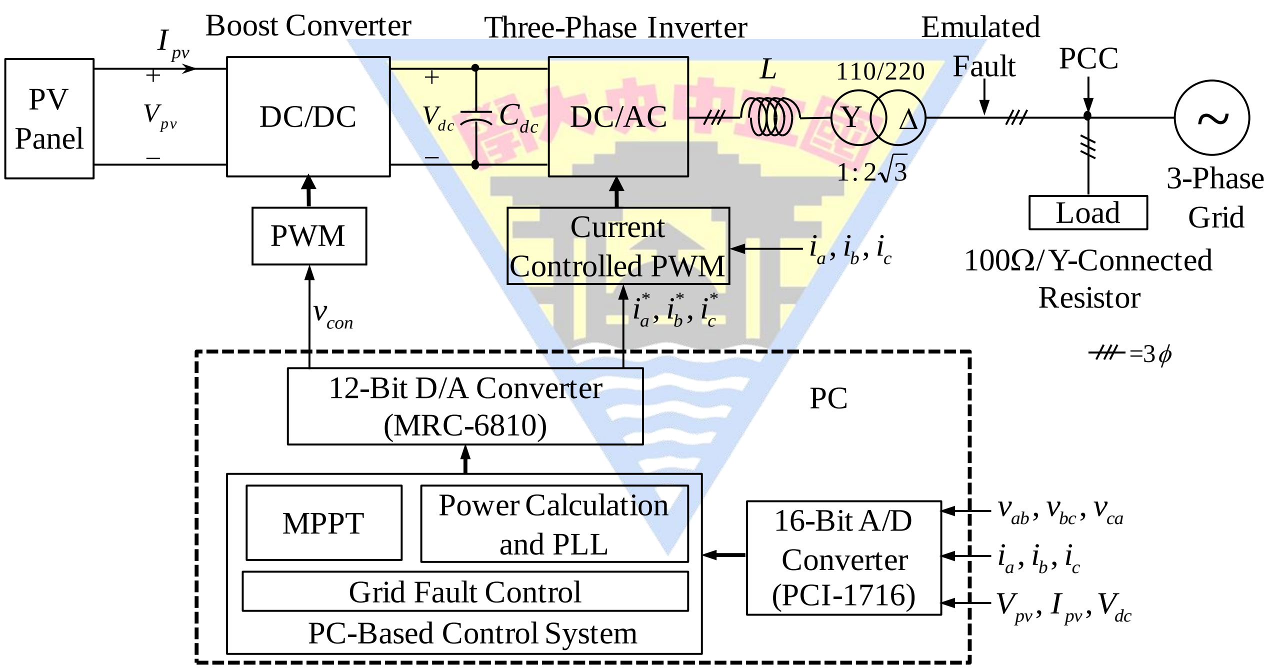

Fig. 2.1

Three-Phase Grid-Connected PV System

Table 2.1 Parameters of experimental setup.

dc-link voltage	V_{dc}	200 V
dc-link capacitor	C_{dc}	3360 μF
grid connection inductor	L	10 mH
inverter output voltage	v_{ab}, v_{bc}, v_{ca}	110 Vrms line-to-line, 60 Hz
inverter maximum current	$I_{\max}$	5 Arms (7.1 A peak current)
emulated PV panel		V_{oc}: 185.6 V, I_{sc}: 6.6 A, 1 kW
switching frequency	f_{sw_C}, f_{sw_I}	18 kHz, 10 kHz

Table 2.2 Specifications of KIKUSUI PCR2000LE.

input voltage /frequency (AC)	170~250 Vrms /47~63 Hz
output capacity	single-phase 2 kVA
voltage	output L range:1 to 150 Vrms output H range:2 to 300 Vrms
voltage resolution	0.1 Vrms
maximum output current	output L range (100 Vrms):20 A output H range (200 Vrms):10 A
maximum reverse current	30% of maximum current
frequency	1Hz~999Hz
frequency resolution	0.01Hz(1.00 Hz to 100.00 Hz) 0.1Hz(100.0 Hz to 999.9 Hz)

Three-Phase Grid-Connected PV System

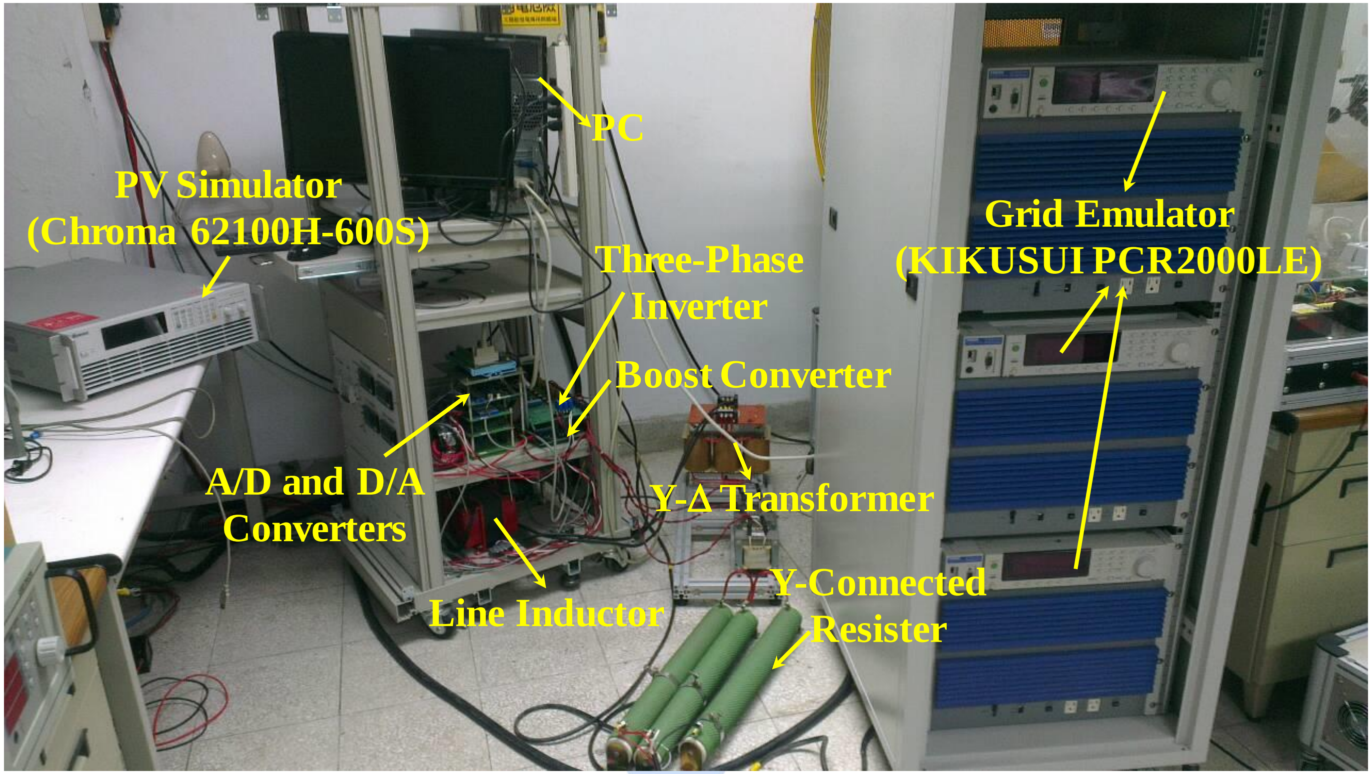

Fig. 2.5

PC-Based Control System

- MPPT control
  - voltage-based perturb-and-observe scheme (output: voltage command V_{pv}^{*}).
- Power calculation and phase-locked loop (PLL) block
  - SRF-PLL.
- Grid fault control
- Control outputs of the PC-based control system: the boost converter PWM control signal v_{con} and the three-phase inverter reference currents i_a^*, i_b^*, i_c^* .
- The SIMULINK control package is adopted for the implementation of the proposed algorithms.
- The proposed intelligent controllers are all realized using the “C” language.

Contents

Requirements of LVRT

- PV systems are largely and widely penetrated into the utility grid in recent year.
  - PV systems may stop the operation or be in unstable operation simultaneously due to transient disturbances.
  - These matters may seriously impact on the stability of the grid, such as power outage, voltage flicker.
- The next-generation PV systems have to provide a full range of services as what the traditional power plants do.
  - Low voltage ride through (LVRT) capability under grid faults.
  - Keeping connected during grid faults.
  - Support the grid by supplying reactive power during grid fault.
- E.ON requires the PV system to support voltage with additional reactive current during voltage sag.
  - The voltage control must take place within 20 ms (one cycle in Europe) after fault occurrence.
  - The amount of the additional reactive current is 2% of the rated current for each percent of the voltage sag.

Requirements of LVRT

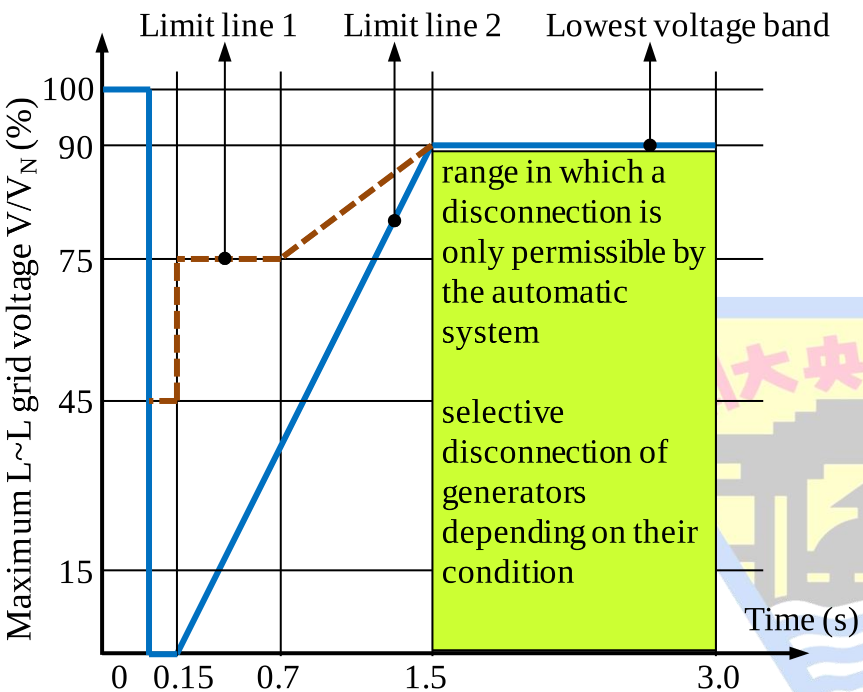

Fig. 2.6

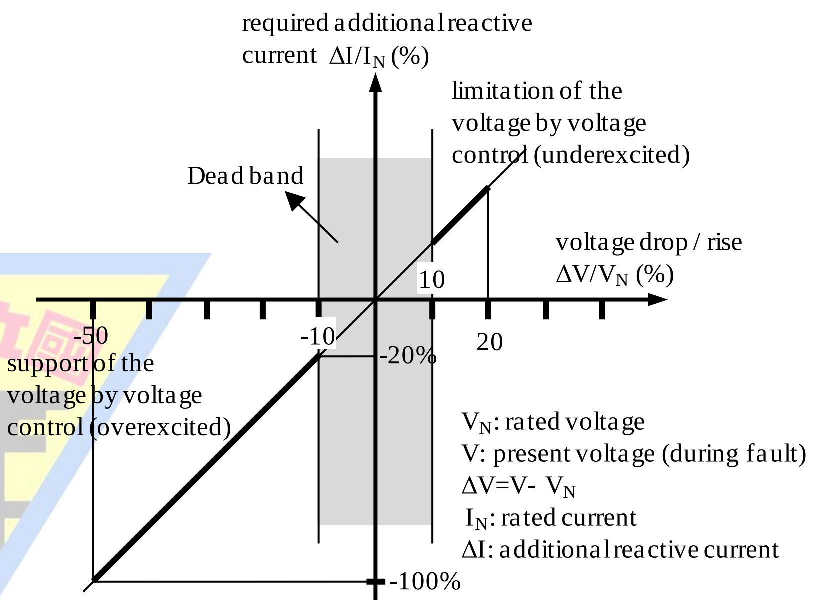

Fig. 2.7

Applications of Fuzzy Logic Systems

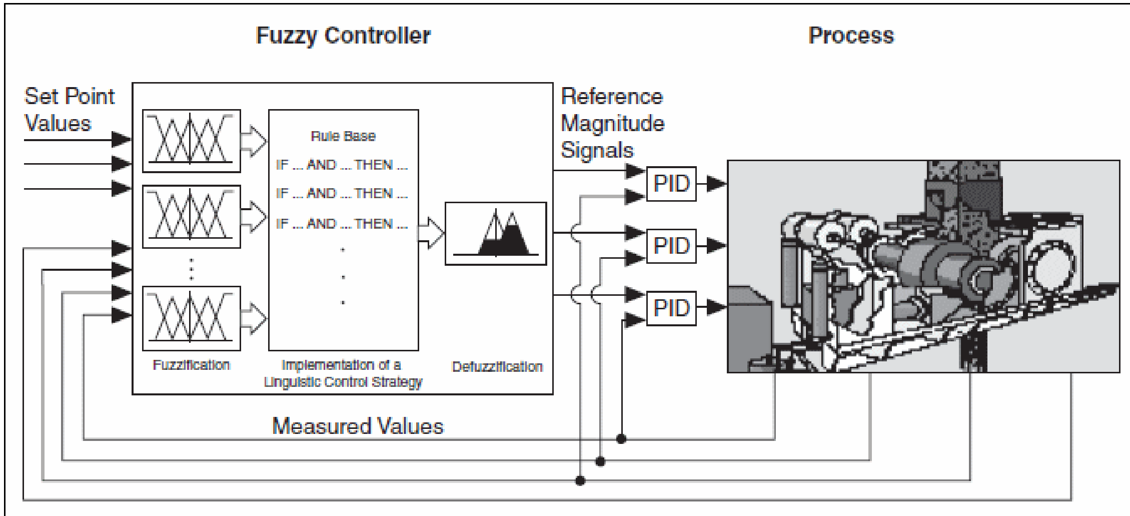

Fuzzy logic application

- household appliances
- animation systems
- industrial automation
- chemical industry
- aerospace
- robotics
- mining and metal processing
- transportation

Applications of Neural Network -- Alphago

New search algorithm that combines Monte-Carlo simulation with value and policy networks

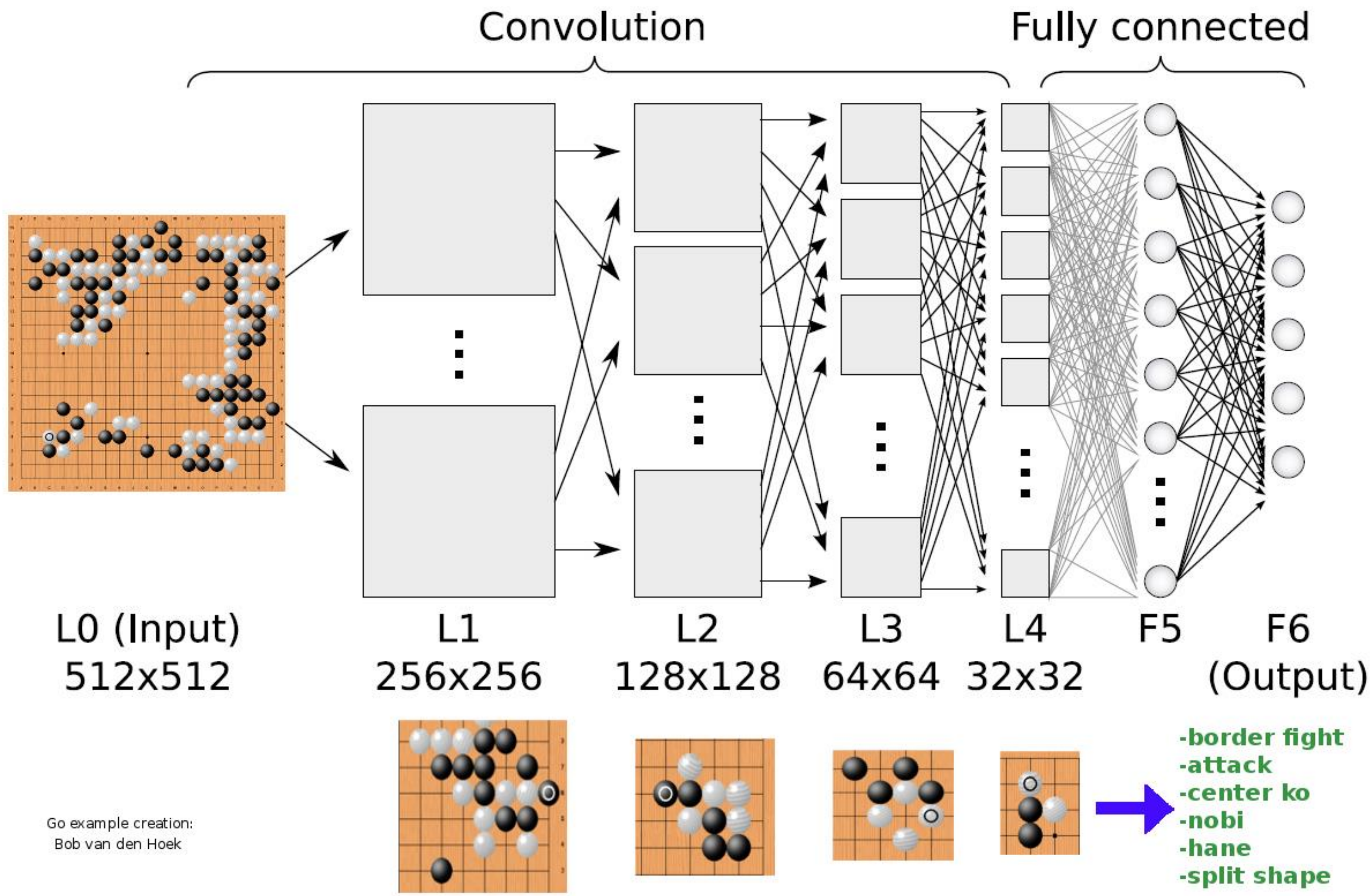

Fuzzy Logic System

Rule: 1	Rule: 1
IF x is A3	IF project_funding is adequate
OR y is B1	OR project_staffing is small
THEN z is C1	THEN risk is low
Rule: 2	Rule: 2
IF x is A2	IF project_funding is marginal
AND y is B2	AND project_staffing is large
THEN z is C2	THEN risk is normal
Rule: 3	Rule: 3
IF x is A1	IF project_funding is inadequate
THEN z is C3	THEN risk is high

Linguistic variables: x, y and z (project funding, project staffing and risk);
Membership functions: A1, A2 and A3 (inadequate, marginal and adequate); B1 and B2(small and large);
C1, C2 and C3 (low, normal and high)

Fuzzy Logic System

Fuzzification:

Rule evaluation:

Aggregation of rule consequents:

Defuzzification: Centre of gravity (COG)

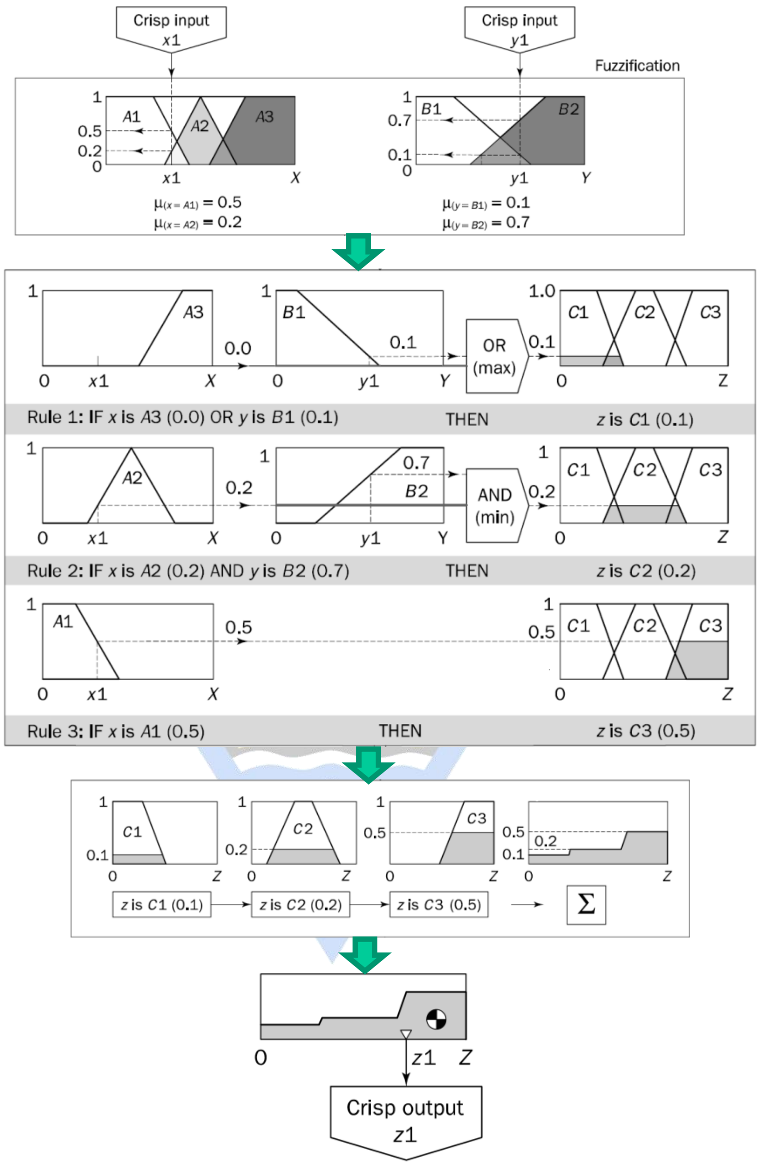

Fig. 1

Fuzzy Logic Control (模糊控制)

IF e is N AND △e is N, THEN z is C1,
IF e is Z AND △e is N, THEN z is C2,
IF e is P AND △e is N, THEN z is C3,
IF e is N AND △e is Z, THEN z is C4,
IF e is Z AND △e is Z, THEN z is C5,
IF e is P AND △e is Z, THEN z is C6,
IF e is N AND △e is P, THEN z is C7,
IF e is Z AND △e is P, THEN z is C8,
IF e is P AND △e is P, THEN z is C9.

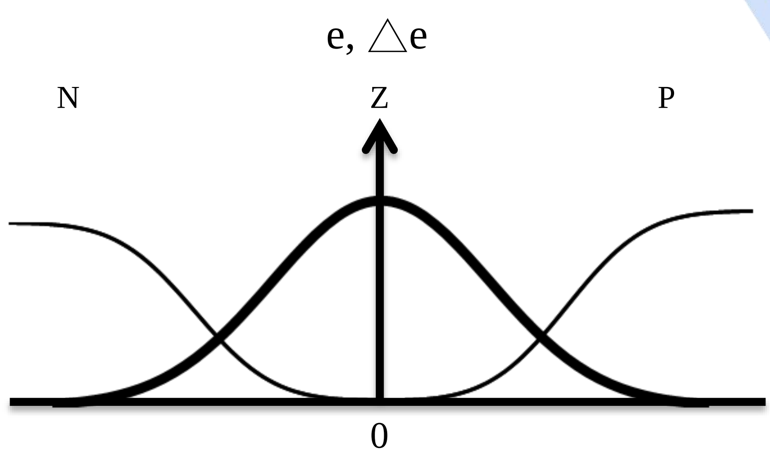

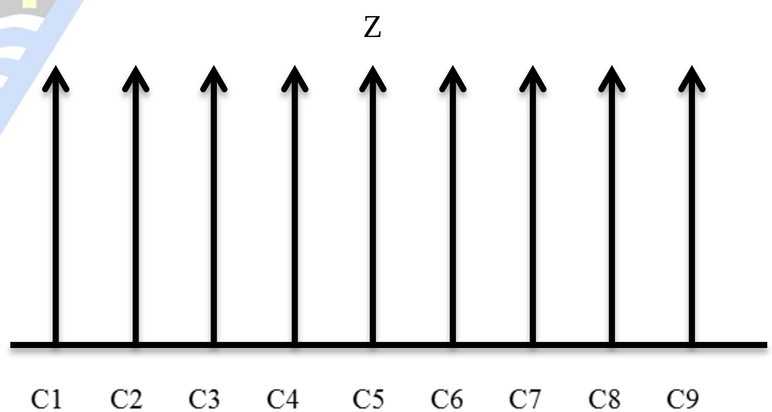

Fuzzy Neural Network (模糊類神經網路)

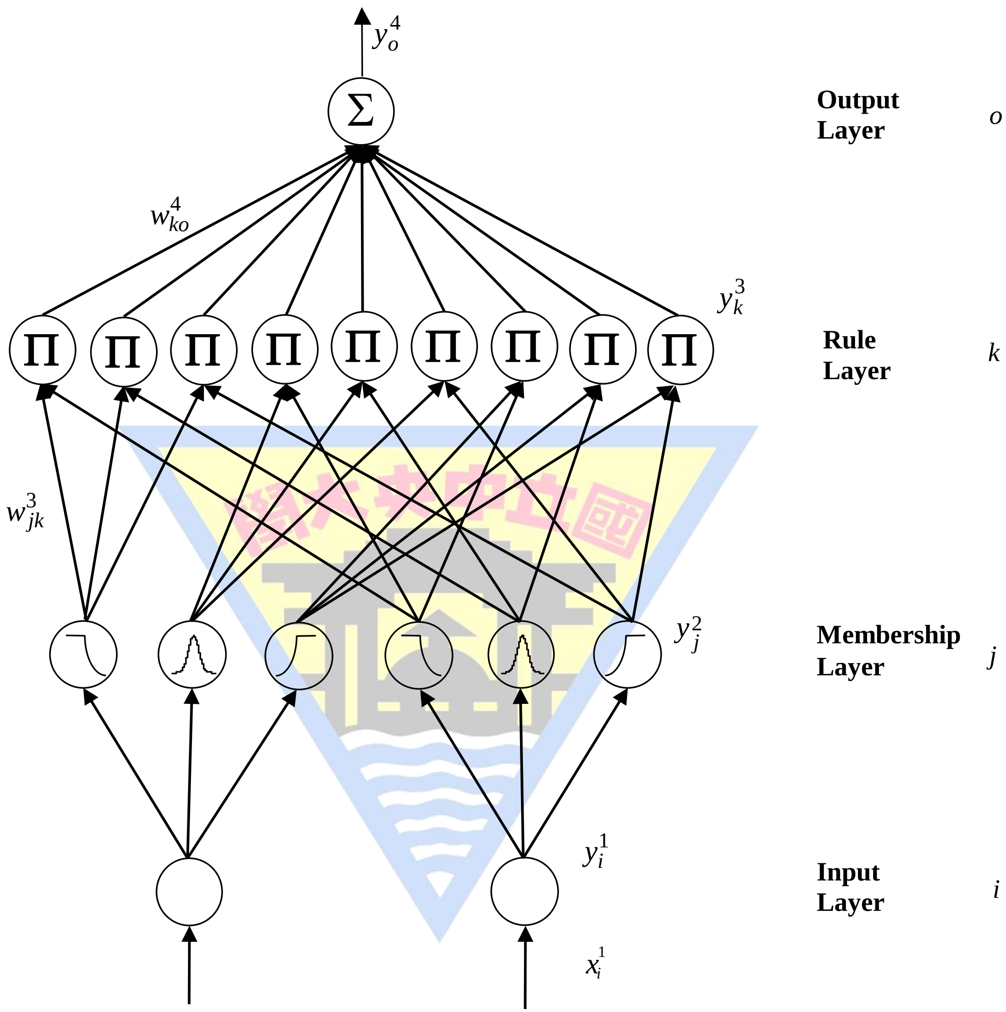

Fig. 5.1

Contents

Power Formulations

$$\begin{bmatrix} v_a \\ v_b \\ v_c \end{bmatrix} = \frac{1}{3}\begin{bmatrix} 1 & 0 & -1 \\ -1 & 1 & 0 \\ 0 & -1 & 1 \end{bmatrix}\begin{bmatrix} v_{ab} \\ v_{bc} \\ v_{ca} \end{bmatrix} \tag{3.1}$$

$$v_{\alpha\beta} = \begin{bmatrix} v_\alpha \\ v_\beta \end{bmatrix} = \frac{2}{3}\begin{bmatrix} 1 & -\frac{1}{2} & -\frac{1}{2} \\ 0 & \frac{\sqrt{3}}{2} & -\frac{\sqrt{3}}{2} \end{bmatrix}\begin{bmatrix} v_a \\ v_b \\ v_c \end{bmatrix} \tag{3.2}$$

$$\begin{bmatrix} v_d \\ v_q \end{bmatrix} = \begin{bmatrix} \cos(\theta_e) & \sin(\theta_e) \\ -\sin(\theta_e) & \cos(\theta_e) \end{bmatrix}\begin{bmatrix} v_\alpha \\ v_\beta \end{bmatrix} \tag{3.3}$$

$$\begin{bmatrix} i_d \\ i_q \end{bmatrix} = \frac{2}{3}\begin{bmatrix} \cos(\theta_e) & \cos(\theta_e - \frac{2}{3}\pi) & \cos(\theta_e + \frac{2}{3}\pi) \\ -\sin(\theta_e) & -\sin(\theta_e - \frac{2}{3}\pi) & -\sin(\theta_e + \frac{2}{3}\pi) \end{bmatrix}\begin{bmatrix} i_a \\ i_b \\ i_c \end{bmatrix} \tag{3.4}$$

$$P = \frac{3}{2}(v_d i_d + v_q i_q), \quad Q = \frac{3}{2}(v_q i_d - v_d i_q) \tag{3.5}$$

$$P = \frac{3}{2} v_q i_q \text{ and } Q = \frac{3}{2} v_q i_d \tag{3.6}$$

Accordingly, P and Q can be regulated by controlling i_q and i_d .

Reactive and Active Power Control

$$I_r^* = \begin{cases} 0\% & , V_{sag} \le 0.1 \\ 200V_{sag}\% , & 0.1 < V_{sag} \le 0.5 \\ 100\% & , V_{sag} > 0.5 \end{cases} \tag{3.7}$$

$$V_{sag} = \left(1 - \frac{\min\left(|v_a|_{rms}, |v_b|_{rms}, |v_c|_{rms} \right)}{V_{base}} \right) \text{ pu} \tag{3.8}$$

$$|S| = \left(|v_a|_{rms} + |v_b|_{rms} + |v_c|_{rms} \right) I_{\max} \tag{3.9}$$

$$Q^* = |S| I_r^* \quad \text{and} \quad P^* = |S| \sqrt{1 - I_r^{*2}} \tag{3.10}$$

v_d

Grid Synchronization

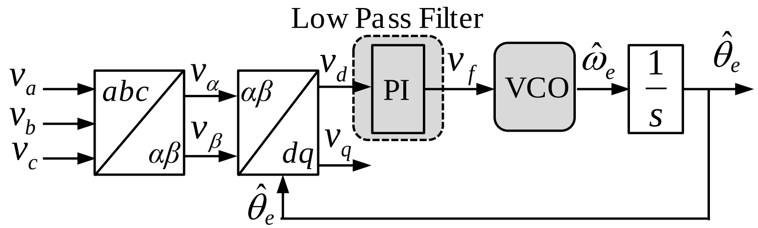

Fig. 3.1

$$\begin{bmatrix} v_a \\ v_b \\ v_c \end{bmatrix} = |V^+| \begin{bmatrix} \sin(\theta_e) \\ \sin\left(\theta_e - \frac{2}{3}\pi\right) \\ \sin\left(\theta_e + \frac{2}{3}\pi\right) \end{bmatrix} + |V^-| \begin{bmatrix} \sin(\theta_e) \\ \sin\left(\theta_e + \frac{2}{3}\pi\right) \\ \sin\left(\theta_e - \frac{2}{3}\pi\right) \end{bmatrix} \quad (3.11)$$

$$\begin{bmatrix} v_\alpha \\ v_\beta \end{bmatrix} = |V^+| \begin{bmatrix} \sin(\theta_e) \\ -\cos(\theta_e) \end{bmatrix} + |V^-| \begin{bmatrix} \sin(\theta_e) \\ \cos(\theta_e) \end{bmatrix} \quad (3.12)$$

$$\begin{bmatrix} v_d \\ v_q \end{bmatrix} = |V^+| \begin{bmatrix} \sin(\theta_e - \hat{\theta}_e) \\ -\cos(\theta_e - \hat{\theta}_e) \end{bmatrix} + |V^-| \begin{bmatrix} \sin(\theta_e + \hat{\theta}_e) \\ \cos(\theta_e + \hat{\theta}_e) \end{bmatrix} \quad (3.13)$$

The negative sequence component voltage of v_d can be filtered by using a properly designed PI low pass filter.

Dual Mode Control Strategy

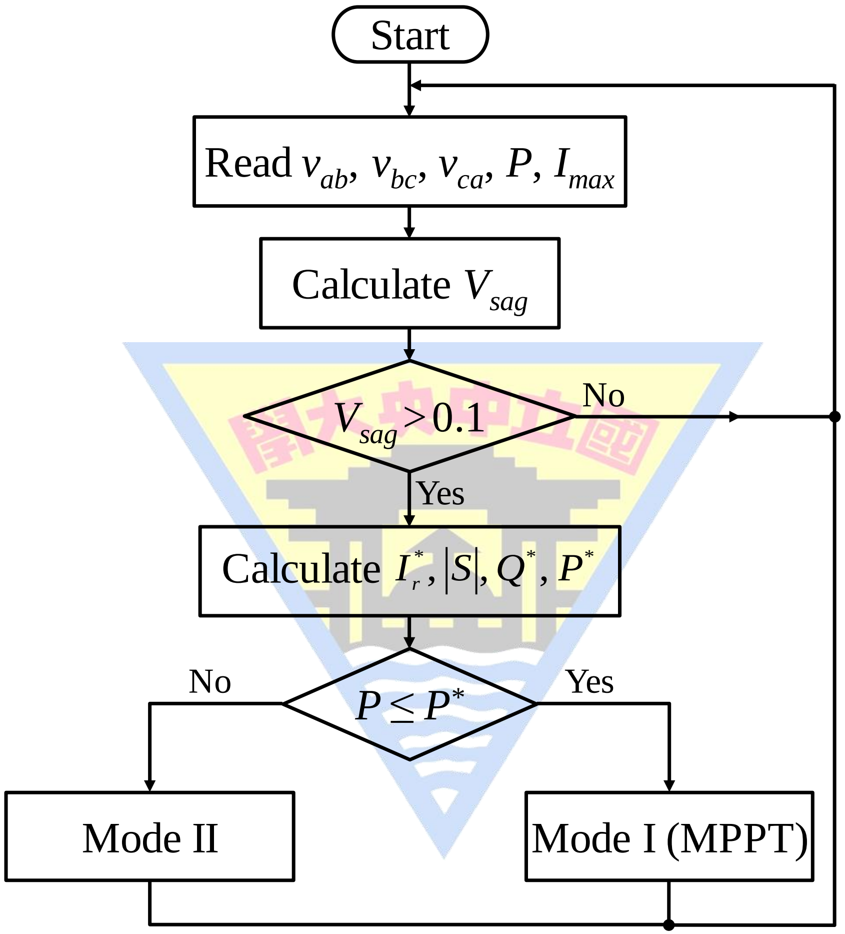

Fig. 3.2

Dual Mode Control Strategy

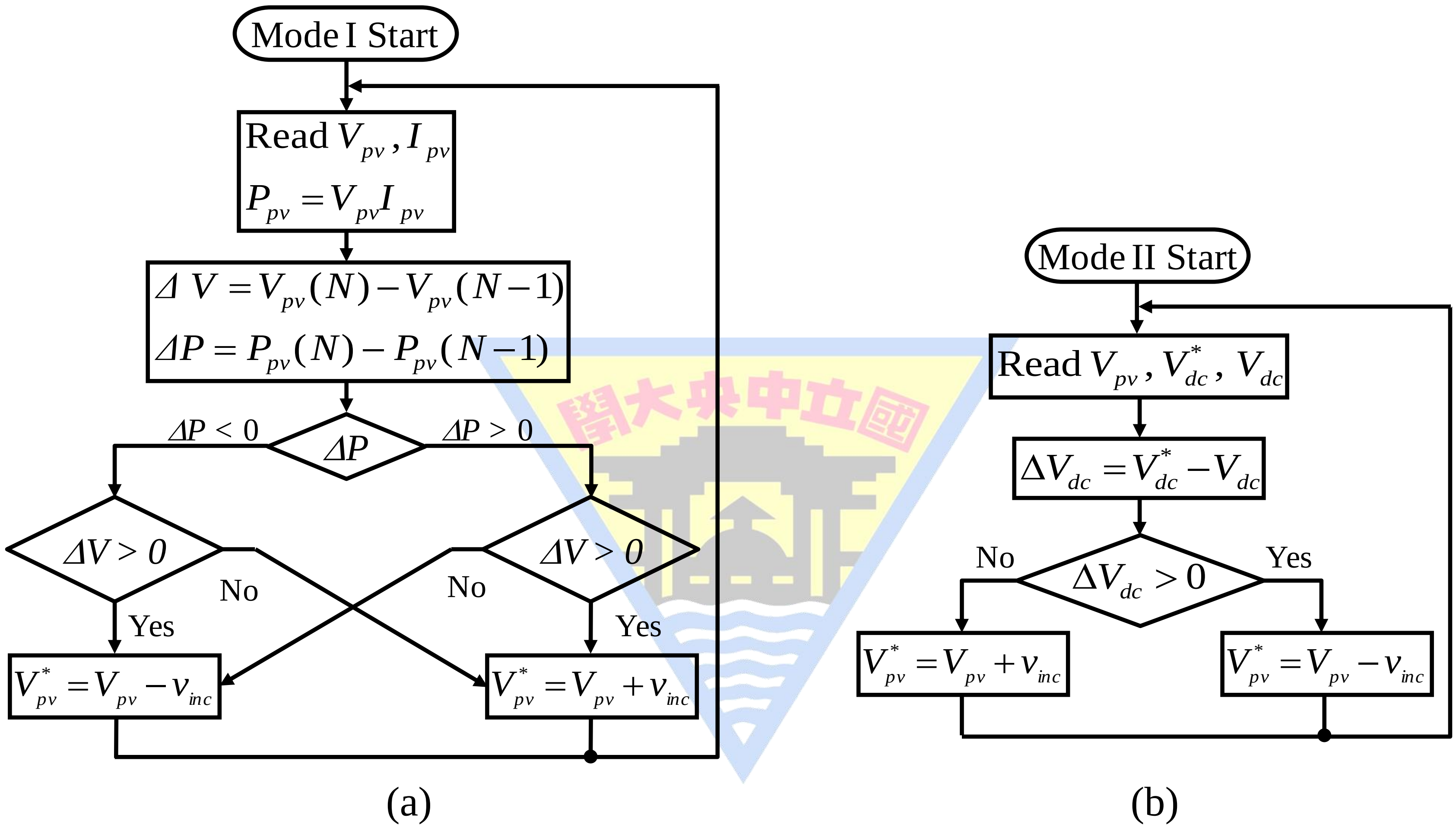

Fig. 3.3

Voltage Sags Classification

- The IEEE standard 1159-1995 has defined that voltage sag is a decrease in rms voltage down to 90% to 10% of nominal voltage for a time greater than 0.5 cycles of the power frequency but less than or equal to one minute.
- "voltage sag" (in U.S.A. English) and "voltage dip" (in U.K. English) differ in meaning.

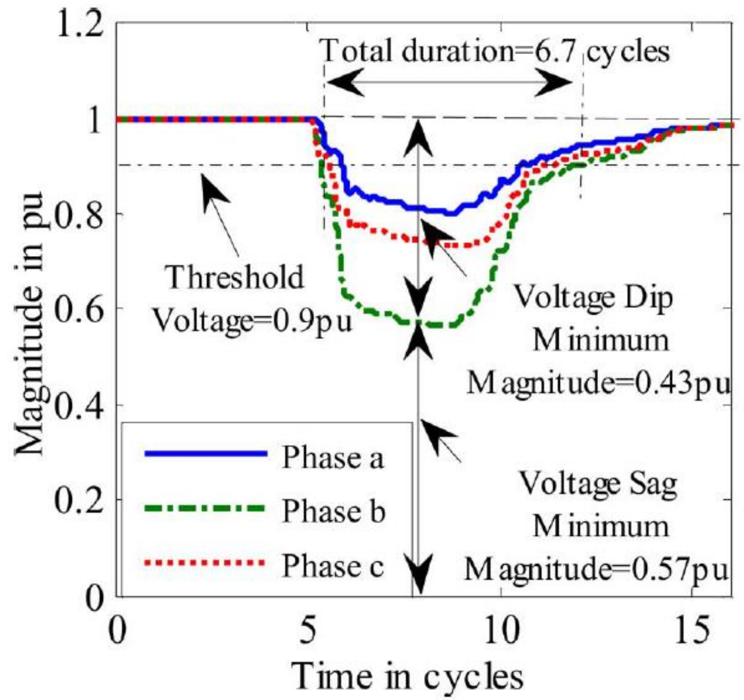

Fig. 3.4

Voltage Sags Classification

- Three-phase faults are symmetrical and called type A, which is not depicted in Fig. 3.5.
- Single phase-to-ground faults are the most common fault type.

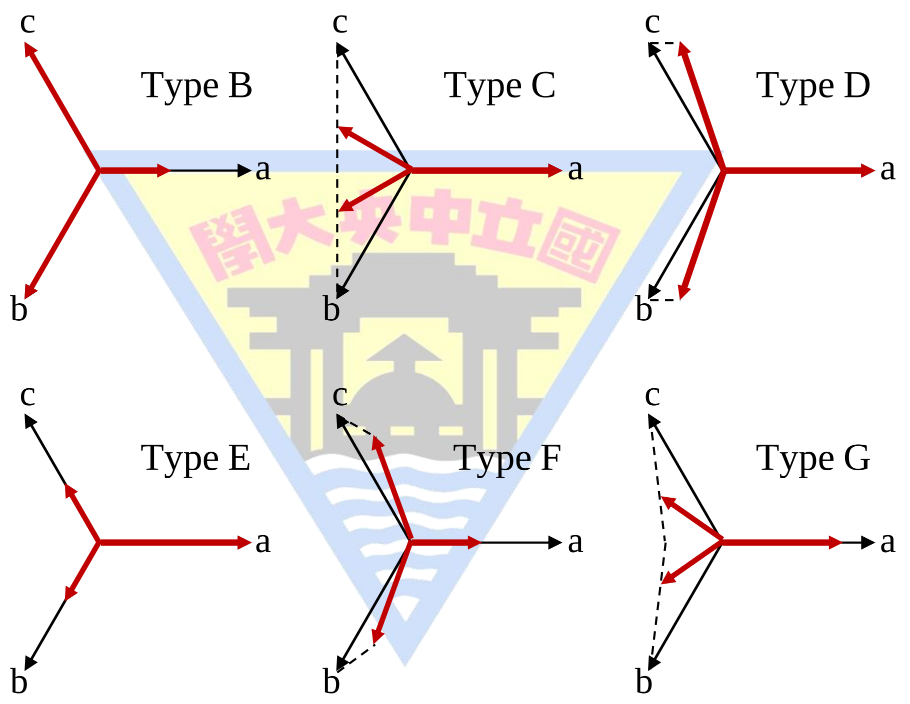

Fig. 3.5

Voltage Sags Classification

- When a fault occurs at bus 3 in Fig. 3.6, a voltage sag appears at bus 1 and propagates to bus 2 (which appears at the terminals of VSI) through the transformer (TR).
- Transformers always eliminate zero-sequence voltage and result in changing the type of voltage sag.
  - Type 1: does not change anything to voltage (e.g. Y grounded/Y grounded)
  - Type 2, which eliminates the zero-sequence voltage (e.g. Δ/Z)
  - Type 3, which swaps line and phase voltage (e.g. Δ/Y, Y/Δ, Y/Z)

Table 3.1 Transformation of voltage sags through TR

TR Type	Sag type at bus 1						
	A	B	C	D	E	F	G
	Sag type at bus 2						
Type 1	A	B	C	D	E	F	G
Type 2	A	D	C	D	G	F	G
Type 3	A	C	D	C	F	G	F

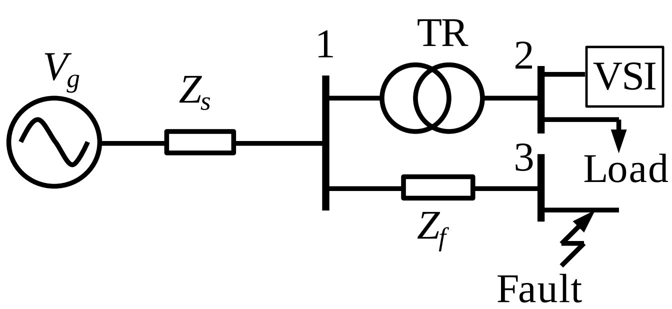

Fig. 3.6

Contents

Network Structure of PWFNN Controller

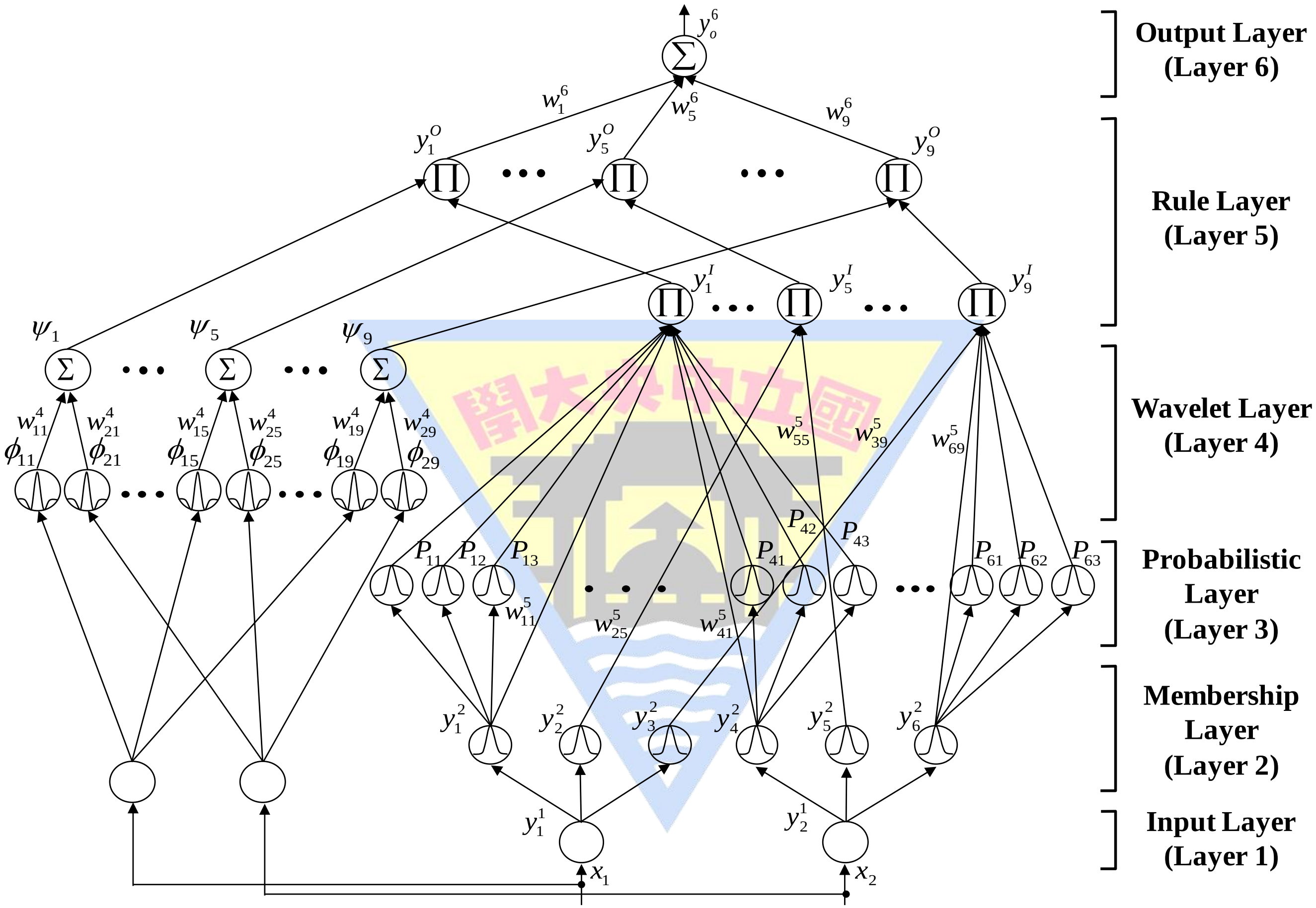

Fig. 4.1

Network Structure of PWFNN Controller

Input layer (Layer 1)

$$net_i^1(N)=x_i,\ y_i^1=f_i^1(net_i^1(N))=net_i^1(N), i=1,2 \quad (4.1)$$

$$x_1=e \qquad \dot{x}_1=\dot{e}=x_2 \qquad e=V_{dc}^*-V_{dc} \text{ or } Q^*-Q$$

Membership layer (Layer 2)

$$net_j^2(N)=-\frac{(y_i^1(N)-m_j^2(N))^2}{(\sigma_j^2(N))^2},$$

$$y_j^2(N)=f_j^2(net_j^2(N))=\exp\left(net_j^2(N)\right), i=1,\ j=1,2,3, \text{ and } i=2,\ j=4,5,6 \quad (4.2)$$

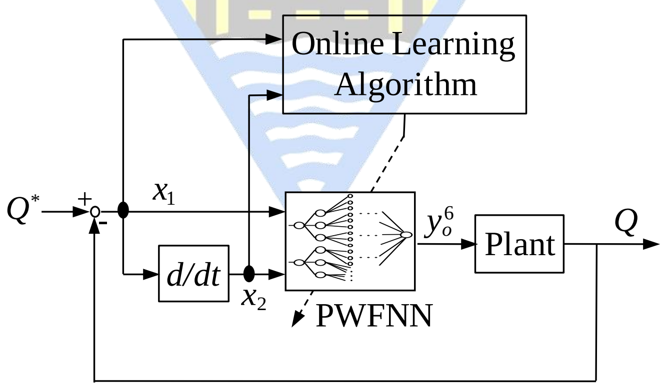

Fig. 4.2

Network Structure of PWFNN Controller

<u>*Probabilistic layer (Layer 3)*</u>

$$P_{jp}(N) = f_{jp}\left(y_j^2(N)\right) = \exp\left(-\frac{\left(y_j^2(N) - m_{jp}^3\right)^2}{\left(\sigma_{jp}^3\right)^2}\right),\ j = 1, 2, \ldots, 6,\ p = 1, 2, 3 \qquad (4.3)$$

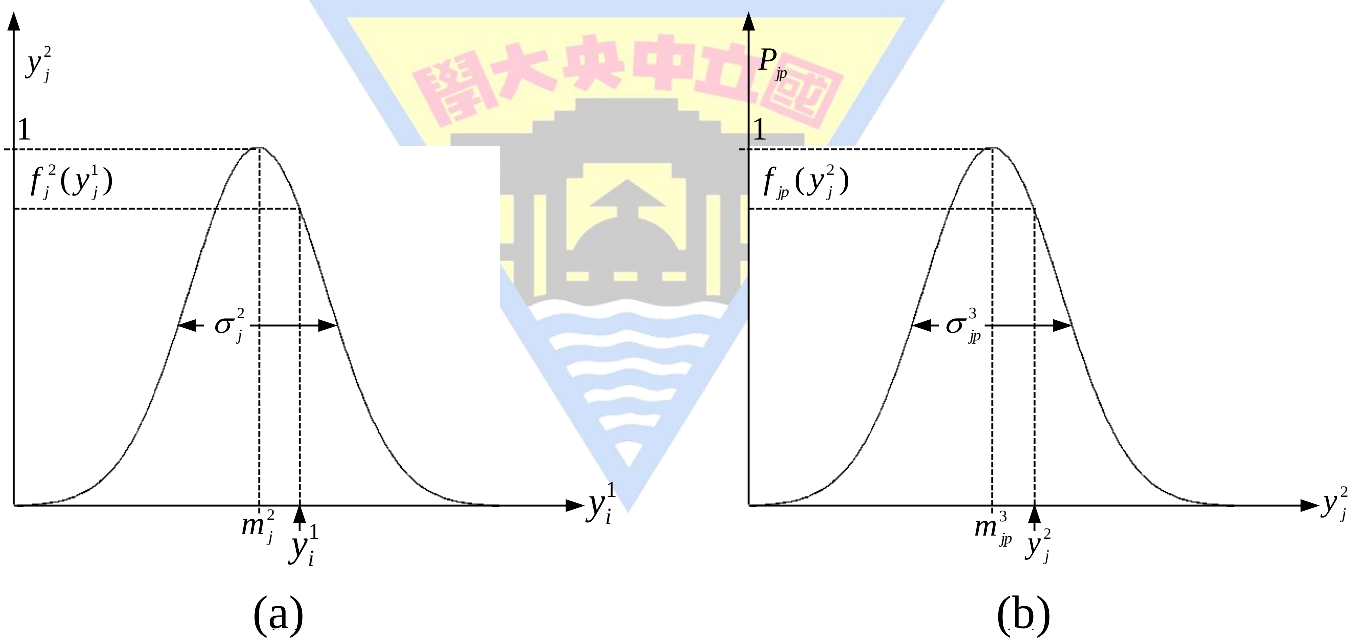

Fig. 4.3

Network Structure of PWFNN Controller

<u>*Wavelet layer (Layer 4)*</u>

$$g_{ik}(N) = \frac{\left(x_i(N) - m_{ik}^4\right)^2}{\left(\sigma_{ik}^4\right)^2},\ i = 1, 2,\ k = 1, 2, \ldots, 9$$

$$\phi_{ik}(N) = \frac{1}{\sqrt{\left|\sigma_{ik}^4\right|}}\left(1 - g_{ik}(N)\right)\exp\left(-\frac{g_{ik}(N)}{2}\right) \tag{4.4}$$

$$\psi_k(N) = \sum_i w_{ik}^4 \phi_{ik}(N),\ i = 1, 2,\ k = 1, 2, \cdots, 9 \tag{4.5}$$

<u>*Rule layer (Layer 5)*</u>

$$y_k^I(N) = \prod_{j,p} w_{jk}^5 y_j^2 P_{jp},\ k = 1, 2, \cdots, 9,\ p = 1, 2, 3 \tag{4.6}$$

$$y_k^O(N) = \psi_k(N) y_k^I(N),\ k = 1, 2, \cdots, 9 \tag{4.7}$$

<u>*Output layer (Layer 6)*</u>

$$y_o^6(N) = \sum_k w_k^6(N) y_k^O(N),\ o = 1;\ k = 1, 2, \cdots, 9 \tag{4.8}$$

Online Learning Algorithm of PWFNN Controller

- Four adjustable parameters $w_k^6,\ w_{ik}^4,\ m_j^2,\ \sigma_j^2$ need to be tuned.
- The purpose of the BP algorithm is to minimize the energy function E

$$E(N) = \frac{1}{2}(y^*(N) - y(N))^2 = \frac{1}{2}e^2(N) \tag{4.9}$$

The gradient error of E

$$\delta_o^6 = -\frac{\partial E}{\partial y_o^6(N)} = -\frac{\partial E}{\partial y}\frac{\partial y}{\partial y_o^6(N)} \tag{4.10}$$

$$\Delta w_k^6 = -\eta_1 \frac{\partial E}{\partial w_k^6(N)} = -\eta_1 \frac{\partial E}{\partial y_o^6(N)}\frac{\partial y_o^6(N)}{\partial w_k^6(N)} = \eta_1 \delta_o^6 y_k^O \tag{4.11}$$

$$w_k^6(N+1) = w_k^6(N) + \Delta w_k^6 \tag{4.12}$$

Online Learning Algorithm of PWFNN Controller

In layer 4

$$\delta_k^4 = -\frac{\partial E}{\partial \psi_k(N)} = -\frac{\partial E}{\partial y_o^6(N)} \frac{\partial y_o^6(N)}{\partial y_k^O(N)} \frac{\partial y_k^O(N)}{\partial \psi_k(N)} = \delta_k^O y_k^I \qquad (4.15)$$

$$\Delta w_{ik}^4 = -\eta_2 \frac{\partial E}{\partial w_{ik}^4(N)} = -\eta_2 \frac{\partial E}{\partial \psi_k(N)} \frac{\partial \psi_k(N)}{\partial w_{ik}^4(N)} = \eta_2 \delta_k^4 \phi_{ik} \qquad (4.16)$$

$$w_{ik}^4(N+1) = w_{ik}^4(N) + \Delta w_{ik}^4 \qquad (4.17)$$

In layer 2

$$\delta_j^2 = -\frac{\partial E}{\partial net_j^2(N)} = -\frac{\partial E}{\partial y_k^I(\mathrm{N})} \frac{\partial y_k^I(N)}{\partial y_j^2(N)} \frac{\partial y_j^2(N)}{\partial net_j^2(N)} = \sum_k w_{jk}^5 \delta_k^I y_k^I \qquad (4.18)$$

$$\Delta m_j^2 = -\eta_3 \frac{\partial E}{\partial m_j^2} = -\eta_3 \frac{\partial E}{\partial net_j^2(N)} \frac{\partial net_j^2(N)}{\partial m_j^2(N)} = \eta_3 \delta_j^2 \frac{2(y_i^1 - m_j^2)}{(\sigma_j^2)^2} \qquad (4.19)$$

$$\Delta \sigma_j^2 = -\eta_4 \frac{\partial E}{\partial \sigma_j^2} = -\eta_4 \frac{\partial E}{\partial net_j^2(N)} \frac{\partial net_j^2(N)}{\partial \sigma_j^2(N)} = \eta_4 \delta_j^2 \frac{2(y_i^1 - m_j^2)^2}{(\sigma_j^2)^2} \qquad (4.20)$$

Online Learning Algorithm of PWFNN Controller

$$m_j^2(N+1) = m_j^2(N) + \Delta m_j^2 \quad (4.21)$$

$$\sigma_j^2(N+1) = \sigma_j^2(N) + \Delta \sigma_j^2 \quad (4.22)$$

Owing to the uncertainties of the grid-connected three-phase PV system, the exact calculation of the sensitivity of the system $\partial y / \partial y_o^6(N)$ cannot be determined exactly.

$$\delta_o^6 \cong (y^* - y) + (\dot{y}^* - \dot{y}) = e + \dot{e} \quad (4.23)$$

Online Learning Algorithm of PWFNN Controller

Online learning algorithm of PWFNN control scheme

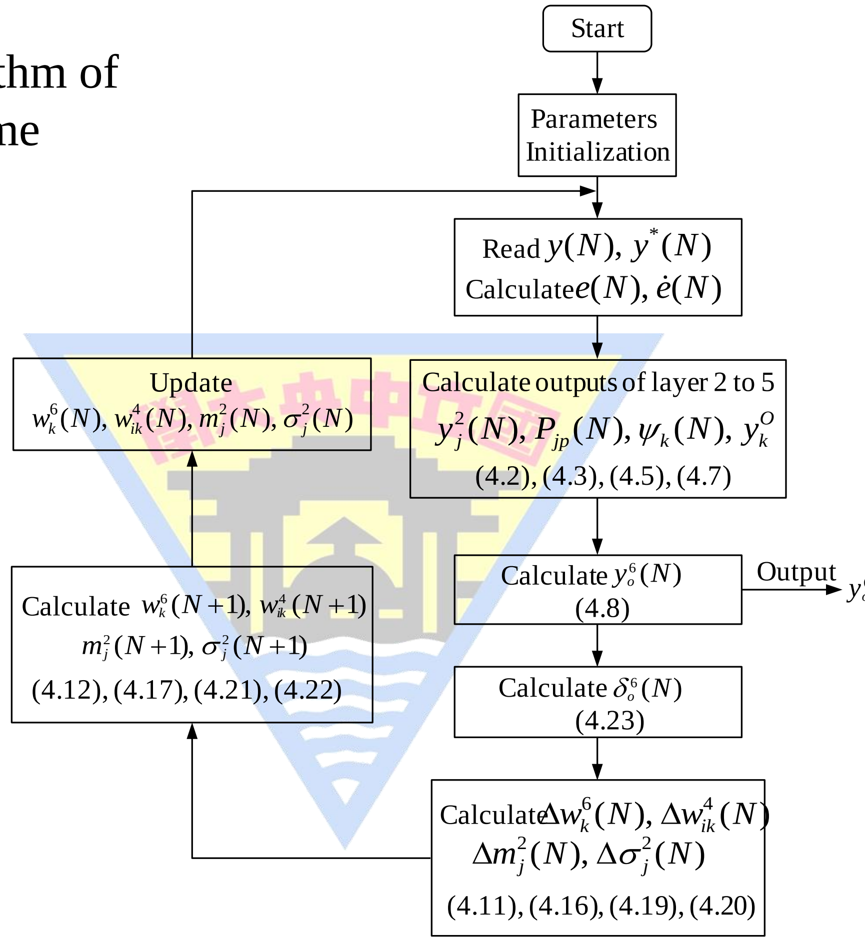

Fig. 4.4

Convergence of PWFNN controller

The resulted varied learning rates are shown in the following equations:

$$\eta_1 = \frac{E(N)/4}{R_1 + \varepsilon}, \text{ where } R_1 = \sum_{k-1}^{9}\left(\frac{\partial E}{\partial y_o^6(N)}\frac{\partial y_o^6(N)}{\partial w_k^6}\right)^2 \tag{4.24}$$

$$\eta_2 = \frac{E(N)/4}{R_2 + \varepsilon}, \text{ where } R_2 = \sum_{k=1}^{9}\sum_{i=1}^{2}\left[\frac{\partial E}{\partial y_o^6(N)}\frac{\partial y_o^6(N)}{\partial w_{ik}^4(N)}\right]^2 \tag{4.25}$$

$$\eta_3 = \frac{E(N)/4}{R_3 + \varepsilon}, \text{ where } R_3 = \sum_{j=1}^{6}\left[\frac{\partial E}{\partial y_o^6(N)}\frac{\partial y_o^6(N)}{\partial m_j^2(N)}\right]^2 \tag{4.26}$$

$$\eta_4 = \frac{E(N)/4}{R_4 + \varepsilon}, \text{ where } R_4 = \sum_{j=1}^{6}\left[\frac{\partial E}{\partial y_o^6(N)}\frac{\partial y_o^6(N)}{\partial \sigma_j^2(N)}\right]^2 \tag{4.27}$$

Convergence of PWFNN controller

$$\Delta E(N) = E(N+1) - E(N) \qquad (4.28)$$

$$\begin{aligned}
E(N+1) &= E(N) + \Delta E(N) \\
&\approx E(N) + \sum_{k=1}^{9}\left(\frac{\partial E(N)}{\partial w_k^6}\Delta w_k^6\right) \\
&\quad + \sum_{k=1}^{9}\sum_{i=1}^{2}\left(\frac{\partial E(N)}{\partial w_{ik}^4}\Delta w_{ik}^4\right) + \sum_{j=1}^{6}\left(\frac{\partial E(N)}{\partial m_j^2}\Delta m_j^2 + \frac{\partial E(N)}{\partial \sigma_j^2}\Delta \sigma_j^2\right) \qquad (4.29) \\
&= \frac{E(N)}{4} - \eta_1 \sum_{k=1}^{9}\left(\frac{\partial E}{\partial y_o^6(N)}\frac{\partial y_o^6(N)}{\partial w_k^6}\right)^2 + \frac{E(N)}{4} - \eta_2 \sum_{k=1}^{9}\sum_{i=1}^{2}\left(\frac{\partial E}{\partial y_o^6(N)}\frac{\partial y_o^6(N)}{\partial w_{ik}^4(N)}\right)^2 \\
&\quad + \frac{E(N)}{4} - \eta_3 \sum_{j=1}^{6}\left(\frac{\partial E}{\partial y_o^6(N)}\frac{\partial y_o^6(N)}{\partial m_j^2(N)}\right)^2 + \frac{E(N)}{4} - \eta_4 \sum_{j=1}^{6}\left(\frac{\partial E}{\partial y_o^6(N)}\frac{\partial y_o^6(N)}{\partial \sigma_j^2(N)}\right)^2
\end{aligned}$$

$$\begin{aligned}
E(N+1) &\approx \varepsilon\left(\sum_{m=1}^{4}\eta_m\right) = \frac{E(N)\varepsilon/4}{R_1+\varepsilon} + \frac{E(N)\varepsilon/4}{R_2+\varepsilon} \\
&\quad + \frac{E(N)\varepsilon/4}{R_3+\varepsilon} + \frac{E(N)\varepsilon/4}{R_4+\varepsilon} < E(N) \qquad (4.30)
\end{aligned}$$

Network Structure of TSKPFNN-AMF Controller

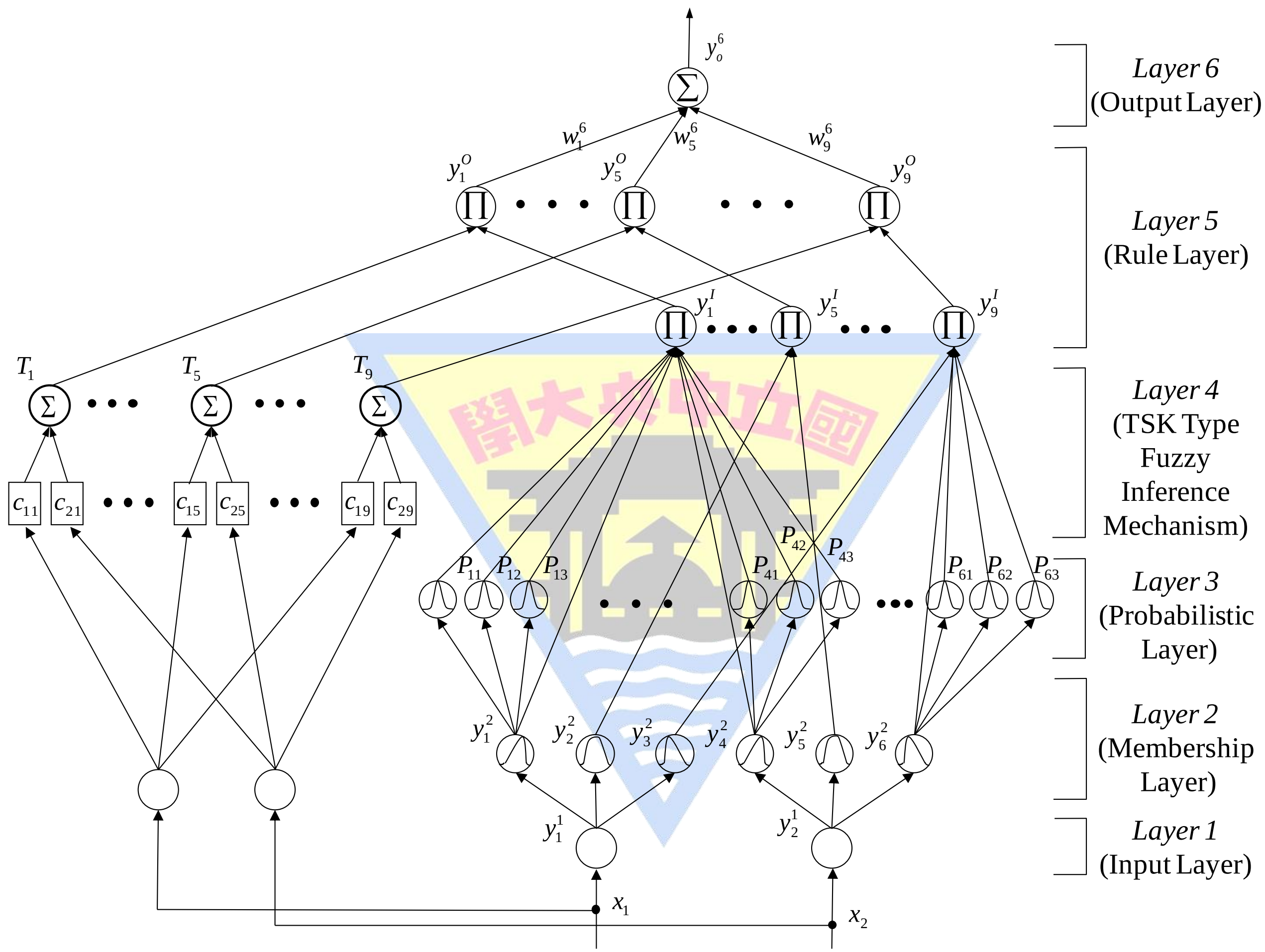

Fig. 4.5

Network Structure of TSKFNN-AMF Controller

Layer 1 (Input layer)

$$net_i^1(N) = x_i^1,\ y_i^1(N) = f_i^1(net_i^1(N)) = net_i^1(N),\ i = 1, 2 \tag{4.32}$$

$$e = V_{dc}^* - V_{dc} \text{ or } P^*\text{-}P \text{ or } Q^* - Q$$

Layer 2 (Membership layer)

$$net_j^2(N) = \begin{cases} -\dfrac{(y_i^1(N) - m_j^2(N))^2}{(\sigma_{L\_j}^2(N))^2}, & -\infty < y_i^1(N) \le m_j^2 \\ -\dfrac{(y_i^1(N) - m_j^2(N))^2}{(\sigma_{R\_j}^2(N))^2}, & m_j^2 < y_i^1(N) < \infty \end{cases} \tag{4.33}$$

$$y_j^2(N) = f_j^2(net_j^2(N)) = \exp\left(net_j^2(N)\right) \tag{4.34}$$

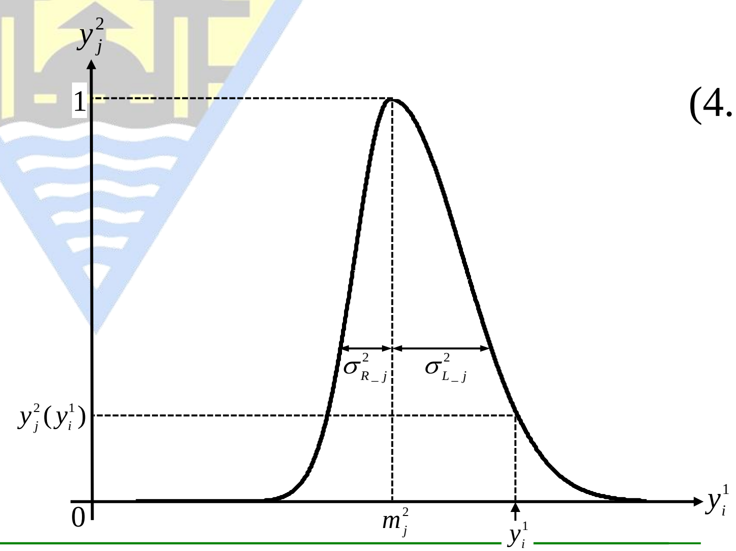

Fig. 4.6

Network Structure of TSKFNN-AMF Controller

Layer 3 (Probability layer)

$$P_{jp}(N) = f_{jp}(y_j^2(N)) = \exp\left[-\frac{(y_j^2(N)-m_{jp}^3)^2}{(\sigma_{jp}^3)^2}\right] \quad (4.35)$$

$$, j = 1, 2, \cdots, 6;\ p = 1, 2, 3$$

Layer 4 (TSK type fuzzy inference mechanism layer)

$$T_k(N) = \sum_i c_{ik}(N)x_i(N), i = 1,2; k = 1, 2, \cdots, 9 \quad (4.36)$$

Layer 5 (Rule layer)

$$y_k^I(N) = y_r^2(N)y_l^2(N)S_r(N)S_l(N), r = 1, 2, 3$$
$$; l = 4, 5, 6; k = 3(r-1)+(l-3) \quad (4.37)$$

$$S_j(N) = \prod_p P_{jp}(N),\ j = 1, 2, \cdots, 6;\ p = 1, 2, 3 \quad (4.38)$$

$$y_k^O(N) = T_k(N)y_k^I(N), k = 1, 2, \cdots, 9 \quad (4.39)$$

Layer 6 (Output layer)

$$y_o^6(N) = \sum_k w_k^6(N)y_k^O(N), o = 1; k = 1, 2, \cdots, 9 \quad (4.40)$$

Online Learning Algorithm of TSKPFNN-AMF Controller

- The purpose of the BP algorithm is to minimize the energy function E

$$E(N)=\frac{1}{2}(y^{*}(N)-y(N))^{2}=\frac{1}{2}e^{2}(N) \tag{4.41}$$

<u>*Layer 6*</u>

$$\delta_{o}^{6}=-\frac{\partial E}{\partial y_{o}^{6}(N)}=-\frac{\partial E}{\partial y}\frac{\partial y}{\partial y_{o}^{6}(N)} \tag{4.42}$$

$$\Delta w_{k}^{6}=-\eta_{1}\frac{\partial E}{\partial w_{k}^{6}(N)}=-\eta_{1}\frac{\partial E}{\partial y_{o}^{6}(N)}\frac{\partial y_{o}^{6}(N)}{\partial w_{k}^{6}(N)}=\eta_{1}\delta_{o}^{6}y_{k}^{O} \tag{4.43}$$

$$w_{k}^{6}(N+1)=w_{k}^{6}(N)+\Delta w_{k}^{6} \tag{4.44}$$

<u>*Layer 5*</u>

$$\delta_{k}^{O}=-\frac{\partial E}{\partial y_{k}^{O}(N)}=-\frac{\partial E}{\partial y_{o}^{6}(N)}\frac{\partial y_{o}^{6}(N)}{\partial y_{k}^{O}(N)}=\delta_{o}^{6}w_{k}^{6} \tag{4.45}$$

$$\delta_{k}^{I}=-\frac{\partial E}{\partial y_{k}^{I}(N)}=-\frac{\partial E}{\partial y_{k}^{O}(N)}\frac{\partial y_{k}^{O}(N)}{\partial y_{k}^{I}(N)}=\delta_{k}^{O}T_{k} \tag{4.46}$$

Online Learning Algorithm of TSKPFNN-AMF Controller

Layer 4

$$\delta_k^4 = -\frac{\partial E}{\partial T_k(N)} = -\frac{\partial E}{\partial y_k^O(N)}\frac{\partial y_k^O(N)}{\partial T_k(N)} = \delta_k^O y_k^I \quad (4.47)$$

$$\Delta c_{ik} = -\eta_2 \frac{\partial E}{\partial c_{ik}(N)} = -\eta_2 \frac{\partial E}{\partial T_k(N)}\frac{\partial T_k(N)}{\partial c_{ik}(N)} = \eta_2 \delta_k^4 x_i \quad (4.48)$$

$$c_{ik}(N+1) = c_{ik}(N) + \Delta c_{ik} \quad (4.49)$$

Layer 2

$$\delta_j^2 = -\frac{\partial E}{\partial net_j^2(N)} = -\frac{\partial E}{\partial y_k^I(N)}\frac{\partial y_k^I(N)}{\partial y_j^2(N)}\frac{\partial y_j^2(N)}{\partial net_j^2(N)}$$
$$= \begin{cases} h_j \sum_r \delta_k^I y_k^I, \; j = 1, 2, 3; \; r = 1, 2, 3; \; k = 3(j-1) + r \\ h_j \sum_r \delta_k^I y_k^I, \; j = 4, 5, 6; \; r = 1, 2, 3; \; k = j + 3(r-2) \end{cases} \quad (4.50)$$

$$h_j = 1 - y_j^2 \sum_p \frac{y_j^2 - m_{jp}^3}{(\sigma_{jp}^3)^2}, \; p = 1, 2, 3 \quad (4.51)$$

Online Learning Algorithm of TSKPFNN-AMF Controller

$$\Delta m_j^2 = -\eta_3 \frac{\partial E}{\partial m_j^2} = -\eta_3 \frac{\partial E}{\partial net_j^2(N)} \frac{\partial net_j^2(N)}{\partial m_j^2(N)}$$

$$= \begin{cases} \eta_3 \delta_j^2 \dfrac{2(y_i^1 - m_j^2)}{(\sigma_{L\_j}^2)^2}, & -\infty < y_i^1 \le m_j^2,\ j = 1, 2, \cdots, 6 \\ \eta_3 \delta_j^2 \dfrac{2(y_i^1 - m_j^2)}{(\sigma_{R\_j}^2)^2}, & m_j^2 < y_i^1 < \infty,\ j = 1, 2, \cdots, 6 \end{cases} \quad (4.52)$$

$$\Delta \sigma_{L\_j}^2 = -\eta_4 \frac{\partial E}{\partial \sigma_{L\_j}^2} = -\eta_4 \frac{\partial E}{\partial net_j^2(N)} \frac{\partial net_j^2(N)}{\partial \sigma_{L\_j}^2(N)}$$

$$= \eta_4 \delta_j^2 \frac{2(y_i^1 - m_j^2)^2}{(\sigma_{L\_j}^2)^3},\ j = 1, 2, \cdots, 6 \quad (4.53)$$

$$\Delta \sigma_{R\_j}^2 = -\eta_5 \frac{\partial E}{\partial \sigma_{R\_j}^2} = -\eta_5 \frac{\partial E}{\partial net_j^2(N)} \frac{\partial net_j^2(N)}{\partial \sigma_{R\_j}^2(N)}$$

$$= \eta_5 \delta_j^2 \frac{2(y_i^1 - m_j^2)^2}{(\sigma_{R\_j}^2)^3},\ j = 1, 2, \cdots, 6 \quad (4.54)$$

Online Learning Algorithm of TSKPFNN-AMF Controller

$$m_j^2(N+1) = m_j^2(N) + \Delta m_j^2 \qquad (4.55)$$

$$\sigma_{L\_j}^2(N+1) = \sigma_{L\_j}^2(N) + \Delta\sigma_{L\_j}^2 \qquad (4.56)$$

$$\sigma_{R\_j}^2(N+1) = \sigma_{R\_j}^2(N) + \Delta\sigma_{R\_j}^2 \qquad (4.57)$$

$$\delta_o^6 \cong (y^* - y) + (\dot{y}^* - \dot{y}) = e + \dot{e} \qquad (4.58)$$

Convergence Analyses of the TSKPFNN-AMF Controller

The varied learning rates based on the analysis of a discrete-type Lyapunov function have been derived as follows:

$$\eta_1 = \frac{E(N)/5}{R_1+\varepsilon}, \text{ where } R_1 = \sum_{k=1}^{9}\left(\frac{\partial E}{\partial y_o^6(N)}\frac{\partial y_o^6(N)}{\partial w_k^6}\right)^2 \tag{4.59}$$

$$\eta_2 = \frac{E(N)/5}{R_2+\varepsilon}, \text{ where } R_2 = \sum_{k=1}^{9}\sum_{i=1}^{2}\left(\frac{\partial E}{\partial T_k(N)}\frac{\partial T_k(N)}{\partial c_{ik}}\right)^2 \tag{4.60}$$

$$\eta_3 = \frac{E(N)/5}{R_3+\varepsilon}, \text{ where } R_3 = \sum_{j=1}^{6}\left(\frac{\partial E}{\partial net_j^2(N)}\frac{\partial net_j^2(N)}{\partial m_j^2(N)}\right)^2 \tag{4.61}$$

$$\eta_4 = \frac{E(N)/5}{R_4+\varepsilon}, \text{ where } R_4 = \sum_{j=1}^{6}\left(\frac{\partial E}{\partial net_j^2(N)}\frac{\partial net_j^2(N)}{\partial \sigma_{L\_j}^2(N)}\right)^2 \tag{4.62}$$

$$\eta_5 = \frac{E(N)/5}{R_5+\varepsilon}, \text{ where } R_5 = \sum_{j=1}^{6}\left(\frac{\partial E}{\partial net_j^2(N)}\frac{\partial net_j^2(N)}{\partial \sigma_{R\_j}^2(N)}\right)^2 \tag{4.63}$$

Convergence Analyses of the TSKPFNN-AMF Controller

The change in the Lyapunov function can be written as

$$\Delta E(N) = E(N+1) - E(N) \tag{4.64}$$

$$\begin{aligned}
E(N+1) &= E(N) + \Delta E(N) \\
&\approx E(N) + \sum_{k=1}^{9}\left(\frac{\partial E(N)}{\partial w_k^6}\Delta w_k^6\right) + \sum_{k=1}^{9}\sum_{i=1}^{2}\left(\frac{\partial E(N)}{\partial c_{ik}}\Delta c_{ik}\right) \\
&\quad + \sum_{j=1}^{6}\left(\frac{\partial E(N)}{\partial m_j^2}\Delta m_j^2\right) + \sum_{j=1}^{6}\left(\frac{\partial E(N)}{\partial \sigma_{L_j}^2}\Delta\sigma_{L_j}^2 + \frac{\partial E(N)}{\partial \sigma_{R_j}^2}\Delta\sigma_{R_j}^2\right) \\
&= \frac{E(N)}{5} - \eta_1\sum_{k=1}^{9}\left(\frac{\partial E}{\partial y_o^6(N)}\frac{\partial y_o^6(N)}{\partial w_k^6}\right)^2 + \frac{E(N)}{5} - \eta_2\sum_{k=1}^{9}\sum_{i=1}^{2}\left(\frac{\partial E}{\partial T_k(N)}\frac{\partial T_k(N)}{\partial c_{ik}(N)}\right)^2 \\
&\quad + \frac{E(N)}{5} - \eta_3\sum_{j=1}^{6}\left(\frac{\partial E}{\partial net_j^2(N)}\frac{\partial net_j^2(N)}{\partial m_j^2(N)}\right)^2 + \frac{E(N)}{5} - \eta_4\sum_{j=1}^{6}\left(\frac{\partial E}{\partial net_j^2(N)}\frac{\partial net_j^2(N)}{\partial \sigma_{L_j}^2(N)}\right)^2 \\
&\quad + \frac{E(N)}{5} - \eta_5\sum_{j=1}^{6}\left(\frac{\partial E}{\partial net_j^2(N)}\frac{\partial net_j^2(N)}{\partial \sigma_{R_j}^2(N)}\right)
\end{aligned} \tag{4.65}$$

Convergence Analyses of the TSKPFNN-AMF Controller

If the learning rates of the TSKPFNN-AMF controller are designed as (4.59) to (4.63), then (4.65) can be rewritten as

$$E(N+1) \approx \varepsilon\left(\sum_{m=1}^{5}\eta_m\right) = \frac{E(N)\varepsilon/5}{R_1+\varepsilon} + \frac{E(N)\varepsilon/5}{R_2+\varepsilon} + \frac{E(N)\varepsilon/5}{R_3+\varepsilon} + \frac{E(N)\varepsilon/5}{R_4+\varepsilon} + \frac{E(N)\varepsilon/5}{R_5+\varepsilon} < E(N) \tag{4.66}$$

$$\Delta E(N) \approx \varepsilon\left(\sum_{m=1}^{5}\eta_m\right) - E(N) = \frac{E(N)}{5}\left[\sum_{m=1}^{5}\left(\frac{\varepsilon}{R_m+\varepsilon}-1\right)\right] = -\frac{E(N)}{5}\left[\sum_{m=1}^{5}\left(\frac{R_m}{R_m+\varepsilon}\right)\right] < 0 \tag{4.67}$$

Therefore, the proof of the convergence of TSKPFNN-AMF controller is completed.

Contents

Power Control Using PWFNN Controllers

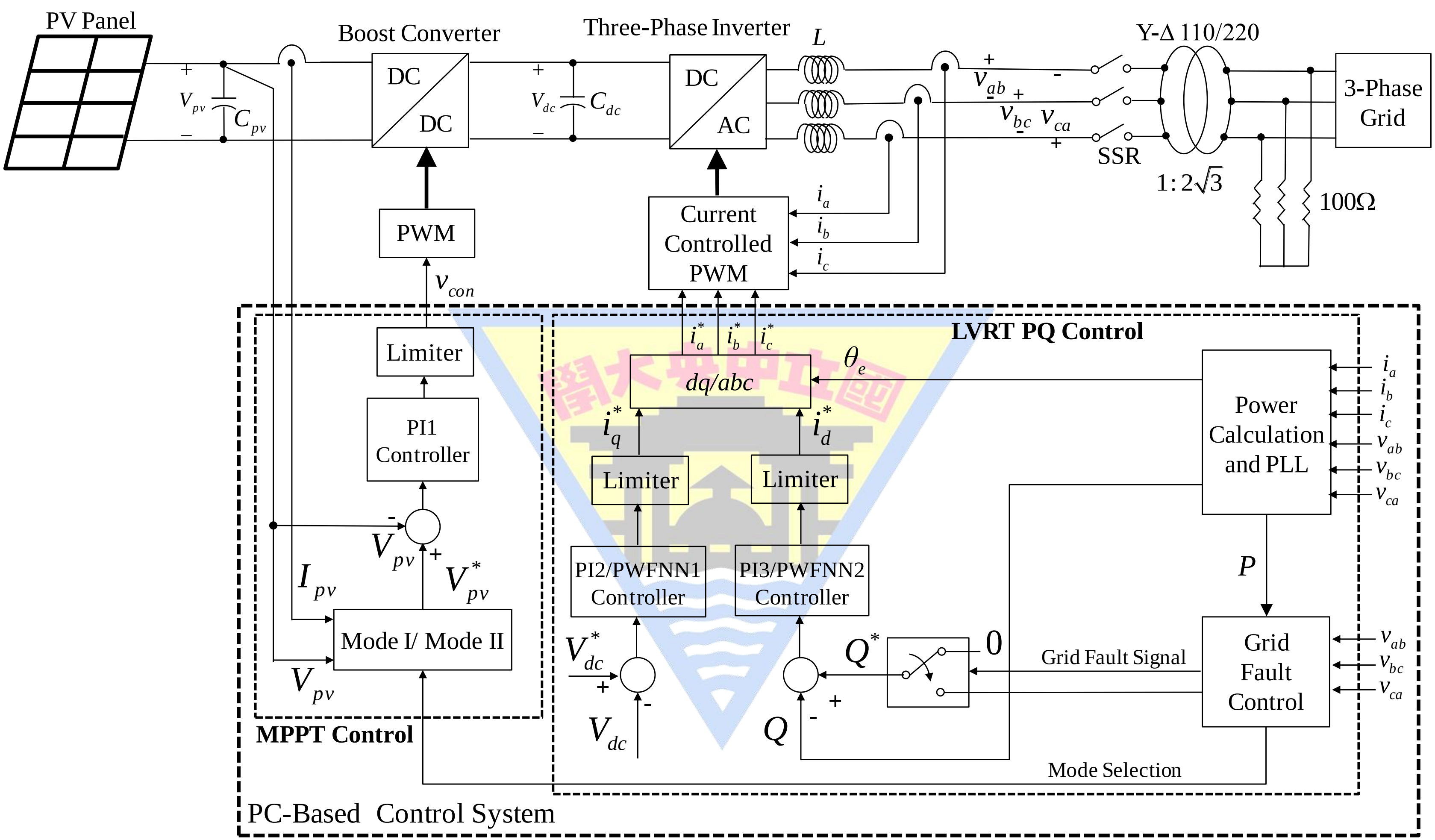

Fig. 5.1

Power Control Using PWFNN Controllers

The average tracking error T_{erravg} , the maximum tracking error T_{MAX} and the standard deviation of the tracking error T_{σ} for the reference tracking are defined as follows:

$$T_{err}(N) = T^*(N) - T(N) \tag{5.1}$$

$$T_{MAX} = \max_{N}\left(\left|T_{err}(N)\right|\right), \quad T_{erravg} = \frac{1}{m}\left(\sum_{N=1}^{m} T_{err}(N)\right) \tag{5.2}$$

$$T_{\sigma} = \sqrt{\frac{1}{m}\left(\sum_{N=1}^{m}\left(T_{err}(N) - T_{erravg}\right)^2\right)} \tag{5.3}$$

Power Control Using PWFNN Controllers

Reactive Power Supporting with Boost Converter Operated at Mode I

Case 1): single phase-to-ground fault occurs with 0.5 pu voltage dip

- P_{pv}= 600 W and P = 526 W
- Q rises to 380 VAR
- voltages: 1.0 pu, 0.77 pu and 0.77 pu
- V_{pv} and I_{pv} remain unchanged due to normal operating of the MPPT control at Mode I.
- V_{mpp} = 150.7 V, irradiance = 600 W/m^2
- V_{pv} = 150.9 V, I_{pv}=4.03 A
- PI controllers:
  - ➢settling time of Q= 0.3 s, overshoot of V_{dc} = 2.6 %
- PWFNN controllers:
  - ➢settling time of Q= 0.1 s, overshoot of V_{dc} = 1.14 %

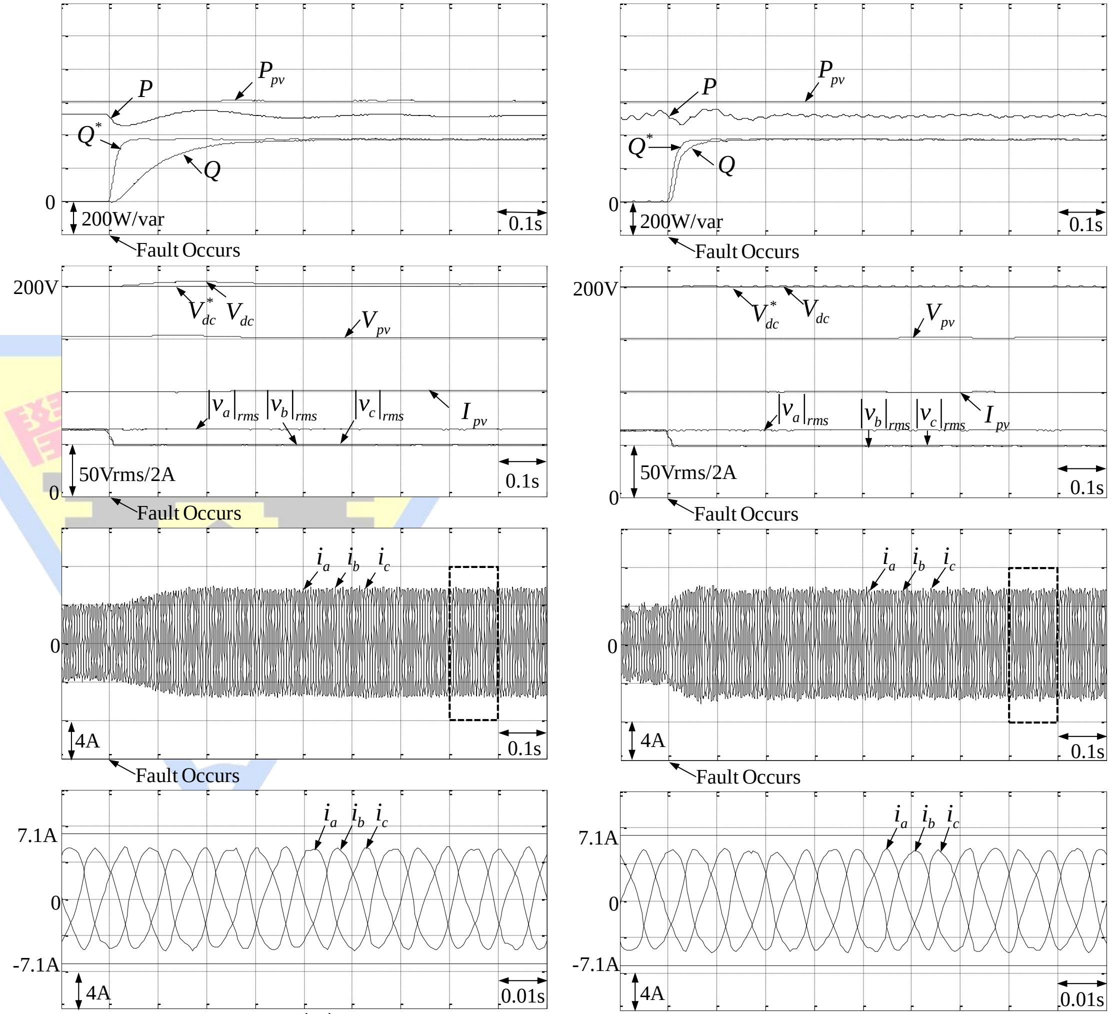

Fig. 5.2 (a) PI (b) PWFNN

Power Control Using PWFNN Controllers

Reactive Power Supporting with Boost Converter Operated at Mode II

Case 2): single phase-to-ground fault occurs with 0.5 pu voltage dip

- P_{pv}= 1000 W → 836 W
- P = 865 W → 720 W
- Q rises to 380 VAR
- voltages: 1.0 pu, 0.77 pu and 0.77 pu
- V_{pv} = 153 V → 164 V
- I_{pv} = 6.5 A → 5.1 A, at Mode II.
- PI controllers:
  - ➢settling time of Q= 0.3 s, overshoot of V_{dc} = 2.5 %
- PWFNN controllers:
  - ➢settling time of Q= 0.1 s, overshoot of V_{dc} = 1.1 %

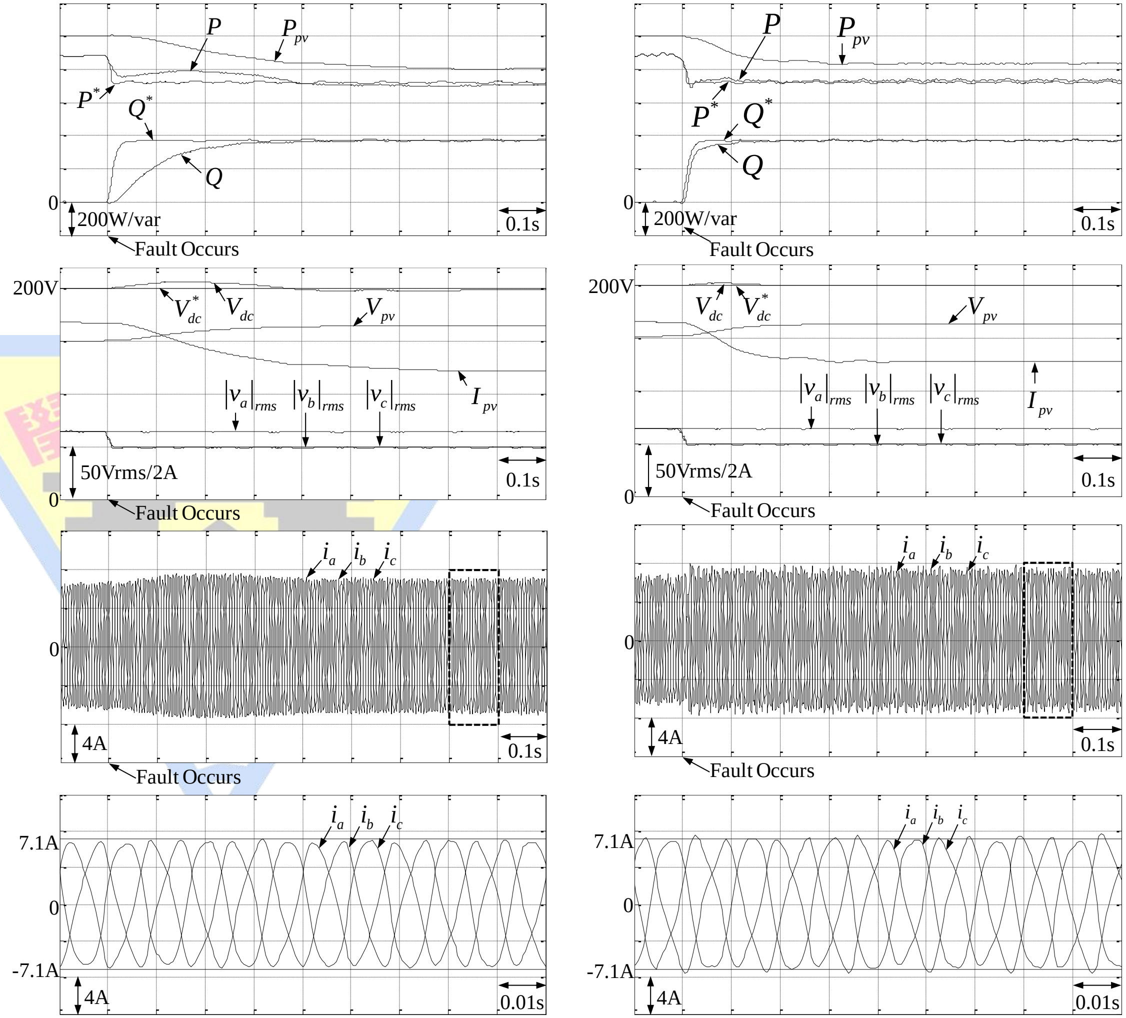

Fig. 5.3 (a) PI (b) PWFNN

Power Control Using PWFNN Controllers

Reactive Power Supporting with Boost Converter Operated at Mode II

Case 3): double phase-to-phase fault occurs with 0.5 pu voltage dip

- P_{pv} = 1000 W → 112 W
- P = 860 W → 55 W
- Q rises to 720 VAR
- voltages: 0.5 pu, 0.92 pu and 0.92 pu
- V_{pv} = 153 V → 174 V
- I_{pv} = 6.5 A → 0.62 A, at Mode II.
- PI controllers:
  - ➢settling time of Q= 0.5 s, overshoot of V_{dc} = 4.63 %
- PWFNN controllers:
  - ➢settling time of Q= 0.2 s, overshoot of V_{dc} = 6.71 %

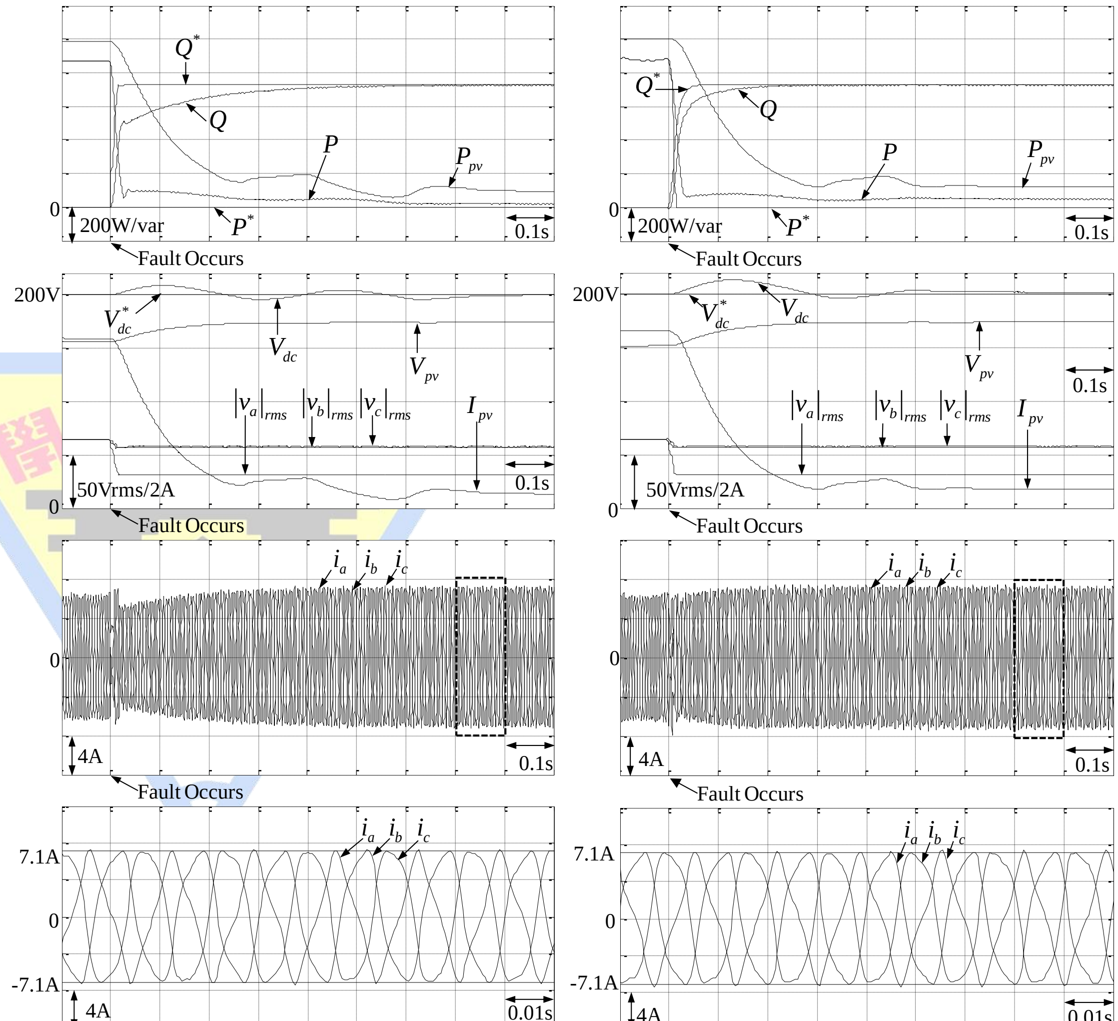

Fig. 5.4 (a) PI (b) PWFNN

Power Control Using PWFNN Controllers

Cases 1 to 3 Using FNN Controllers (1/2)

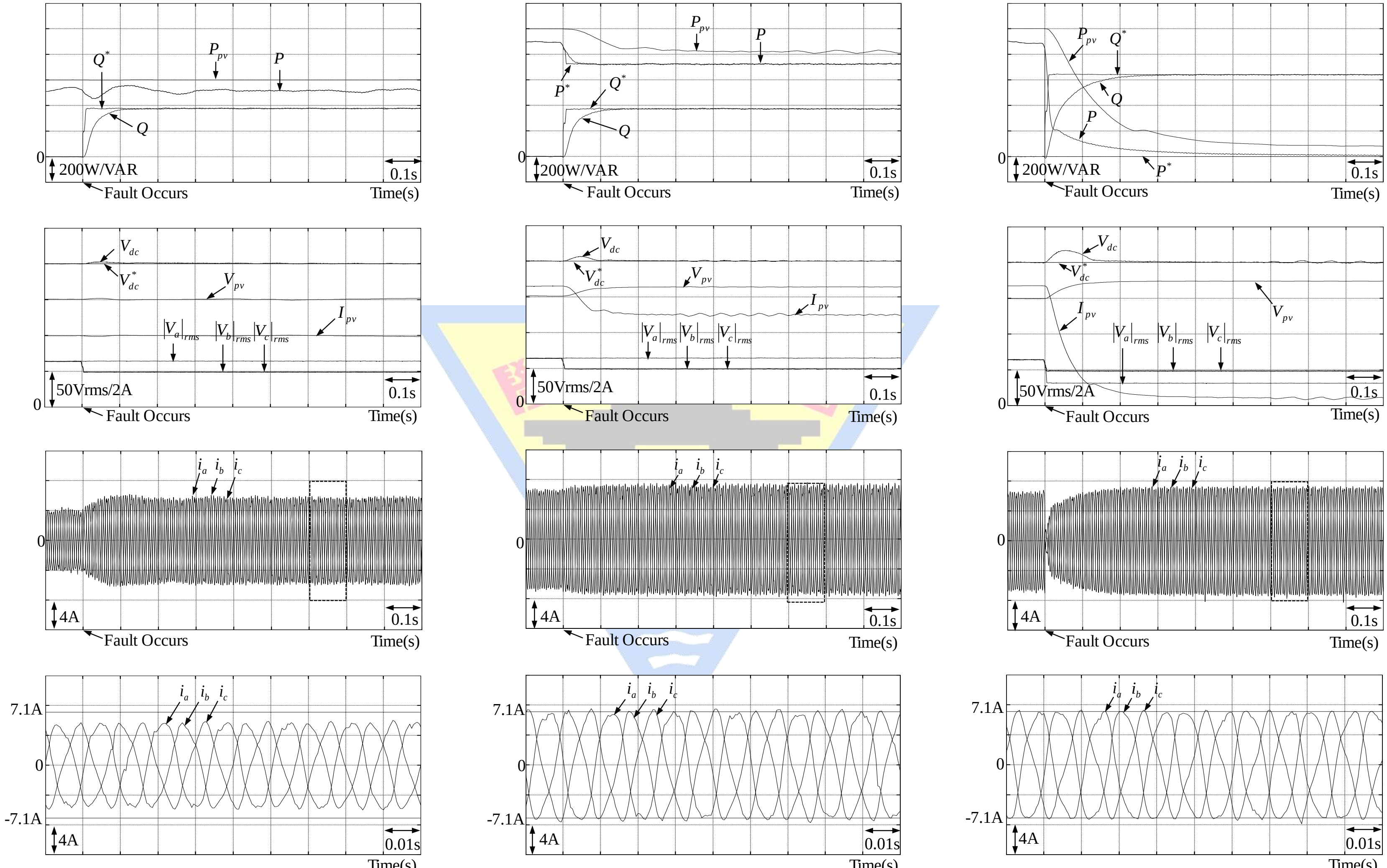

Fig. 5.5 (a) Case 1 (b) Case 2 (c) Case 3

Power Control Using PWFNN Controllers

Cases 1 to 3 Using FNN Controllers (2/2)

Case 1):

- P_{pv}= 600 W and P = 530 W
- Q rises to 378 VAR
- voltages: 1.0 pu, 0.76 pu and 0.76 pu
- V_{pv} and I_{pv} unchanged (Mode I).
- V_{mpp} = 150.5 V, irradiance = 600 W/m^2
- V_{pv} = 150.0 V, I_{pv}=3.99 A
- PI controllers:
  - settling time of Q= 0.3 s
  - overshoot of V_{dc} = 2.6 %
- FNN controllers:
  - settling time of Q= 0.12 s
  - overshoot of V_{dc} = 1.2 %
- PWFNN controllers:
  - settling time of Q= 0.1 s
  - overshoot of V_{dc} = 1.14 %

Case 2):

- P_{pv}= 1000 W → 820 W
- P = 896 W → 720 W
- Q rises to 377 VAR
- voltages: 1.0 pu, 0.76 pu and 0.76 pu
- V_{pv} = 151.2 V → 164 V
- I_{pv} = 6.6 A → 5.0 A, at Mode II.
- PI controllers:
  - settling time of Q= 0.3 s
  - overshoot of V_{dc} = 2.5 %
- FNN controllers:
  - settling time of Q= 0.15 s
  - overshoot of V_{dc} = 3.3 %
- PWFNN controllers:
  - settling time of Q= 0.1 s
  - overshoot of V_{dc} = 1.1 %

Case 3):

- P_{pv}= 1000 W → 88 W
- P = 886 W → 15 W
- Q rises to 655 VAR
- voltages: 0.5 pu, 0.91 pu and 0.9 pu
- V_{pv} = 151.4 V → 174 V
- I_{pv} = 6.6 A → 0.44 A, at Mode II.
- PI controllers:
  - settling time of Q= 0.5 s
  - overshoot of V_{dc} = 4.63 %
- FNN controllers:
  - settling time of Q= 0.25 s
  - overshoot of V_{dc} = 7.5 %
- PWFNN controllers:
  - settling time of Q= 0.2 s
  - overshoot of V_{dc} = 6.71 %

Power Control Using PWFNN Controllers

Performance Discussion

- The performance measurements of PWFNN controller are superior to the other controllers (PI, FNN).
- When the FNN and PWFNN controllers are implemented, the overshoot of V_{dc} is larger owing to more energy accumulated in C_{dc} during the transient period.
- computation complexity
  - ➢ PWFNN: 753 computation steps.
  - ➢ PI: 3 computation steps.
- implementation complexity
  - ➢ PWFNN: 427 code lines/ 14k bytes.
  - ➢ PI: only three function blocks by using Simulink.

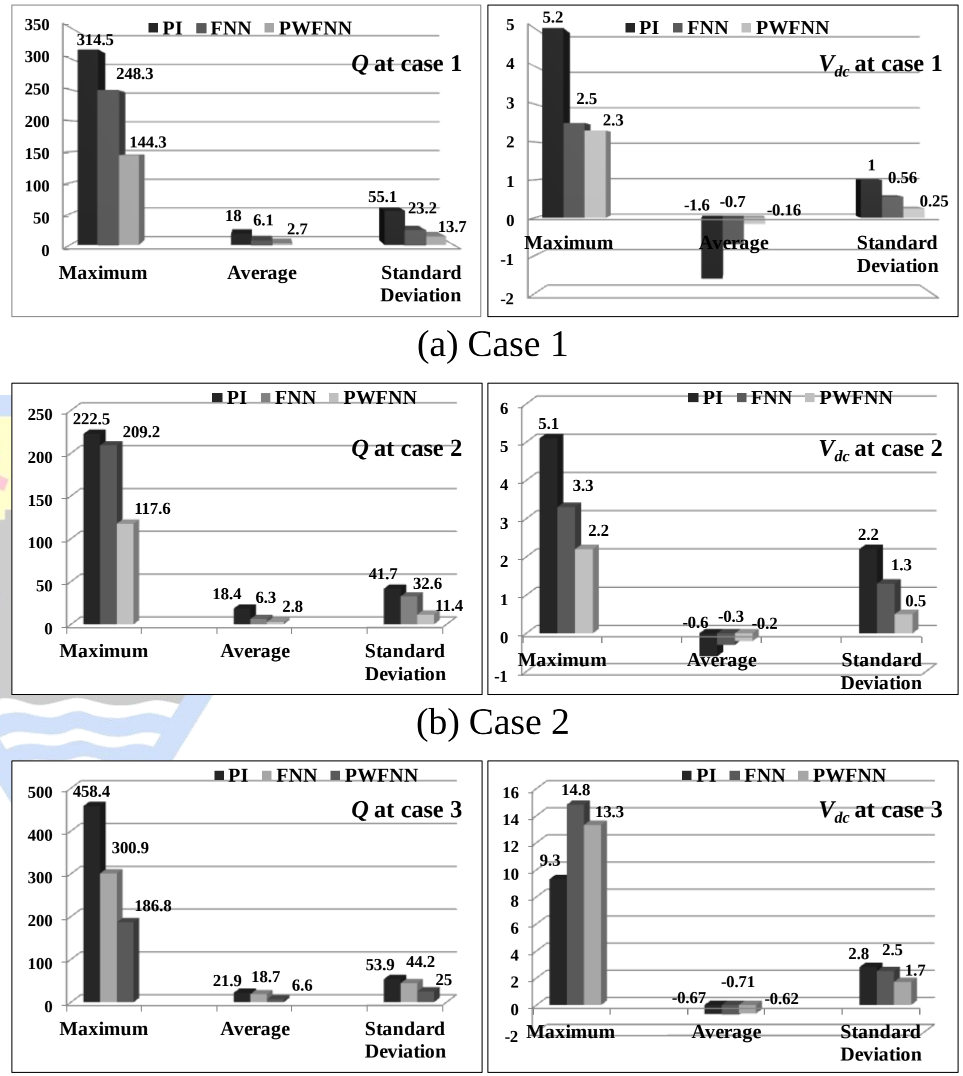

Fig. 5.6 (c) Case 3

Power Control Using PWFNN Controllers

Decreasing of Irradiance with Boost Converter Operated at Mode I

Case 4): single phase-to-ground fault occurs with 0.5 pu voltage dip

- t = 0.2 s: voltage sag occurrence
- P_{pv} = 603 W, P = 533 W (unchanged)
- Q rises to 383 VAR
- voltages: 1.0 pu, 0.77 pu and 0.77 pu
- V_{pv} = 150.3 V, I_{pv} = 4.1 A, at Mode I
- t = 1.0 s; irradiance 600 → 300 W/m^2
- P_{pv}= 603 W → 305 W
- P = 533 W → 243 W
- Q = 383 VAR (unchanged)
- V_{pv} = 151.6 V, I_{pv} = 2.1 A, at Mode I
- The irradiance change after grid fault may cause the response of P oscillating for both the PI or PWFNN controllers with stable response of Q.

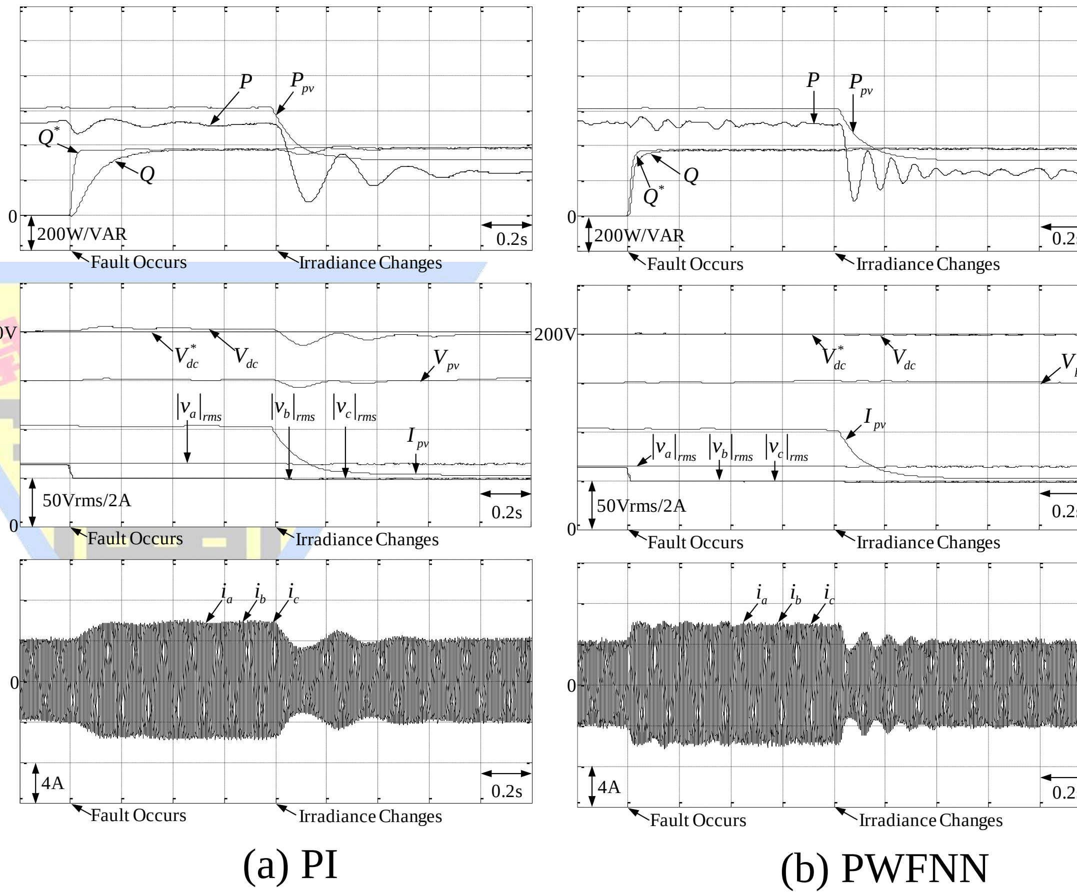

Fig. 5.7

Power Control Using PWFNN Controllers

Decreasing of Irradiance with Boost Converter Operated at Mode I

<u>*Case 5)*:</u> single phase-to-ground fault occurs with 0.5 pu voltage dip

- irradiance = 30 W/m^2
- t = 0.2 s: voltage sag occurrence
- P_{pv} = 30 W, P = 0 W
- Q rises to 391 VAR
- voltages: 1.0 pu, 0.77 pu and 0.77 pu
- V_{pv} = 158.9 V, I_{pv} = 0.23 A, at Mode I
- If the output power of PV panel is less than 30 W, the generated power can't support the electronic circuits to operate and the boost converter and three-phase inverter will shut down.

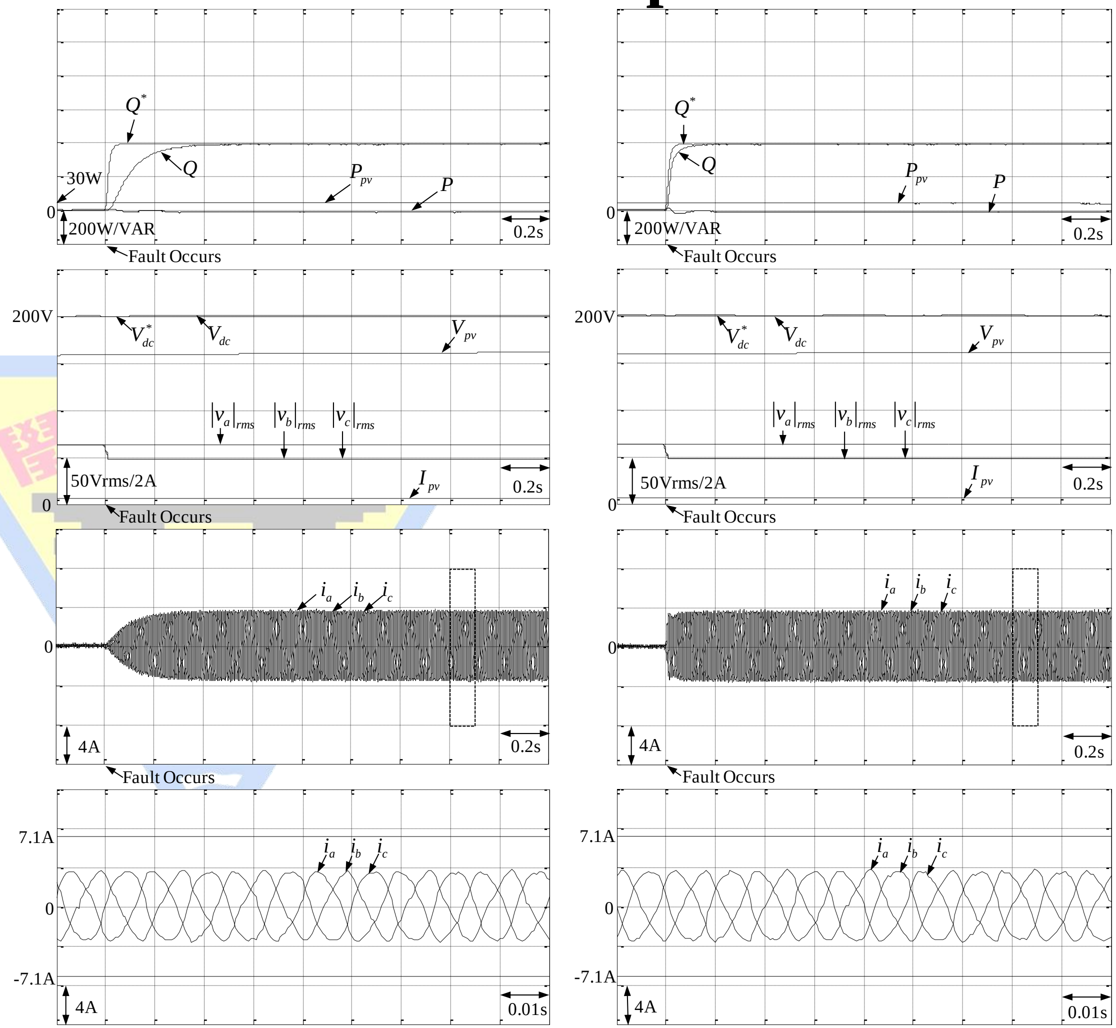

Fig. 5.8 (a) PI (b) PWFNN

Power Control Using TSKPFNN-AMF Controllers

Fig. 5.9

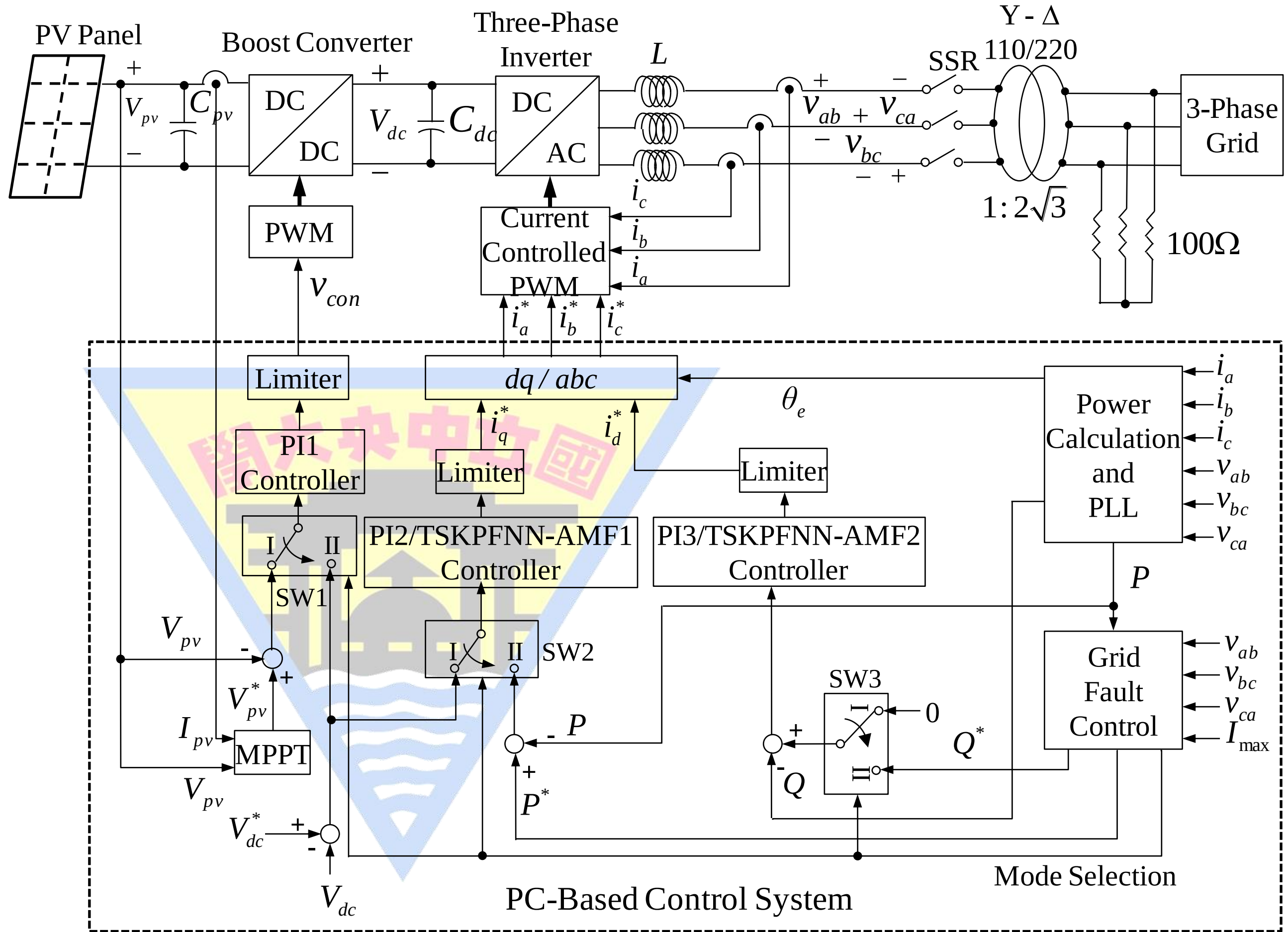

The integral of squared error (ISE) of the tracking error T_{ISE} :

$$T_{ISE} = \int_0^{\infty} \{e(t)\}^2 dt \approx \Delta T \sum_{N=1}^{m} \left(T_{err}(N)\right)^2, \quad T_{err}(N) = T^*(N) - T(N) \qquad (5.4)$$

Power Control Using TSKPFNN-AMF Controllers

Reactive Power Supporting at Mode I

<u>*Case 1):* </u>double phase-to-ground fault occurs with 0.3 pu voltage dip

- P_{pv}= 612 W and P = 524 W
- Q rises to 456 VAR
- voltages: 0.7 pu, 0.87 pu and 0.87 pu
- V_{pv} = 150.9 V, I_{pv}=4.05 A, at mode I
- i_q^* changes from 4.1 A to 4.9 A; i_d^* rises to 2.9 A
- PI controllers:
  - ➢settling time of Q= 0.45 s, overshoot of V_{dc} = 4.9 %
- TSKPFNN-AMF controllers:
  - ➢settling time of Q= 0.3 s, overshoot of V_{dc} = 1.45 %
- The settling time of Q is decreased by 33.3 % and the overshoot of V_{dc} is decreased by 70.4 % by using the TSKPFNN-AMF controllers.

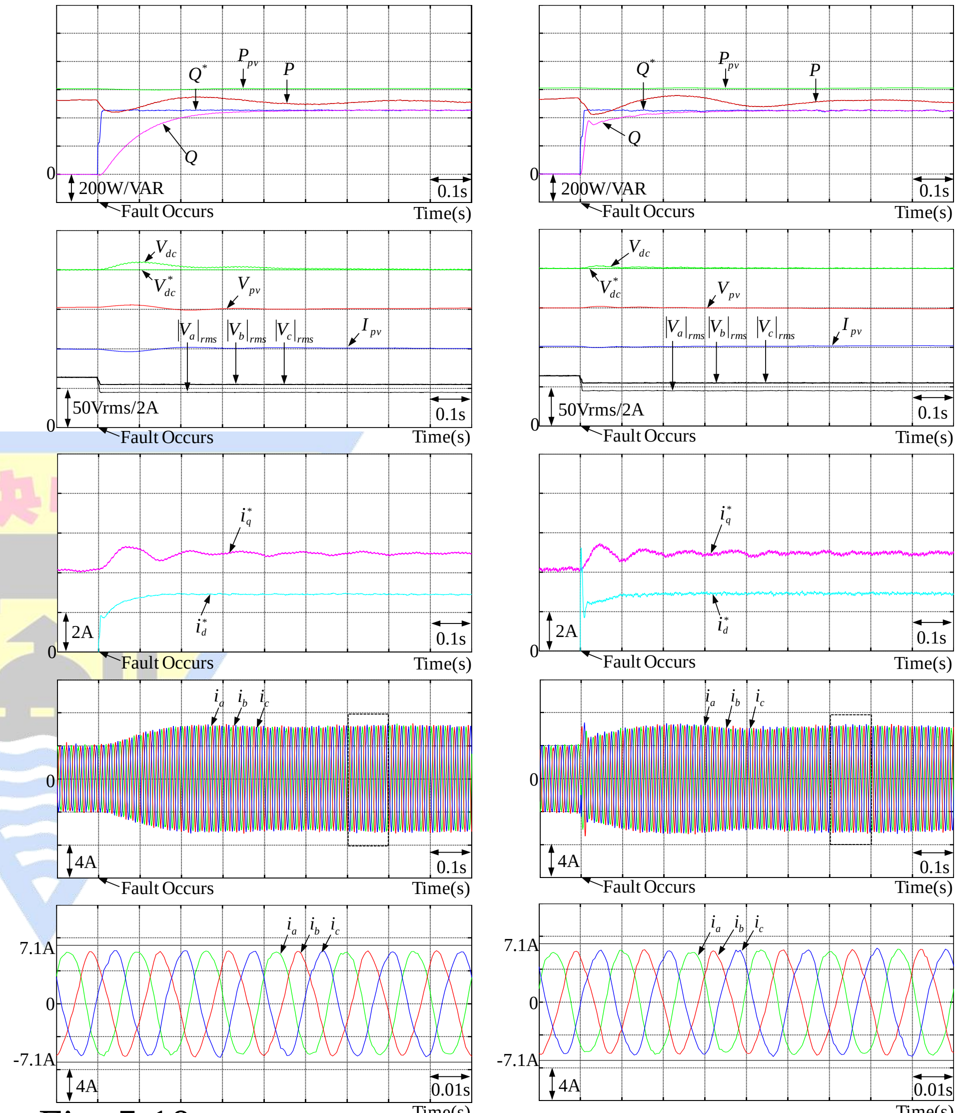

Fig. 5.10 (a) PI (b) TSKPFNN-AMF

Power Control Using TSKPFNN-AMF Controllers

Reactive Power Supporting at Mode II

<u>Case 2):</u> double phase-to-ground fault occurs with 0.7 pu voltage dip

- P_{pv}= 1005 W → 102 W; P = 882 W → 21 W
- Q rises to 527 VAR, , at mode II
- voltages: 0.3 pu, 0.67 pu and 0.68 pu
- V_{pv} = 150.4 → 173.9 V, I_{pv}= 6.6 → 0.52 A
- i_q^* drops from 6.2 A to 1.3 A; i_d^* rises to 5.9 A
- PI controllers:
  - ➢settling time of Q= 0.7 s, overshoot of V_{dc} = 5.4 %
- TSKPFNN-AMF controllers:
  - ➢settling time of Q= 0.16 s
  - ➢ overshoot of V_{dc} = 7 % (by PI1)
- The settling time of Q is decreased by 77.1 % by using the TSKPFNN-AMF controllers.

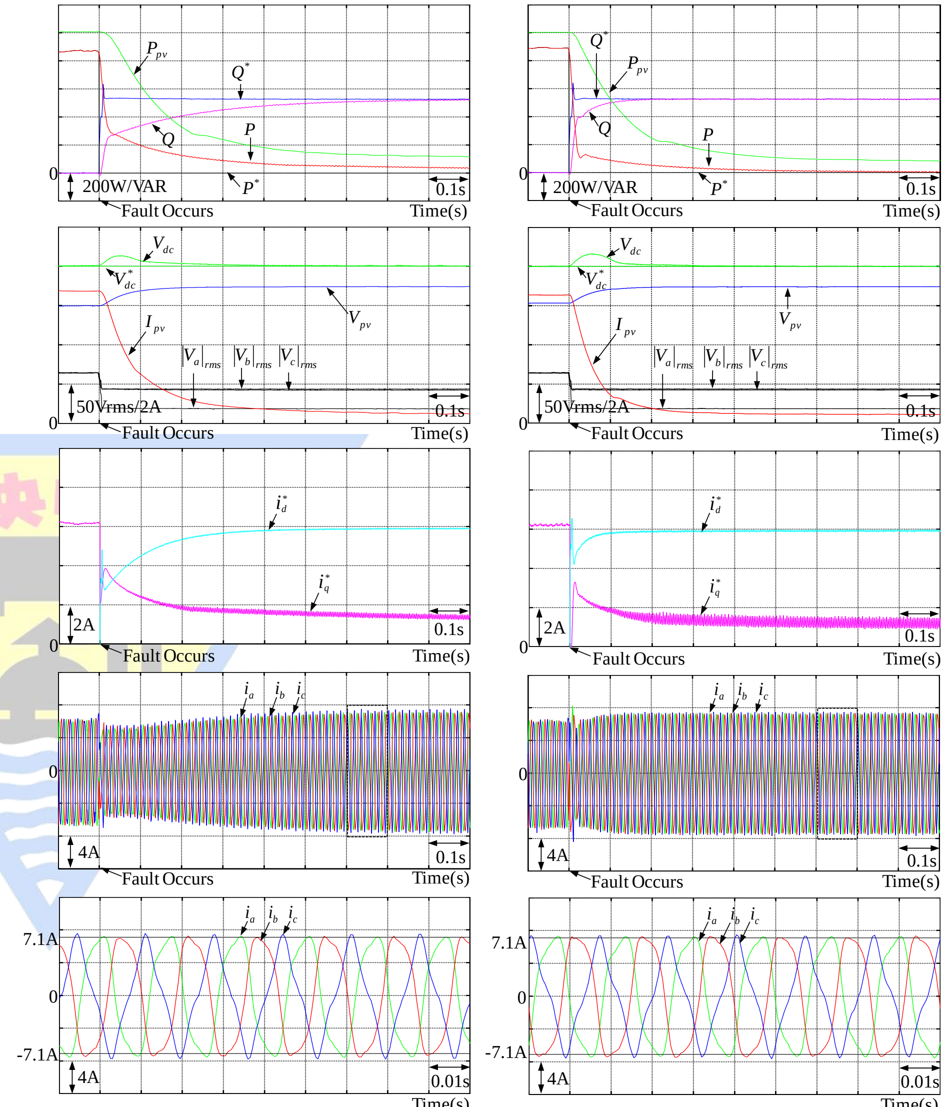

Fig. 5.11 (a) PI (b) TSKPFNN-AMF

Power Control Using TSKPFNN-AMF Controllers

Reactive Power Supporting at Low Irradiance

Case 3): double phase-to-ground fault occurs with 0.7 pu voltage dip

- Irradiance: 100 W/m^2
- P_{pv}= 106 W $\rightarrow$ 77.6 W; P = 63.8 W $\rightarrow$ 1.4 W
- Q rises to 522 VAR, , at mode II
- voltages: 0.29 pu, 0.67 pu and 0.68 pu
- V_{pv} = 158 $\rightarrow$ 168 V, I_{pv}= 0.67 $\rightarrow$ 0.46 A
- i_q^* 1.37 $\rightarrow$ 1.23 A; i_d^* rises to 5.9 A
- PI controllers:
  - ➢settling time of Q= 0.65 s, overshoot of V_{dc} = 1.9 %
- TSKPFNN-AMF controllers:
  - ➢settling time of Q= 0.2 s
  - ➢ overshoot of V_{dc} = 1.4 % (by PI1)
- The settling time of Q is decreased by 77.1 % by using the TSKPFNN-AMF controllers.

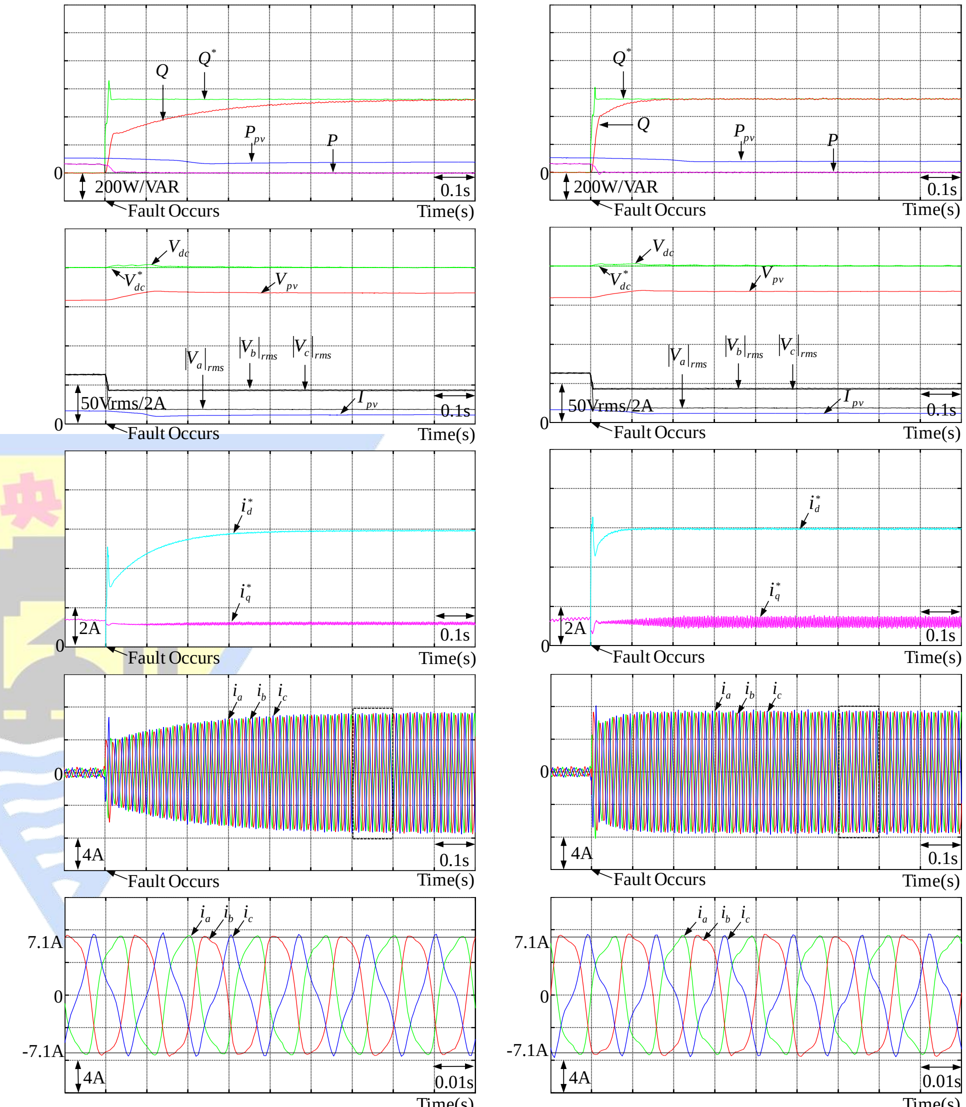

Fig. 5.12 (a) PI (b) TSKPFNN-AMF

Power Control Using TSKPFNN-AMF Controllers

Reactive Power Supporting at Unsymmetrical Unbalance Fault Condition

<u>*Case 4)*: </u>double phase-to-ground fault unsymmetrical balance fault with 0.3 pu and 0.5 pu voltage dip

- P_{pv}= 609 W → 546 W; P = 532 W → 449 W
- Q rises to 556 VAR, , at mode II
- voltages: 0.61 pu, 0.77 pu and 0.86 pu
- V_{pv} = 152 → 162 V, I_{pv}= 4.0 → 3.3 A
- i_q^* 4.1 → 4.9 A; i_d^* rises to 4.1 A
- PI controllers:
  - ➢settling time of Q= 0.45 s, overshoot of V_{dc} = 4.1 %
- TSKPFNN-AMF controllers:
  - ➢settling time of Q= 0.3 s
  - ➢ overshoot of V_{dc} = 0.6 % (by PI1)

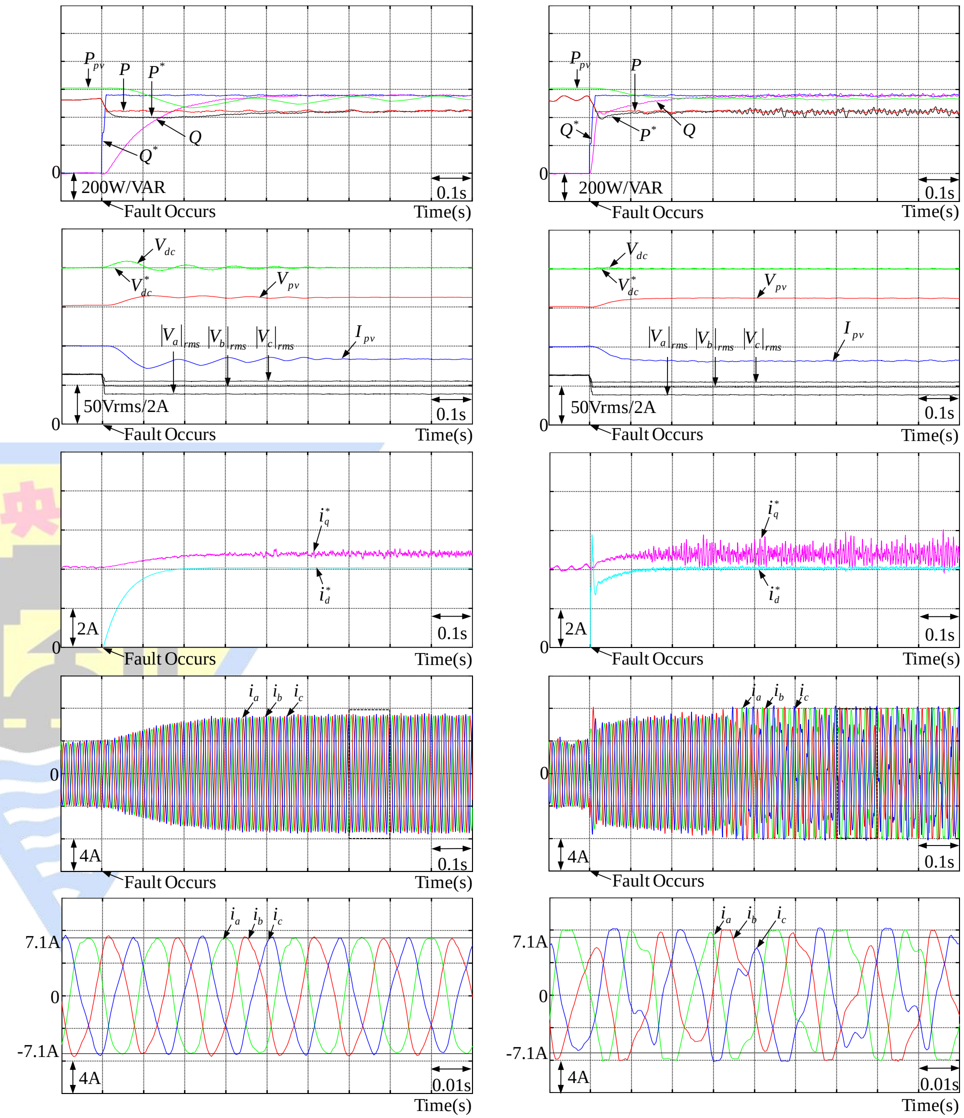

Fig. 5.13 (a) PI (b) TSKPFNN-AMF

Power Control Using TSKPFNN-AMF Controllers

Cases 1 and 2 Using FNN Controllers (1/2)

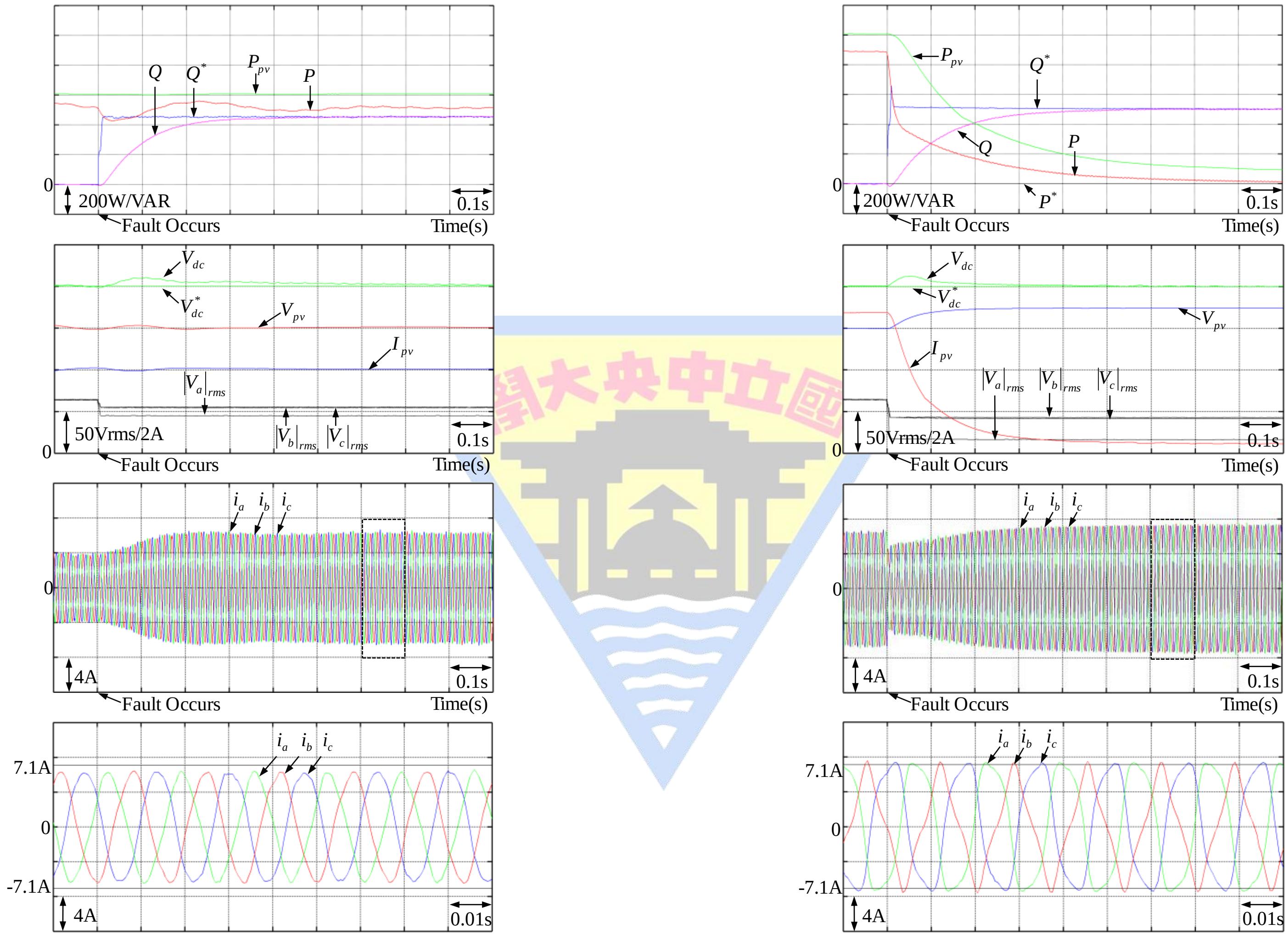

Fig. 5.14 (a) Case 1 (b) Case 2

Power Control Using TSKPFNN-AMF Controllers

Cases 1 and 2 Using FNN Controllers (2/2)

Case 1):

- P_{pv}= 608 W and P = 520 W
- Q rises to 457 VAR
- voltages: 0.7 pu, 0.87 pu and 0.87 pu
- V_{pv} = 150.6 V, I_{pv}=4.03 A, at mode I
- PI controllers:
  - settling time of Q= 0.45 s
  - overshoot of V_{dc} = 4.9 %
- FNN controllers:
  - settling time of Q= 0.42 s
  - overshoot of V_{dc} = 4.5 %
- TSKPFNN-AMF controllers:
  - settling time of Q= 0.3 s
  - overshoot of V_{dc} = 1.45 %.

Case 2):

- P_{pv}= 1008 W → 96 W; P = 887 W → 13 W
- Q rises to 504 VAR, , at mode II
- voltages: 0.3 pu, 0.67 pu and 0.67 pu
- V_{pv} = 151.4 → 174 V, I_{pv}= 6.6 → 0.0.46 A
- PI controllers:
  - settling time of Q= 0.7 s
  - overshoot of V_{dc} = 5.4 %
- FNN controllers:
  - settling time of Q= 0.55 s
  - overshoot of V_{dc} = 5.7 % (by PI1)
- TSKPFNN-AMF controllers:
  - settling time of Q= 0.16 s
  - overshoot of V_{dc} = 7 % (by PI1)

Power Control Using TSKPFNN-AMF Controllers

Table 5.1 THDs of Three-Phase Currents for Case 1 to Case 4

Test Case	Controller	i_a (%)	i_b (%)	i_c (%)	Average (%)
Case 1	PI	8.73	8.72	7.16	8.20
	TSKPFNN-AMF	8.23	7.23	8.82	8.09
Case 2	PI	15.98	14.24	18.26	16.16
	TSKPFNN-AMF	16.90	16.55	21.45	18.30
Case 3	PI	17.59	16.62	21.87	18.69
	TSKPFNN-AMF	20.65	18.86	26.22	21.91
Case 4	PI	9.20	10.79	11.58	10.52
	TSKPFNN-AMF	19.99	25.74	34.20	26.64

- In Case 4, the THDs of i_a, i_b, and i_c are 9.2 %, 10.79 % and 11.58 % when the PI controllers are used, and the THDs of i_a, i_b, and i_c and are 19.99 %, 25.74 %, and 34.2 % when the TSKPFNN-AMF controllers are used.

Power Control Using TSKPFNN-AMF Controllers

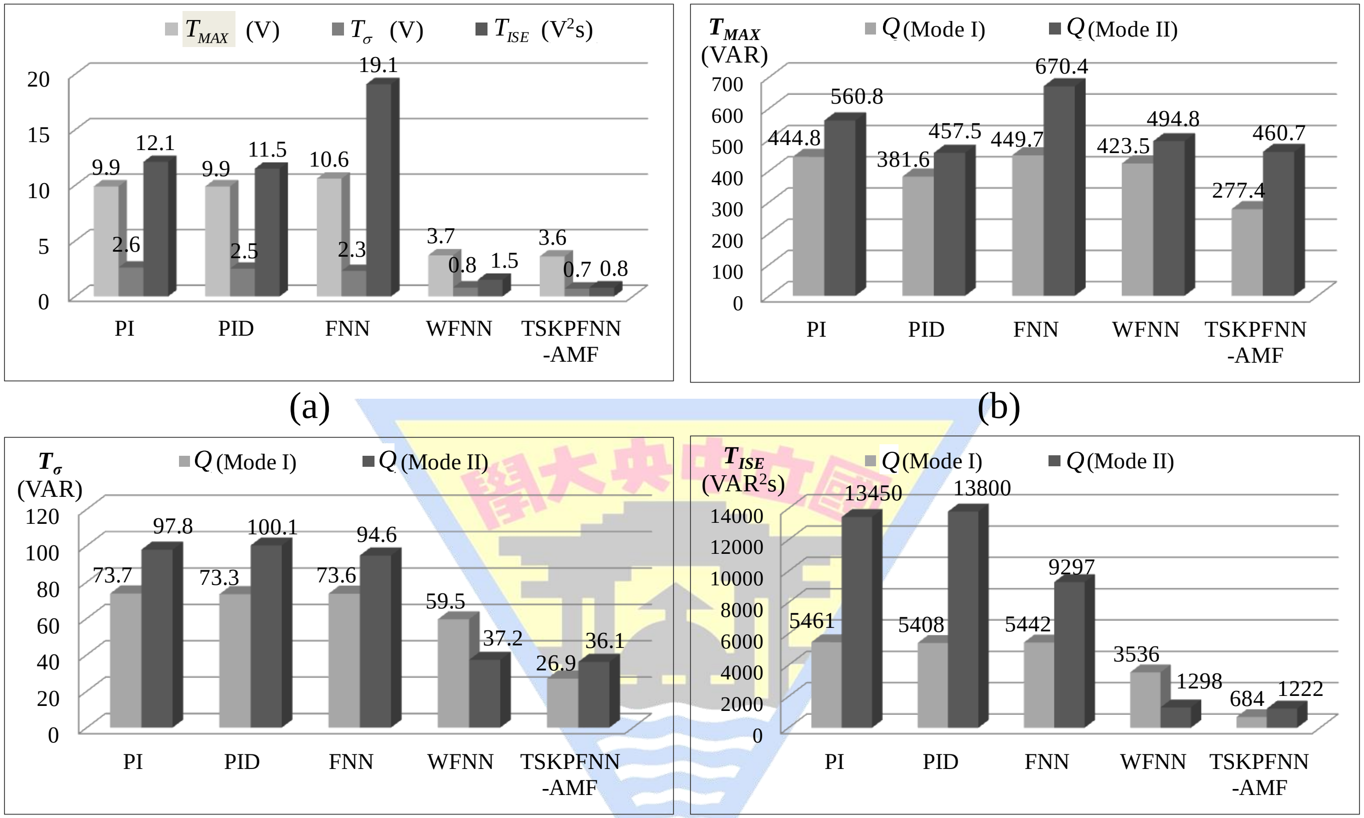

Fig. 5.15

- The performances of TSKPFNN-AMF controllers are superior to the other controllers.
- Computation complexity: TSKPFNN-AMF controller: 662 steps; PI controller: 3 steps
- Implementation complexity: TSKPFNN-AMF controller: 377 code lines/ 13k bytes; PI controller: 3 blocks

Contents

Conclusions

Conclusions

- Voltages and currents analyses of PV system during the grid faults were described.
- A dual mode operation control method is developed.
- Network structure, online learning algorithm~~s~~ and convergence analysis.
- Performances of the proposed controllers are better than PI, PID, FNN and WFNN controllers.
- Major contributions
  - The formula for the depth of the unsymmetrical voltage sags is proposed and used to determine the injected reactive power during grid faults considering the current limit.
  - The dual mode control strategy is developed to maintain the balance of power between boost converter and three-phase inverter during grid faults
  - Two intelligent controllers are developed to control the active and reactive power of the grid-connected three-phase PV system
  - The BP-based online learning algorithm of the PWFNN and TSKPFNN-AMF controllers with self-tuning learning rates.
  - The proposed controllers are successful implemented to control the power and DC-link bus voltage of a three-phase grid-connected PV system during grid faults.

Academic Performance

Journal Papers

[1] K. C. Lu, F. J. Lin, and B. H. Yang, "Profit Optimization Based Power Compensation Control Strategy for Grid-Connected PV System," *IEEE Systems Journal*, vol. 12, no. 3, pp. 2878-2881, 2018.

[2] F. J. Lin, K. C. Lu, and B. H. Yang, "Recurrent Fuzzy Cerebellar Model Articulation Neural Network Based Power Control of Single-Stage Three-Phase Grid-Connected Photovoltaic System during Grid Faults," *IEEE Trans. Industrial Electronics*, vol. 64, no. 2, pp. 1258-1268, 2017. (SCI)

[3] F. J. Lin, S. Y. Lu, J. Y. Chao, and J. K. Chang, "Intelligent PV power smoothing control using probabilistic fuzzy neural network with energy storage system," *International Journal of Photoenergy*, vol. 2017, article ID 8387909, 15 pages, 2017.

[4] F. J. Lin, K. C. Lu, T. H. Ke, and Y. R. Chang, "Probabilistic Wavelet Fuzzy Neural Network Based Reactive Power Control for Grid-Connected Three-Phase PV System during Grid Faults Renewable Energy," *Renewable Energy*, vol. 92, pp. 437-449, 2016. (SCI)

[5] F. J. Lin, K. C. Lu, T. H. Ke, and H. Y. Li, "Reactive Power Control of Three-Phase PV System during Grids Faults Using Takagi-Sugeno-Kang Probabilistic Fuzzy Neural Network Control," *IEEE Trans. Industrial Electronics*, vol. 62, no. 9, pp. 5516-5528, 2015. (SCI)

[6] F. J. Lin, K. C. Lu, T. H. Ke, and Y. R. Chang, "Reactive Power Control of Single-Stage Three-phase Photovoltaic System during Grid Faults Using Recurrent Fuzzy Cerebellar Model Articulation Neural Network," *International Journal of Photoenergy*, vol. 2014, Article ID 760743, 13 pages, 2014. (SCI)

Patents

[1] F. J. Lin, K. C. Lu, and H. Y. Lee, *Photovoltaic Power Generation System*, USA Patent, US 9,276,498 B2, March 2016

[2] F. J. Lin, K. C. Lu, and H. Y. Lee, *Photovoltaic Energy Power Generation System*, Patent No. I522767, R. O. C., Feb. 2016